

Models with competing interactions

Cristian Micheletti
Christ Church

Department of Physics, Theoretical Physics
University of Oxford



Thesis submitted for the degree of Doctor of Philosophy
in the University of Oxford

Trinity Term 1996

Models with competing interactions

Cristian Micheletti

Christ Church

Department of Physics, Theoretical Physics
University of Oxford



University of Oxford

Abstract

We examine the occurrence of spatially modulated structures in several models with competing interactions. Of particular interest are the situations where, for given values of the interactions, the ground-state is infinitely degenerate. Most of the work presented here concerns the analysis of how this zero-temperature multidegeneracy can be removed by the introduction of weak perturbations such as spin anisotropy, external magnetic fields, or quantum fluctuations.

In Chapters 2-4, we consider models of finite or semi-infinite chains of spins, where the competition between surface and bulk effects creates a domain wall (kink) in the ground state. In particular in Chapter 2 we show that, in a chain of ferromagnetically-coupled XY spins with p -fold anisotropy ($p \geq 3$), the softening of the spins removes the degeneracy by stabilizing a sequence of layering transitions. It is also argued that, when $p = 2$, the persistence of multidegeneracy in the classical model can be eliminated by quantum effects. In Chapter 3 the effects of quantum fluctuations on the behaviour of an interface are considered further for the case of the three-dimensional transverse Ising model.

Finally we study a chain of antiferromagnetically-coupled XY spins with two-fold anisotropy in an external magnetic field. The analytical and numerical results, presented in Chapter 4, reveal that, in semi-infinite and finite chains of even length, there is a sequence of layering transitions in the bulk that has not been previously identified.

The second part of the thesis focuses on the splitting of the multidegeneracy in infinite systems. In particular, in Chapter 5, we examine the effect of quantum fluctuations near the multiphase point of a generalised, quantum, axial next-nearest-neighbour Ising model. It is shown that the sequence of phases stabilized by quantum and thermal fluctuations are dramatically different.

In Chapter 6 we consider the Falicov-Kimball model, which describes a one-dimensional system of interacting ions and electrons. By using Green's functions techniques we recursively construct the phase diagram in the limit of large ion-electron coupling. Hence, it is shown that the ion density has a behaviour characteristic of a devil's staircase.

Finally we consider a model consisting of a chain of XY spins with six-fold anisotropy and chiral interactions in the presence of a magnetic field. The analysis presented in Chapter 7 gives evidence for the occurrence of an epsilon point (an infinite checkerboard of modulated phases) in the phase diagram. By using a recursive analysis technique it is shown that the checkerboard has a self-similar, fractal structure.

Thesis submitted for the degree of Doctor of Philosophy
in the University of Oxford

Trinity Term 1996

Acknowledgements

It is a great pleasure to thank my supervisor, Dr. Julia Yeomans, for the constant help and encouragement that she has given to me over the past few years and for suggesting the problems that are presented in this thesis.

I have enjoyed very much working with her; for me it has been an enriching experience, both from the scientific and human point of view.

I am also grateful to her for giving to me the opportunity to meet and collaborate with other researchers. In particular I would like to express my gratitude to the members of the Condensed Matter group in Padua, to Prof. A. B. Harris and R. B. Griffiths (who I would also like to thank for their hospitality during my visits to Philadelphia and Pittsburgh).

I am also indebted to Prof. M. E. Fisher, Dr. L. M. Floria, Prof. M. Rasetti, Dr. L. Trallori and Dr. G. I. Watson for helpful discussions.

Naturally, having spent three years in Oxford, there are really many other people that I should like to thank. Above all I wish to thank my parents, my brothers and Sabina for all their help and support.

Many thanks also to the several people with whom, over the years, I have shared the office 2.7, Alexander, Andrew, Bobby, David, Jean-Sebastian, Roderich, Roger and William, and also to the graduate members of Christ Church and Trinity, in particular Brad, Greg, Kostas, Paul and Richard.

To my family.

Contents

1	Introduction	3
1.1	Modulated structures	3
1.2	The ANNNI model	4
1.3	The ANNNI model at finite temperature.	5
1.4	Domain-wall interactions	7
1.5	Removal of multidegeneracy in models with a surface	8
2	Unbinding of interfaces mediated by spin softening	12
2.1	Introduction	12
2.2	The model	13
2.3	Qualitative remarks	14
2.4	The inverse-anisotropy expansion	14
2.5	Calculation of $E_{\langle n \rangle} - E_{\langle n+1 \rangle}$	15
2.6	The phase diagram	17
2.7	Persistence of degeneracy for $p = 2$	19
2.8	Quantum fluctuations	21
2.9	Conclusions	24
3	Quantum fluctuations in the transverse Ising model	25
3.1	Introduction	25
3.2	The model	26
3.3	Qualitative remarks	27
3.4	Calculation of ΔE_k	28
3.5	The phase diagram	34
3.6	The (3+1)-dimensional classical model	35
3.7	Calculation of ΔE_0	37
3.8	Conclusions	40
4	Layering transitions in an anisotropic antiferromagnet	41
4.1	Introduction	41
4.2	Infinite Chain	42
4.3	Semi-infinite chains	48
4.4	Analytical results	53
4.5	Finite chain	55
4.6	Conclusions	57
5	Quantum fluctuations in the ANNNI model	59
5.1	Introduction	59
5.2	The model	60
5.3	Perturbation expansion	63
5.4	The wall-wall interaction formalism	63
5.5	Wall energy	68

5.6	Two-wall interactions	68
5.7	Three-wall interactions	73
5.8	Conclusions	76
6	Complete devil's staircase in the Falicov-Kimball model	78
6.1	Introduction	78
6.2	The model	79
6.3	The phase diagram for $t = 0$	79
6.4	The defect-defect interaction expansion	81
6.5	Calculation of $V_2(n)$ using Green's function methods	84
6.6	Calculation of the general V_m term	86
6.7	Hyperfine structure of the phase diagram	87
6.8	Conclusions	87
7	An epsilon point in a spin model	89
7.1	Introduction	89
7.2	The model	90
7.3	The interface-interface interaction formalism	92
7.4	The $\langle\alpha\rangle$ boundary	93
7.5	The $\langle\beta\rangle$ boundary	96
7.6	Hyperfine structure	97
7.7	Conclusions	99
A		101
A.1	Stability of the $\langle 2 \rangle - \langle 3 \rangle$ boundary	101
B		108
B.1	Calculation of the two-interface interaction.	108

Chapter 1

Introduction

1.1 Modulated structures

In this thesis we examine the occurrence of spatially modulated structures in models with competing interactions. Typically the competition arises from the presence of two or more physical parameters that tend to favour states with different periodicity, symmetry or structure. Due to the presence of this type of competition the stable phases can show complex spatial modulations.

One of the best known examples of a material with many different modulated phases is cerium antimonide, $CeSb$. The crystal structure of this alloy is $NaCl$ -like, with the ions of Ce and Sb occupying alternate vertices of a simple cubic lattice. At low temperatures ($T \lesssim 8K$) the crystal field splitting causes the lowest energy state of the Ce ions to be a singlet, so that the total magnetic moment (that for simplicity we shall call *spin*) of the ions has an Ising-like behaviour.

Several experiments based on neutron scattering have revealed that $CeSb$ samples have a uniaxial magnetic modulation [1, 2]. In other words, in the planes perpendicular to the modulation vector, the spins of the Ce ions are essentially parallel while, perpendicular to the planes, complicated sequences of alternating bands of up and down spins are observed. The various magnetic structures seen in cerium antimonide are shown in Fig. 1.1.

The phase diagram of Fig. 1.1 is so rich that it seems implausible that it should be possible to explain it using a simple model. However, it is often the case that the complicated behaviour of materials with uniaxial modulation can be accounted for by very simple, schematic, models with competing interactions.

Arguably, the best known example of these is the axial next-nearest-neighbour (ANNNI) model which was introduced by Elliott (1961) to explain rare-earth magnetism [3]. The simplicity of the ANNNI model makes it an ideal example for discussing the physics of modulated structures. Therefore we will devote the next section to a qualitative description of the model and its phase diagram.

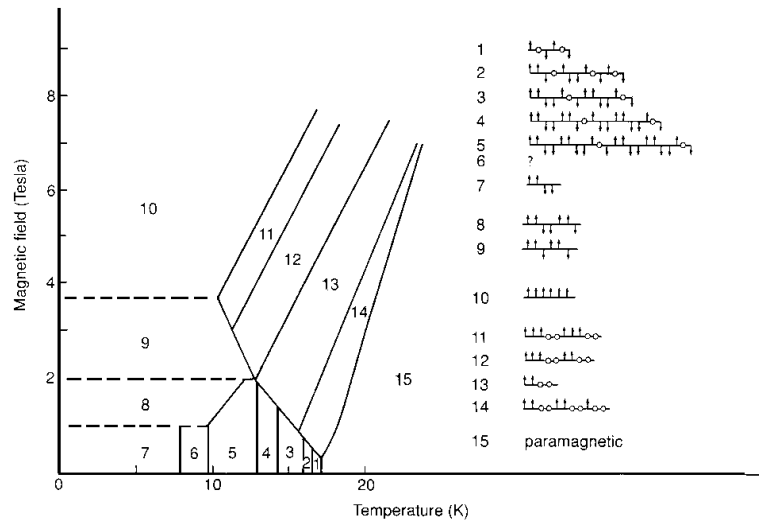


Figure 1.1: Experimental phase diagram for *CeSb* (after [2]). The arrows denote the orientation of the magnetic moments of *Ce* ions in the ferromagnetic planes. The open circles indicate planes where the magnetization is zero to within experimental accuracy.

1.2 The ANNNI model

The ANNNI model consists of a three-dimensional system of Ising spins occupying the sites of a cubic lattice. Along one lattice direction the interaction between nearest-neighbour spins, J_1 , is chosen to be ferromagnetic, while the next-nearest-neighbour exchange, J_2 , is antiferromagnetic. In planes perpendicular to the privileged lattice direction, nearest-neighbour spins interact via a ferromagnetic exchange, J_0 . The Hamiltonian for the system is

$$\mathcal{H} = -J_0 \sum_{i\langle jj' \rangle} S_{i,j} S_{i,j'} - J_1 \sum_{i,j} S_{i,j} S_{i+1,j} + J_2 \sum_{i,j} S_{i,j} S_{i+2,j}, \quad (1.1)$$

where i labels the ferromagnetic planes and j the sites within the plane. Also $\langle jj' \rangle$ indicates a sum over pairs of nearest neighbours in the same plane and $S_{i,j}$ is an Ising spin at site (i, j) . A schematic representation of the model is given in Fig. 1.2.

At zero temperature the ground state is ferromagnetic for $J_2/J_1 < 1/2$ (all spins up or all down) while, for $J_2/J_1 > 1/2$, the favoured configuration is the one corresponding to two planes up, two down and so on. The point $J_2/J_1 = 1/2$ is a multiphase point where all spin configurations consisting of a sequence of domains of two or more parallel planes with alternate orientation have the same energy.

The presence of a multiphase point is not an uncommon feature in models with competing interactions. As for the ANNNI case, the multidegeneracy is usually encountered when configurations built by mixing segments of two or more neighbouring phases are degenerate. Usually this type of multidegeneracy is not robust to small perturbations introduced, for example, by thermal fluctuations, surface effects or additional external fields.

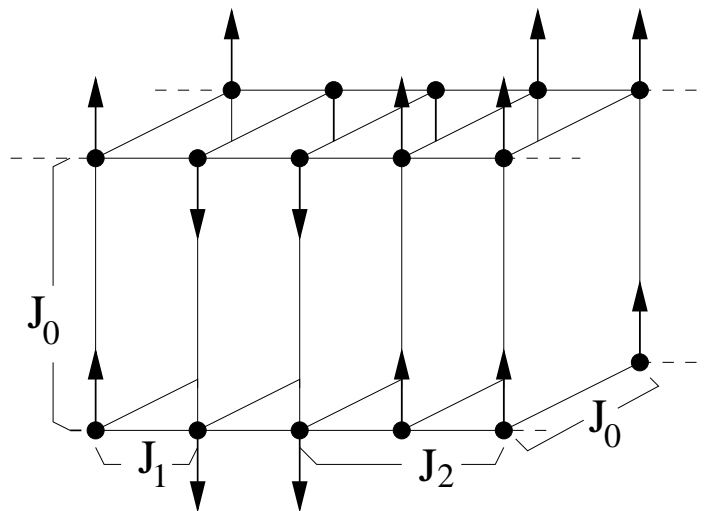


Figure 1.2: Schematic representation of the ANNNI model. The ferromagnetic nearest-neighbour interaction J_1 favours a homogeneous arrangement of spins (all spins up or all down), while the antiferromagnetic exchange J_2 prefers the periodic arrangement of two spins up, two down and so on.

Indeed most of the work presented in this thesis is devoted to an investigation of how the multidegeneracy is removed by applications of different perturbations.

1.3 The ANNNI model at finite temperature.

In the case of the ANNNI model, the multidegeneracy encountered at $T = 0$ is removed at finite temperature by entropic contributions to the free energy. This is clearly visible in the phase diagram of Fig. 1.3 where the notation $\langle n_1 n_2 \dots n_m \rangle$ is used to denote a state consisting of domains of parallel planes with alternate orientation whose widths repeat periodically the sequence $\{n_1, n_2, \dots, n_m\}$. It is important to point out that strictly speaking, this notation should be used only at zero temperature, where the domain walls, which separate bands of planes pointing in opposite directions are perfectly flat. Nevertheless, at temperatures below the roughening temperature [4], T_R , the walls will be statistically smooth, and the notation introduced above can still be used.

The first systematic study of the phase diagram of the ANNNI model at finite temperature was carried out by Fisher and Selke in 1980 [6]. By using a low-temperature analysis, these authors showed that an infinite sequence of phases,

$$\langle 2 \ 3 \rangle, \langle 2 \ 2 \ 3 \rangle, \langle 2 \ 2 \ 2 \ 3 \rangle, \dots \quad (1.2)$$

springs out from the multiphase point. This result was later corrected by Bak and Von Boehm and Selke and Duxbury [7, 8] who used mean-field analysis techniques to prove that, at finite temperature, long-period states appear between the phases of the Fisher-Selke sequence (1.2).

A major step in the direction of understanding modulated structures is represented by the work of

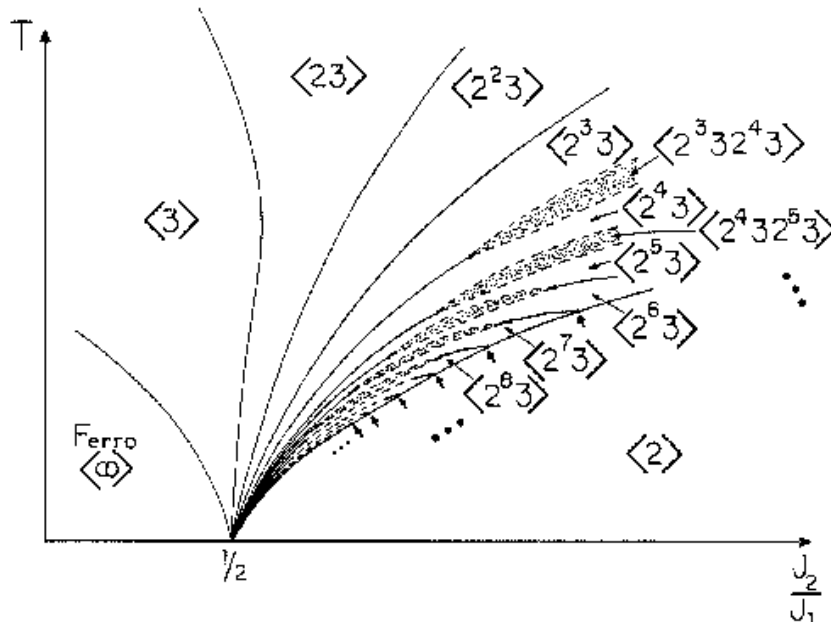


Figure 1.3: Schematic representation of the finite-temperature phase diagram of the ANNNI model (after [5]). At the point $(T = 0, J_2/J_1 = 1/2)$ all the phases appearing in the figure become degenerate (for a more detailed discussion see Chapter 5). The notation n_1^x is used as shorthand to refer to $x + 1$ successive domain walls with the same separation, n_1 .

Villain and Gordon [9]. These authors suggested that the mechanism responsible for the appearance of modulated states was an effective interaction between pairs of neighbouring walls. Villain and Gordon showed that, for the ANNNI model at finite temperature, this effective interaction was due to thermal excitations of domain walls which caused the latter to occasionally be in contact (see Fig. 1.4).

The intuition of Villain and Gordon was later perfected by Fisher and Szpilka [10] who turned it into a rigorous and powerful tool for the analysis of modulated phases. Their technique, which is known as the wall-wall interaction formalism, differs from the original method of Villain and Gordon by the inclusion of three- and higher-order wall interactions.

Since it was introduced in 1987, the wall-wall interaction formalism has become an indispensable tool for analyzing models where modulated structures appear. It is used extensively in this thesis to examine the series of phases which originate from the splitting of multiphase points. Therefore in the next section we shall present a qualitative overview of the Fisher-Szpilka technique and discuss the different models to which we have applied it.

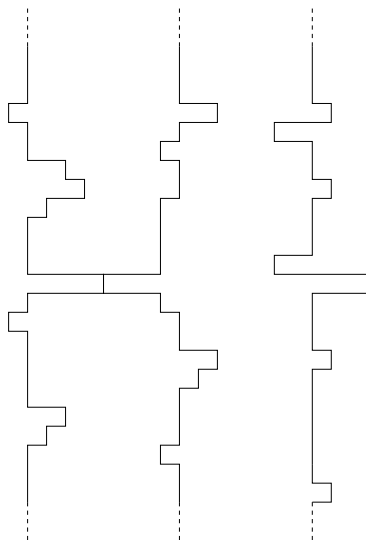


Figure 1.4: Schematic illustration of a contact interaction induced by thermal excitations of two neighbouring domain walls.

1.4 Domain-wall interactions

To illustrate the wall-wall interaction formalism we follow Fisher and Szpilka and write the free energy of a phase with N_w domain walls with separation $\{n_1, n_2, \dots, n_{N_w-1}\}$ as

$$E = E_0 + N_w E_w + \sum_i V_2(n_i) + \sum_i V_3(n_i, n_{i+1}) + \sum_i V_4(n_i, n_{i+1}, n_{i+2}) + \dots, \quad (1.3)$$

where E_0 is the free energy of the system when no walls are present, E_w is the creation energy of a domain wall, and $V_m(x_1, x_2, \dots, x_{m-1})$ is the interaction energy of m walls with separation x_1, x_2, \dots, x_{m-1} . The question is to determine the sequence of wall spacings that minimizes the expression (1.3).

Since the effective interactions between the walls are mediated by the short range spin interactions, J_1 and J_2 , the V 's will typically decay exponentially as a function of the wall separation. For this reason, the dominant term in expression (1.3) is usually the one proportional to E_w .

Indeed, when the wall-wall interaction contribution to (1.3) can be neglected, the lowest energy phases can be established by simply looking at the sign of E_w . If E_w is positive then the stable phase is the homogeneous one (no walls) while, if it is negative, the favoured configuration is the one with the largest density of domain walls, i.e. $\uparrow\uparrow\downarrow\downarrow \dots$.

However, near the multiphase point, E_w is approximately equal to 0 and, therefore, the contribution of the V_m 's to the energy cannot be neglected. Fisher and Szpilka have shown that, in these circumstances, the detailed structure of the phase diagram can be established by considering in turn the effect of V_2 , V_3 and so on.

Details of the method are explained in Chapter 5 where we apply the wall-wall interaction

formalism to study the modulated structures arising in a generalized quantum version of the ANNNI model. The aim of this work is to analyse how robust the multidegeneracy is against a novel type of perturbation, quantum fluctuations. These appear to split the multidegeneracy in a way similar to thermal fluctuations. However, the sequence of phases springing out from the multiphase point in the quantum and thermal case are dramatically different.

Although the energy expansion scheme of Fisher and Szpilka was originally introduced for treating interacting domain walls in magnetic systems, it can be applied to study other types of binary modulated structures, where segments of two distinct phases are separated by domain walls (or, more generally, defects).

An example of the flexibility of the method is given in Chapter 6 where we study the phase diagram of the Falicov-Kimball model. This is a model for interacting ions and electrons on a one-dimensional lattice in the limit of zero ion mobility. In this case the effective ion-ion interaction replaces the wall-wall interactions. By using a perturbative technique the general ion-ion interactions are calculated in the limit of strong ion-electron coupling. The recursive study of the phase diagram reveals that the ion density has a behaviour characteristic of a devils staircase, as conjectured by Barma and Subrahmanyam [11].

The defect-defect interaction scheme can also be naturally extended to more complicated cases, as shown by Bassler, Sasaki and Griffiths [12]. We exploit this in Chapter 7 to explain the effect of another type of perturbation, the softening of discrete spins on a system with competing interactions. We consider a spin model with six-fold spin anisotropy and chiral interactions under the influence of a magnetic field. When the spin anisotropy is infinite, the phase diagram exhibits points where two multiphase lines meet at a first order transition, as sketched in Fig. 1.5a. As the spin anisotropy is reduced from infinity, an infinite sequence of phases springs out from each of the multiphase lines. Near the point P (see Fig. 1.5b) the two sequences interpenetrate, giving rise to a checkerboard structure of phases which include segments of all three coexisting states A , B and C . By constructing the phase diagram iteratively, we show that the checkerboard has a self-similar, fractal structure.

1.5 Removal of multidegeneracy in models with a surface

We now turn to consider the effect of multidegeneracy which arises from a competition between surface and bulk effects rather than a competition between different interactions. This can be observed in models of finite and semi-infinite chains of spins where the competition occurs because surface and bulk effects tend to stabilize different spin configurations. Below the roughening transition temperature [4], T_R , a statistically flat interface (kink) will separate the bulk and surface phases. In this case the interesting question regards the determination of the stable positions of the interface as the temperature or other parameters are varied. In particular it is important to establish whether the kink is always localised near the surface or if it can depin from it [13, 14].

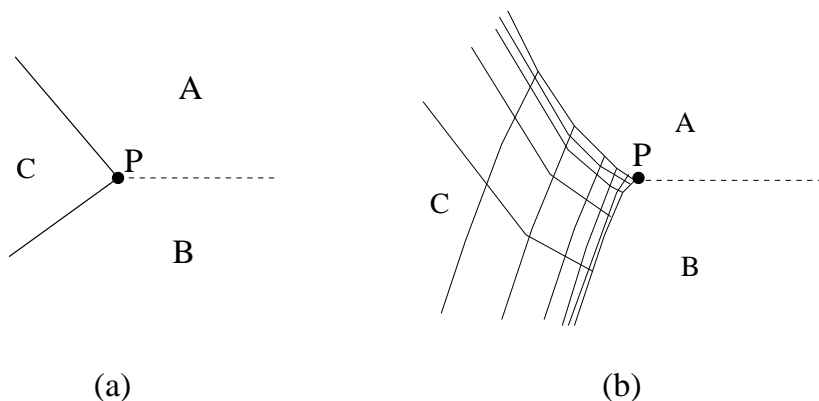


Figure 1.5: (a) Two multiphase lines, AC and CB meet at a first order-transition (dashed line) in P . (b) When the multidegeneracy is removed a checkerboard of phases with ternary modulation can appear near the point P .

This type of problem is probably best illustrated with the aid of an example. To this purpose we follow Duxbury and Yeomans in considering a model which consists of a system of Ising spins occupying the sites of a three-dimensional cubic lattice [15]. The lattice is chosen to be infinitely extended in two dimensions and with free surfaces in the third, as shown in Fig. 1.6. An interface is imposed on the system by applying two infinite opposite fields at the surfaces so that the Hamiltonian for the system is

$$\mathcal{H} = -J \sum_{i\langle j,j'\rangle} S_{i,j} S_{i',j'} - h \sum_{i,j} S_{i,j} - H_S \sum_j (S_{0,j} - S_{L,j}), \quad (1.4)$$

where i labels the planes in the lattice ($0 \leq i \leq L$) and j the sites within the planes, J is the exchange interaction between neighbouring spins, h is the bulk field and H_S the surface field (assumed to tend to infinity). Also, with $\langle j, j' \rangle$ we have indicated a sum over pairs of nearest neighbours in the same plane.

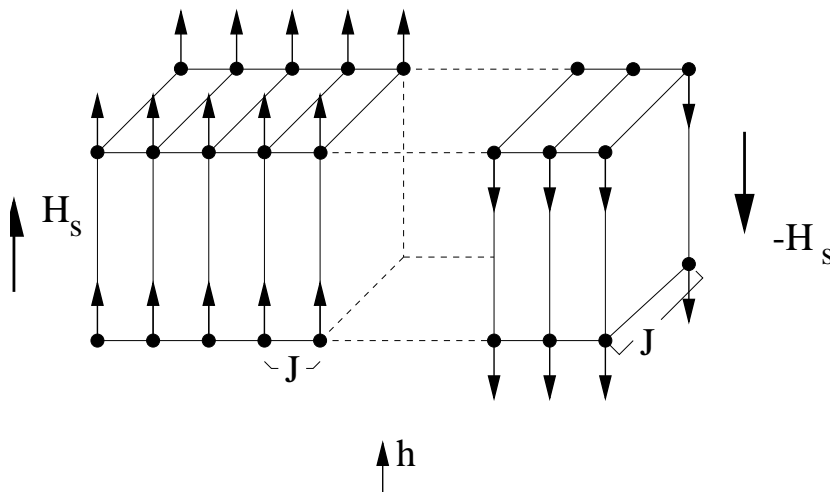


Figure 1.6: Schematic representation of a three-dimensional Ising model with imposed surface fields.

We first consider the behaviour of the interface at $T = 0$. If the bulk field, h , is positive [negative] the interface is pinned to the right [left] surface. Indicating by $\langle k \rangle$ the ground state where the flat interface lies between planes k and $k + 1$, we can write its energy (modulo an irrelevant energy shift) as

$$E_{\langle k \rangle} = Ahk , \quad (1.5)$$

where A is a positive number. When $h = 0$ a multidegeneracy is encountered, since all the $E_{\langle k \rangle}$'s are equal to zero. By analogy with the ANNNI case, it seems reasonable to expect that thermal excitations of the interface can introduce an effective coupling between the surface and the interface,

$$E_{\langle k \rangle} = Ahk + V(k) . \quad (1.6)$$

Indeed, the low-temperature analysis of Duxbury and Yeomans showed that, for $T > 0$, the effective surface-kink potential, $V(k)$ is non-zero. Hence the interface multidegeneracy is removed by thermal fluctuations. More precisely, since $V(k)$ is repulsive, one has that, as h changes from positive to negative, the interface depins from the left surface through a series of layering transitions, where the position of the kink increases discontinuously [15].

Of particular interest to us are the cases where the interface multidegeneracy is removed at zero temperature. This possibility was first pointed out by de Oliveira and Griffiths who considered a pseudo-spin model with a long-range attractive surface potential [16]. They showed that this type of interactions gives rise to a series of layering transitions even at zero temperature. This is intuitively plausible since long-range interactions can be expected to introduce a coupling between the surface and the kink, no matter what their separation is.

It is interesting that quantum fluctuations can have an analogous effect. This is discussed in detail in Chapter 2, where we consider a quantum generalization of the Duxbury-Yeomans model. The depinning of interfaces induced by quantum fluctuations is also addressed in Chapter 3, where we study the behaviour of a kink in the three-dimensional transverse Ising model.

Finally, working by analogy with the mechanisms that remove the multidegeneracy in infinite systems, we also consider the possibility of raising the interface multidegeneracy by allowing spin softening. In Chapter 2 we analyse the behaviour of an interface in chains of XY spins with p -fold spin anisotropy and with ferromagnetic interactions. By calculating the effective surface-kink coupling induced by the softening of the spins, we show that a series of layering transitions is stabilized.

In Chapter 4 we show that a similar mechanism is responsible for the appearance of several surface-induced phase transitions in a model of an antiferromagnet with two-fold spin anisotropy in a magnetic field. In particular, numerical and analytical calculations reveal that, in semi-infinite and finite chains of even length, there is a sequence of layering transitions in the bulk that has not

been previously identified. This clarifies the mechanism for the crossover between the surface and the bulk spin-flop states. The relevance of these results for Fe/Cr multilayers is discussed.

The work presented in this thesis forms the basis of the following publications

- C. Micheletti and J. M. Yeomans, **The role of spin anisotropy in the unbinding of interfaces**, *Europhys. Lett.* **28**, 465 (1994)
- A.B. Harris, C. Micheletti and J. M. Yeomans, **Quantum fluctuations in the ANNNI model**, *Phys. Rev. Lett.* **74**, 3045 (1995)
- C. Micheletti, F. Seno and J. M. Yeomans, **Upsilon point in a spin model**, *Phys. Rev. B* **52**, 4353 (1995)
- A. B. Harris, C. Micheletti and J. M. Yeomans, **Lifting of multiphase degeneracy by quantum fluctuations**, *Phys. Rev. B* **52**, 6684 (1995)
- A. B. Harris, C. Micheletti and J. M. Yeomans, **Compete wetting in the three-dimensional transverse Ising model** *J. Stat. Phys.*, in press
- A. B. Harris, C. Micheletti and J. M. Yeomans, **A devil's staircase in the Falicov-Kimball model** preprint OUTP-96-22-S.
- C. Micheletti, R. B. Griffiths and J. M. Yeomans, **Surface spin-flop phases and bulk discommensurations in antiferromagnets** preprint OUTP-96-23-S

Chapter 2

Unbinding of interfaces mediated by spin softening

2.1 Introduction

There is a considerable body of literature discussing the way in which interfaces depin from surfaces [17]. Depending on the details of the macroscopic interactions and external parameters, such as the temperature or a magnetic field [18], the unbinding of the interface can occur through a first or second order transition or, on a lattice, via a sequence of first order transitions.

The latter possibility was first pointed out by De Oliveira and Griffiths[16] for a model in which the layering is driven by the competition between a long-range bulk interaction and a surface field. The presence of long range interactions stabilizes the layering transitions even at zero temperature. Later Duxbury and Yeomans[15] showed that, if the position of the interface relative to the surface was degenerate at zero temperature, the degeneracy could be split by thermal fluctuations giving an infinite series of layering transitions at finite temperatures. The stable interface position is determined as a balance between the binding effect of a bulk field and the entropic advantage for the interface lying further from the surface.

In this Chapter we aim to discuss the role of a hithertofore unexplored parameter on the unbinding transition: the spin anisotropy. We shall show that, as discrete spins with p -fold spin anisotropy soften, layering transitions can be stabilised in simple, short-range clock models, even at zero temperature (for $p \geq 3$). An expansion in inverse spin anisotropy allows us to prove that an infinite sequence of layering phase transitions exist. Moreover, because the interesting features occur at zero temperature it is possible to follow the phase diagram numerically for all values of the spin anisotropy. In particular, for $p \geq 3$, we are able to demonstrate how the boundaries between the different interface phases end in critical points and to pinpoint these with considerable precision [19].

Then we consider the special case $p = 2$, where the multidegeneracy cannot be lifted for small values of $1/D$. In this case we consider the quantum version of the model and show that quantum fluctuations can raise the multidegeneracy stabilizing an infinite sequence of layering transitions [20].

2.2 The model

We consider the classical XY model with p -fold spin anisotropy, D , in a magnetic field, H , at zero temperature. The model is defined by the Hamiltonian

$$\mathcal{H} = \sum_{i=1}^N \{ -J \cos(\theta_{i-1} - \theta_i) - H(\cos \theta_i - 1) - D(\cos p\theta_i - 1)/p^2 \} \quad (2.1)$$

where i labels the spins on a one-dimensional lattice and θ_i can take values between 0 and 2π . The model (2.1) is used in the theoretical description of rare-earth metals and compounds [21, 22, 23, 24, 25]. In fact, as the physical parameters J , H , D and p are varied, the corresponding ground states display a variety of periodic spin arrangements that closely resemble the uniaxial magnetic modulation observed, for example, in Ho and Er .

In order to study the behaviour of an interface in the system we need to create a kink in the chain. To do so we shall choose

$$\begin{aligned} \theta_0 &= 2\pi/p, \\ \theta_N &= 0, \end{aligned} \quad (2.2)$$

and let $N \rightarrow \infty$. If the interface lies between the spins at sites $n-1$ and n , so that

$$\theta_i < \pi/p \quad \text{for } i \leq n-1, \quad (2.3)$$

$$\theta_i > \pi/p \quad \text{for } i \geq n \quad (2.4)$$

the corresponding interface phase will be labelled $\langle n \rangle$, as shown in Fig. 2.1. We shall show *a posteriori* that this choice for the definition of different interface phases is appropriate also for finite values of D .

Finally we note that, although for simplicity we consider a one-dimensional Hamiltonian, the study applies to any space dimension with the ground states translationally invariant in the direction parallel to the boundary plane.

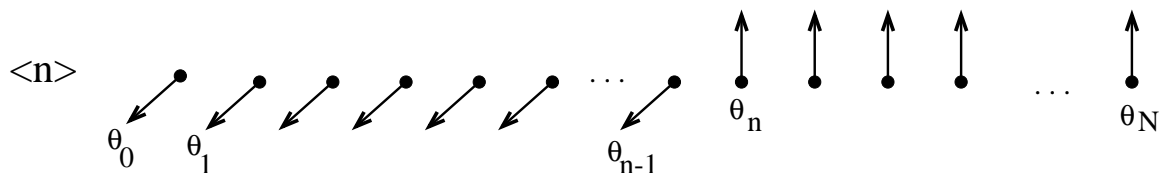


Figure 2.1: Schematic representation of phase $\langle n \rangle$ for $p = 3$ and $D = \infty$.

2.3 Qualitative remarks

For infinite D the Hamiltonian (2.1) describes a p -state clock model. For $H > 0$ the interface is bound to the surface in state $\langle 1 \rangle$ while, for $H < 0$, the ground state is $\langle \infty \rangle$. The point ($H = 0$, $D = \infty$) is a multiphase point where the interface has the same energy whatever its position on the lattice. It is known that such a degeneracy can be lifted by thermal fluctuations [15]. Here we will be interested in the raising of degeneracy operated by the anisotropy D . In fact, for $p \geq 3$, as the anisotropy is reduced from infinity it becomes energetically favourable for the spin angles, $\{\theta_i\}$, to relax from their clock positions, $\{\theta_i^0\}$'s, in a way that depends on the distance between the surface and the interface. Thus the softening of the spins introduces an effective coupling between the surface and the interface that can be expected to raise the multidegeneracy.

Depending on the sign of the effective coupling, the transition from phase $\langle 1 \rangle$ to $\langle \infty \rangle$ can occur either discontinuously or through a sequence of intermediate states, $\langle k \rangle$, in which k decreases monotonically with H . This sequence can be finite, so that there is a first-order transition from a state with $k = k_{\max}$ to $\langle \infty \rangle$, or it can be infinite. In general, one expects the first possibility when the effective interaction between the surface and the interface is attractive and the second when this effective interaction is repulsive. Our results indicate that reducing the anisotropy from ∞ , gives rise to the second possibility and that the sequence of layering transitions $\langle 1 \rangle, \langle 2 \rangle, \langle 3 \rangle \dots$ is an infinite one.

2.4 The inverse-anisotropy expansion

Since we are interested in studying how the degeneracy is lifted near the multiphase point, we will consider $1/D$ as a small parameter in our theory. As a consequence the spin deviations from the clock positions

$$\tilde{\theta}_i = \theta_i - \theta_i^0 \quad (2.5)$$

will be considered sufficiently small to expand the Hamiltonian (2.1) keeping only terms quadratic in the $\{\tilde{\theta}_i\}$'s

$$\mathcal{H} = \sum_{i=1}^{\infty} \left\{ -Jc_i - H(\cos \theta_i^0 - 1) + Jc_i \{ \tilde{\theta}_{i-1} - \tilde{\theta}_i + s_i/c_i \}^2 / 2 - Js_i^2 / 2c_i + H \cos \theta_i^0 \{ \tilde{\theta}_i + \tan \theta_i^0 \}^2 / 2 - H \sin^2 \theta_i^0 / 2 \cos \theta_i^0 + D \tilde{\theta}_i^2 / 2 \right\} \quad (2.6)$$

where

$$s_i = \sin(\theta_{i-1}^0 - \theta_i^0), \quad c_i = \cos(\theta_{i-1}^0 - \theta_i^0). \quad (2.7)$$

The equilibrium values of the $\tilde{\theta}_i$ are given by minimising the Hamiltonian (2.6). This leads to linear recursion equations

$$-Jc_i \{ \tilde{\theta}_{i-1} - \tilde{\theta}_i + s_i/c_i \} + Jc_{i+1} \{ \tilde{\theta}_i - \tilde{\theta}_{i+1} + s_{i+1}/c_{i+1} \} + H \cos \theta_i^0 (\tilde{\theta}_i + \tan \theta_i^0) + D \tilde{\theta}_i = 0. \quad (2.8)$$

If the full Hamiltonian (2.1) is used non-linearities appear in the recursion relations (2.8). However, these do not affect the leading order terms needed for the subsequent calculations.

The best strategy to find the leading order angle deviations $\tilde{\theta}_i$ for phase $\langle n \rangle$ is to start by calculating $\tilde{\theta}_n$ and $\tilde{\theta}_{n-1}$ to leading order in $1/D$ using (2.8),

$$\begin{aligned}\tilde{\theta}_n &= (J/D) \sin(2\pi/p) + \mathcal{O}(1/D^2) \\ \tilde{\theta}_{n-1} &= -J/D \sin(2\pi/p) + \mathcal{O}(H/D, 1/D^2).\end{aligned}\tag{2.9}$$

The deviations of the remaining spins on the left [right] side of the interface can then be found using (2.9) and solving iteratively (2.8) for decreasing [or increasing] values of i , thus obtaining

$$\begin{aligned}& \vdots \\ \tilde{\theta}_{n+2} &= (J/D)^3 \sin(2\pi/p) + \mathcal{O}(1/D^4) \\ \tilde{\theta}_{n+1} &= (J/D)^2 \sin(2\pi/p) + \mathcal{O}(1/D^3) \\ \tilde{\theta}_n &= (J/D) \sin(2\pi/p) + \mathcal{O}(1/D^2) \\ & \vdots \\ \tilde{\theta}_{n-1} &= -J/D \sin(2\pi/p) + \mathcal{O}(H/D, 1/D^2) \\ \tilde{\theta}_{n-2} &= -(J/D)^2 \sin(2\pi/p) + \mathcal{O}(H/D, 1/D^3) \\ & \vdots \\ \tilde{\theta}_1 &= -(J/D)^{n-1} \sin(2\pi/p) + \mathcal{O}(H/D, 1/D^n).\end{aligned}\tag{2.10}$$

The final result for the interface phase boundaries derived below will demonstrate that it is consistent to neglect terms $\mathcal{O}(H/D)$ in (2.10). Note that for $p = 2$, for D large, the $\{\tilde{\theta}_i\}$'s are all zero, suggesting that the spins do not lower their energy by canting. This will be proven in section 2.7. Meanwhile we will implicitly restrict ourselves to the case $p \geq 3$.

2.5 Calculation of $E_{\langle n \rangle} - E_{\langle n+1 \rangle}$

In this section we shall use the harmonic approximation (2.6) to calculate the energy differences, $E_{\langle n \rangle} - E_{\langle n-1 \rangle}$, between neighbouring interface states. For simplicity we will evaluate the energy difference for a chain of finite length, N , and take the limit $N \rightarrow \infty$ at the end of the calculations.

Let $\langle n-1 \rangle$ have spins $\{\alpha_i\}$ with α_1 the surface spin and $\langle n \rangle$ have spins $\{\beta_i\}$ with β_0 the surface spin. Then in both cases the interface lies between $i = n-1$ and $i = n$ and $\alpha_i^0 \equiv \beta_i^0$, as shown below.

With this choice of labelling we have

$$E_n - E_{n-1} = -H \left[\cos(2\pi/p) - 1 \right]$$

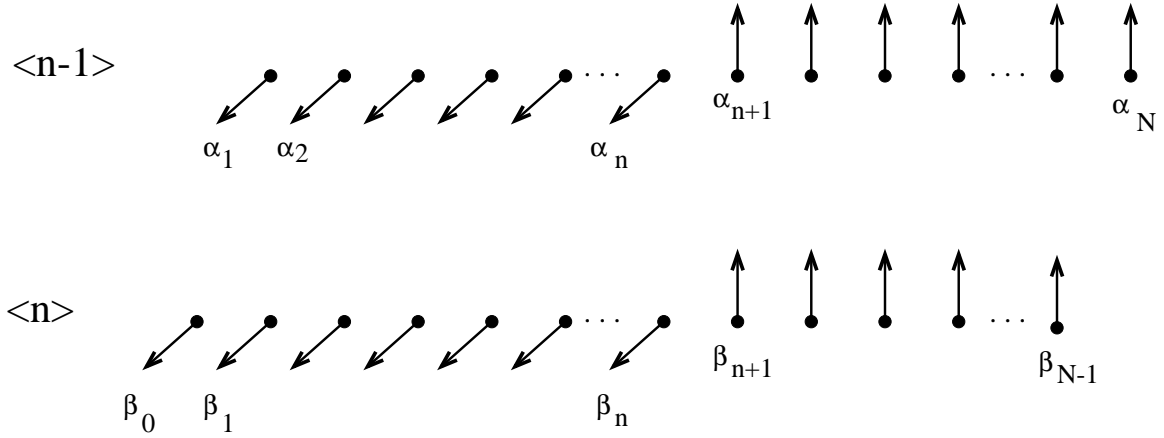


Figure 2.2: Schematic illustration of the labelling chosen for phases $\langle n-1 \rangle$ and $\langle n \rangle$.

$$\begin{aligned}
& + \sum_{i=2}^{N-1} \frac{1}{2} J c_i \left\{ [(\tilde{\beta}_{i-1} - \tilde{\beta}_i) + \frac{s_i}{c_i}]^2 - [(\tilde{\alpha}_{i-1} - \tilde{\alpha}_i) + \frac{s_i}{c_i}]^2 \right\} \\
& + \sum_{i=1}^{N-1} \frac{1}{2} H \cos \beta_i^0 [(\tilde{\beta}_i + \tan \beta_i^0)^2 - (\tilde{\alpha}_i + \tan \alpha_i^0)^2] + \frac{1}{2} \sum_{i=1}^{N-1} D(\tilde{\beta}_i^2 - \tilde{\alpha}_i^2) \\
& + \frac{1}{2} J \tilde{\beta}_1^2 - \frac{1}{2} J \tilde{\alpha}_{N-1}^2
\end{aligned} \tag{2.11}$$

where, according to our choice of boundary conditions (2.2), $\tilde{\alpha}_1$, $\tilde{\alpha}_N$, $\tilde{\beta}_0$ and $\tilde{\beta}_{N-1}$ must be set equal to zero.

The expression for $E_n - E_{n-1}$, (2.11) can be simplified considerably using the linearised recursion equations (2.8). To this purpose it is convenient to define the quantity

$$A = \sum_{i=2}^{N-1} \frac{1}{2} J c_i \left\{ [(\tilde{\beta}_{i-1} - \tilde{\beta}_i) + \frac{s_i}{c_i}]^2 - [(\tilde{\alpha}_{i-1} - \tilde{\alpha}_i) + \frac{s_i}{c_i}]^2 \right\} \tag{2.12}$$

and rewrite it in the form

$$\begin{aligned}
A & = \sum_{i=2}^{N-1} \frac{1}{2} J c_i (\tilde{\beta}_{i-1} - \tilde{\beta}_i + \tilde{\alpha}_{i-1} - \tilde{\alpha}_i + 2 \frac{s_i}{c_i}) \left[(\tilde{\beta}_{i-1} - \tilde{\alpha}_{i-1}) - (\tilde{\beta}_i - \tilde{\alpha}_i) \right] \\
& = \sum_{i=2}^{N-2} \left[-\frac{1}{2} J c_i (\tilde{\beta}_{i-1} - \tilde{\beta}_i + \tilde{\alpha}_{i-1} - \tilde{\alpha}_i + 2 \frac{s_i}{c_i}) \right. \\
& \quad \left. + \frac{1}{2} J c_{i+1} (\tilde{\beta}_i - \tilde{\beta}_{i+1} + \tilde{\alpha}_i - \tilde{\alpha}_{i+1} + 2 \frac{s_{i+1}}{c_{i+1}}) \right] (\tilde{\beta}_i - \tilde{\alpha}_i) \\
& \quad + \frac{1}{2} J c_2 (\tilde{\beta}_1 - \tilde{\beta}_2 + \tilde{\alpha}_1 - \tilde{\alpha}_2 + 2 \frac{s_2}{c_2}) (\tilde{\beta}_1 - \tilde{\alpha}_1) \\
& \quad - \frac{1}{2} J c_{N-1} (\tilde{\beta}_{N-2} - \tilde{\beta}_{N-1} + \tilde{\alpha}_{N-2} - \tilde{\alpha}_{N-1} + 2 \frac{s_{N-1}}{c_{N-1}}) (\tilde{\beta}_{N-1} - \tilde{\alpha}_{N-1}).
\end{aligned} \tag{2.13}$$

Substituting (2.13) back into (2.11) and using the recursion equations (2.8) the energy difference simplifies to

$$\begin{aligned}
E_n - E_{n-1} &= -H \left[\cos(2\pi/p) - 1 \right] + \frac{1}{2} J \tilde{\beta}_1^2 + \frac{1}{2} H \cos \beta_1^0 (\tilde{\beta}_1 + \tan \beta_1^0)^2 \\
&+ \frac{1}{2} D \tilde{\beta}_1^2 + \frac{1}{2} J c_2 (\tilde{\beta}_1 - \tilde{\beta}_2 + \tilde{\alpha}_1 - \tilde{\alpha}_2 + 2 \frac{s_2}{c_2}) (\tilde{\beta}_1 - \tilde{\alpha}_1) \\
&- \frac{1}{2} J \tilde{\alpha}_{N-1}^2 - \frac{1}{2} H \cos \alpha_{N-1}^0 (\tilde{\alpha}_{N-1} - \tan \alpha_{N-1}^0)^2 - \frac{1}{2} D \tilde{\alpha}_{N-1}^2 \\
&\frac{1}{2} J c_{N-1} (\tilde{\beta}_{N-2} - \tilde{\beta}_{N-1} + \tilde{\alpha}_{N-2} - \tilde{\alpha}_{N-1} + 2 \frac{s_{N-1}}{c_{N-1}}) (\tilde{\beta}_{N-1} - \tilde{\alpha}_{N-1})
\end{aligned} \tag{2.14}$$

where we set $\tilde{\alpha}_1 = \tilde{\alpha}_N = \tilde{\beta}_0 = \tilde{\beta}_{N-1} = 0$. Then, taking the limit $N \rightarrow \infty$, one has

$$\begin{aligned}
E_{\langle n \rangle} - E_{\langle n-1 \rangle} &= -H \{ \cos(2\pi/p) - 1 \} + H \tilde{\beta}_1 \sin \beta_1^0 / 2 - J \tilde{\beta}_1 \tilde{\alpha}_2 / 2 & n \geq 3 \\
E_{\langle 2 \rangle} - E_{\langle 1 \rangle} &= -H \{ \cos(2\pi/p) - 1 \} + H \tilde{\beta}_1 \sin \beta_1^0 / 2 \\
&\quad - J \cos(2\pi/p) \tilde{\beta}_1 \tilde{\alpha}_2 / 2 + J \sin(2\pi/p) \tilde{\beta}_1 / 2 .
\end{aligned} \tag{2.15}$$

The formulae (2.15) are exact for the quadratic Hamiltonian (2.6). Higher order terms in the full Hamiltonian (2.1) appear as higher order corrections.

Substituting in the values for the surface spins from (2.10) gives, for $n \geq 2$,

$$E_{\langle n \rangle} - E_{\langle n-1 \rangle} = -H(\cos(2\pi/p) - 1) - J^{2n-2} \sin^2(2\pi/p) / (2D^{2n-3}) + \mathcal{O}(1/D^{2n-2}) \tag{2.16}$$

It follows immediately from (2.16) that the boundary between phases $\langle n-1 \rangle$ and $\langle n \rangle$ is given, to leading order, by

$$H_{\langle n-1 \rangle : \langle n \rangle} = J^{2n-2} \sin^2(2\pi/p) \{ 2(1 - \cos(2\pi/p)) D^{2n-3} \}^{-1} \tag{2.17}$$

indicating that the unbinding proceeds via an infinite series of phases $\langle n \rangle$ of widths $\mathcal{O}(1/D^{2n-3})$. Although these conclusions are rigorously based on the leading order calculation of $E_{\langle n \rangle} - E_{\langle n-1 \rangle}$ it must be noticed that neglected higher-order interactions could dominate for large values of n , and therefore they could qualitatively change the phase diagram. However, we notice that in Hamiltonian (2.1) we do not have any competing interactions that could make $E_{\langle n \rangle} - E_{\langle n-1 \rangle}$ oscillatory as a function of n . Therefore, since for large n we do not expect the sign of $E_{\langle n \rangle} - E_{\langle n-1 \rangle}$ to change, it is unlikely that higher-order terms in (2.17) can introduce qualitative modifications in the phase diagram.

2.6 The phase diagram

These results were confirmed numerically for the case $p = 3$ by iteratively studying the equations (2.1) which minimize the energy. The numerical approach allowed us to obtain the interface phase diagram for all values of D which is shown in Fig. 2.3.

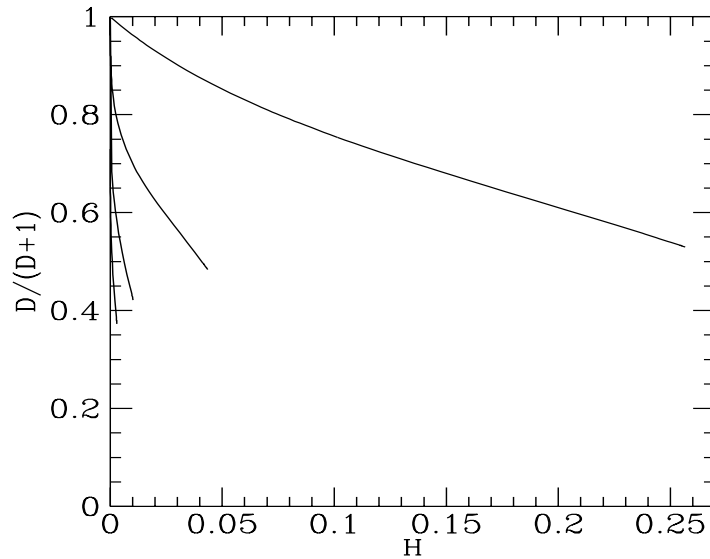


Figure 2.3: Phase diagram of the classical X-Y model in a magnetic field, H , with three-fold spin anisotropy, D , and an imposed interface. There are an infinite number of interface layering transitions. The first order boundaries between them terminate in critical points.

The first order boundaries between the different interface phases end at a series of critical points at

$$\langle 1 \rangle : \langle 2 \rangle \quad D_{1,2}^* = 1.1268 \pm 0.0003 \quad H_{1,2}^* = 0.2566 \pm 0.0009 \quad (2.18)$$

$$\langle 2 \rangle : \langle 3 \rangle \quad D_{2,3}^* = 0.9360 \pm 0.0003 \quad H_{2,3}^* = 0.04357 \pm 0.00001 \quad (2.19)$$

$$\langle 3 \rangle : \langle 4 \rangle \quad D_{3,4}^* = 0.7281 \pm 0.0005 \quad H_{3,4}^* = 0.01029 \pm 0.00004 \quad (2.20)$$

$$\langle 4 \rangle : \langle 5 \rangle \quad D_{4,5}^* = 0.5931 \pm 0.0003 \quad H_{4,5}^* = 0.00295 \pm 0.00002 \quad (2.21)$$

\vdots

These were identified as the points where both the energy E and its partial derivative with respect to H become the same in the two phases, as shown in Fig. 2.4.

Assuming that $D_{n,n+1}^*$ and $H_{n,n+1}^*$ have a power law dependence on n , extrapolation to $n \rightarrow \infty$ shows that $(D_\infty^*, H_\infty^*) = (0, 0)$ is consistent with the data. However, due to finite numerical accuracy, it was only possible to obtain results for $n \leq 5$, and so we cannot be confident that this is the true asymptotic behaviour.

The mechanism for the occurrence of the end-points can be understood by considering the softening of the interface spins. From equation (2.10) it is clear that, as D is lowered, the spins move to close the gap at the interface, $\tilde{\beta}_n - \tilde{\beta}_{n+1}$ and $\tilde{\alpha}_n - \tilde{\alpha}_{n+1}$. As we move along the $\langle n \rangle | \langle n-1 \rangle$ phase boundary for decreasing values values of D , the interface angles α_{n+1} and β_n will move in opposite

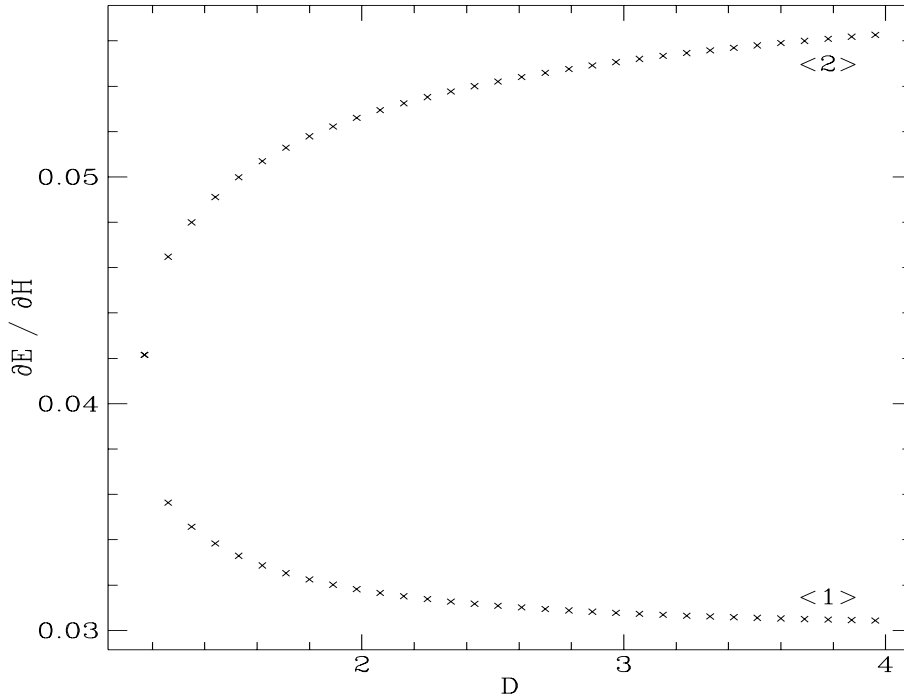


Figure 2.4: Plot of the derivative $\partial E/\partial H$ for phases $\langle 1 \rangle$ and $\langle 2 \rangle$ along the $\langle 1 \rangle : \langle 2 \rangle$ boundary for $p = 3$.

directions as shown in the example of Fig. 2.5.

When the critical point is reached, the angles α_{n+1} and β_n have the same value and, consequently the two chains $\{\alpha_i\}$ and $\{\beta_i\}$ become identical. The critical value for α_{n+1} (or equivalently β_n) for which the end point is attained is π/p . This justifies, *a posteriori* our definition of the interface phases given in (2.4).

Finally, we conclude the description of the phase diagram noting that, for $D = 0$ the interface shape varies continuously from being a domain wall at the surface for H large to a uniform spiral for $H = 0$.

2.7 Persistence of degeneracy for $p = 2$

In the rest of this Chapter we will consider the model (2.1) for $p = 2$. As previously observed, this is a special case, since equation (2.10) shows that the leading order expressions for the $\{\tilde{\theta}_i\}$'s vanish. As we show this result is not approximate but is exactly true if D is sufficiently large.

To see this consider the full recursion equations for $p = 2$

$$\begin{aligned} \frac{\partial \mathcal{H}}{\partial \theta_i} &= Jc_i \sin(\tilde{\theta}_i - \tilde{\theta}_{i-1}) + Jc_{i+1} \sin(\tilde{\theta}_i - \tilde{\theta}_{i+1}) \\ &= Hc_i^0 \sin \tilde{\theta}_i + \frac{D}{2} \sin 2\tilde{\theta}_i = 0 . \end{aligned} \quad (2.22)$$

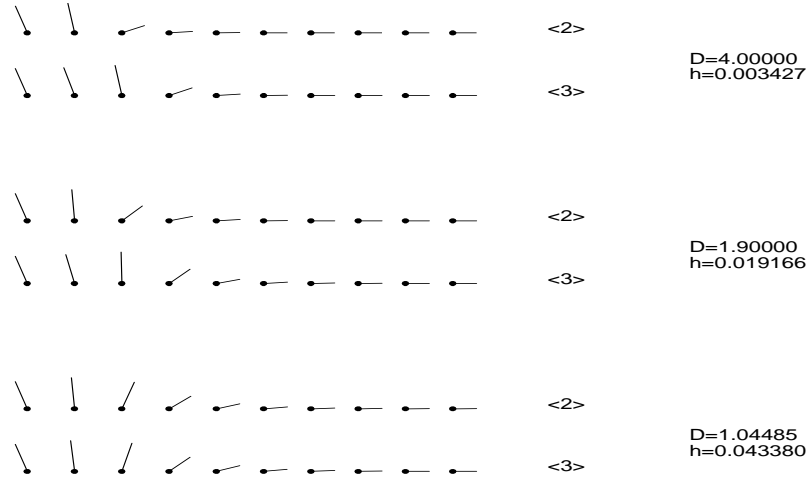


Figure 2.5: Configurations of the first 10 spins for phases $\langle 2 \rangle$, $\langle 3 \rangle$ along the $\langle 2 \rangle : \langle 3 \rangle$ boundary for $p = 3$ (the surface spins are the left-most ones). As the critical point ($H_{2,3}^* = 0.04357, D_{2,3}^* = 0.9360$) is approached, the third spin from the surface tends to the value $\pi/3$ for both chains.

For very large D , equation (2.22) shows that $\tilde{\theta}_i$ must be at least of order $1/D$. Now suppose that the $\tilde{\theta}_i$'s are not all identically zero. Then consider the spin deviation $\tilde{\theta}_k$ of maximum modulus

$$|\tilde{\theta}_k| = \max_i \{|\tilde{\theta}_i|\} . \quad (2.23)$$

For simplicity we assume that there is only one value of k satisfying (2.23), but this is not essential for the following discussion. The recursion equations $\partial\mathcal{H}/\partial\theta_k = 0$ give

$$(D + Hc_k^0) \sin \tilde{\theta}_k \cos \tilde{\theta}_k + Jc_k \sin(\tilde{\theta}_k - \tilde{\theta}_{k-1}) + Jc_{k+1} \sin(\tilde{\theta}_k - \tilde{\theta}_{k+1}) = 0 . \quad (2.24)$$

The last two terms of (2.24) are, at most, of order $J \sin(2\tilde{\theta}_k)$, while the first one is of order $D \sin(\tilde{\theta}_k)$. When D is sufficiently large the recursion equation (2.24) cannot be satisfied if $\tilde{\theta}_k \neq 0$ since the term $D \sin \tilde{\theta}_k \cos \tilde{\theta}_k$ can never be cancelled out by the contribution of the other two (remember that the $\tilde{\theta}_i$ are $\mathcal{O}(1/D)$). Therefore, for large D , the spin deviations must be exactly zero.

Since, for large D , the spins remain locked in their Ising positions, it implies that, for $H = 0$, the multidegeneracy for $D = \infty$ persists for finite values of D .

In the next section we will study how quantum fluctuations affect this multidegeneracy. We show that, for $p = 2$, zero-temperature quantum fluctuations are strong enough to modify the phase diagram by raising the multidegeneracy.

2.8 Quantum fluctuations

We consider the quantum mechanical version of the model (2.1) for spins with two-fold anisotropy,

$$\mathcal{H} = -\frac{J}{S^2} \sum_{i=0}^{N-1} \vec{S}_i \cdot \vec{S}_{i+1} + \frac{H}{S} \sum_{i=0}^N S_i^z - \frac{D}{S^2} \sum_{i=1}^N (S_i^z)^2 - \frac{K}{S} (S_i^z - S_N^z) \quad (2.25)$$

where \vec{S}_i is a quantum mechanical spin of modulus S at site i and, K is thought to tend to ∞ in order to enforce the appropriate boundary conditions, cf. relations (2.2), on the chain.

We will consider the case $S \gg 1$. In the limit $S \rightarrow \infty$ we expect to recover the results for the classical $p = 2$ case. As for the classical case, we are interested in determining the qualitative features of the phase diagram near the multiphase point, ($D = \infty, H = 0$). Therefore, $1/D$ will be treated as a small parameter.

For $D = \infty$ the spins will be locked in the Ising positions $S_i^z = \sigma_i S$, where $\sigma_i = \pm 1$. To study the effect of quantum fluctuation for small $1/D$ we introduce the Dyson-Maleev transformation [26, 27].

$$\begin{aligned} S_i^z &= \sigma_i (S - a_i^\dagger a_i), \\ S_i^+ &= \sqrt{2S} \left(\delta_{\sigma_i, 1} \left[1 - \frac{a_i^\dagger a_i}{2S} \right] a_i + \delta_{\sigma_i, -1} a_i^\dagger \left[1 - \frac{a_i^\dagger a_i}{2S} \right] \right), \\ S_i^- &= \sqrt{2S} \left(\delta_{\sigma_i, 1} a_i^\dagger + \delta_{\sigma_i, -1} a_i \right), \end{aligned} \quad (2.26)$$

where a_i^\dagger and a_i are bosonic operators that create/destroy a spin excitation at site i and $S_i^\pm = S_i^x \pm iS_i^y$. The Dyson-Maleev transformation, which is often regarded as a truncated Holstein-Primakov transformation [28, 29, 30], preserves the canonical commutation relations between S^z , S^+ and S^- . The advantage of using (2.26) is that, when the Hamiltonian (2.25) is recasted in bosonic form, only terms involving at most four bosonic operators (a^\dagger and a) appear, while the Holstein-Primakov transformation involves an infinite expansion in terms of a^\dagger and a . The Holstein-Primakov transformation is accompanied by the additional requirement that the number of spin deviations at any site cannot exceed $2S$, (so that $-S \leq S_i^z \leq +S$). This physical requirement is not enforced by the Dyson-Maleev transformation, where the bosonic occupation numbers, $a_i^\dagger a_i$, can be arbitrary large. This has the consequence of introducing some spurious eigenvalues in the eigenspectrum of \mathcal{H} . However, Dyson has shown that these spurious eigenvalues are separated by a gap of order T_N (T_N being the Néel temperature for the system) from the physical band of eigenvalues [26]. Hence, for temperatures not too close to T_N , the Dyson-Maleev transformation allows an almost exact treatment of spin models. However, as we shall point out later, we will eliminate rigorously the effect of spurious states by using standard Schrödinger-Rayleigh perturbation theory.

When recasting (2.25) in bosonic operator form, it is important to notice that the product $\vec{S}_i \cdot \vec{S}_{i+1}$ will take different forms for $\sigma_i = \sigma_{i+1}$ or $\sigma_i = -\sigma_{i+1}$. If $\sigma_i = \sigma_{i+1}$

$$\frac{-J \vec{S}_i \cdot \vec{S}_{i+1}}{S^2} = -J + \frac{J}{S} (a_i^+ - a_{i+1}^+) (a_i - a_{i+1}); \quad (2.27)$$

whereas if $\sigma_i = -\sigma_{i+1}$

$$-\frac{J\vec{S}_i \cdot \vec{S}_{i+1}}{S^2} = J - \frac{J}{S}(a_i^+ + a_{i+1})(a_i + a_{i+1}^+) + \frac{J}{S}, \quad (2.28)$$

where the last term comes from normally ordering the boson operators. Likewise the magnetic field term becomes

$$\frac{HS_z(i)}{S} = H - \frac{a_i^+ a_i}{S} \quad (2.29)$$

for $\sigma_i = 1$ and

$$\frac{HS_z(i)}{S} = -H + \frac{a_i^+ a_i}{S} \quad (2.30)$$

for $\sigma_i = -1$. The anisotropy energy becomes

$$\frac{-DS_z(i)^2}{S^2} = -D + \frac{2D}{S} \sum_i a_i^+ a_i - \frac{D}{S^2} \sum_i a_i^+ a_i a_i^+ a_i. \quad (2.31)$$

Now we can discuss how quantum fluctuations break the degeneracy with respect to the wall position which exists classically when $h = 0$. We will denote with $|0\rangle_k$ the ground state that reduces to $\{\sigma_1, \sigma_2 = 1, \dots, \sigma_k = 1, \sigma_{k+1} = -1, \dots, \sigma_N = -1\}$ when $D = \infty$, as shown in Fig. 2.6.

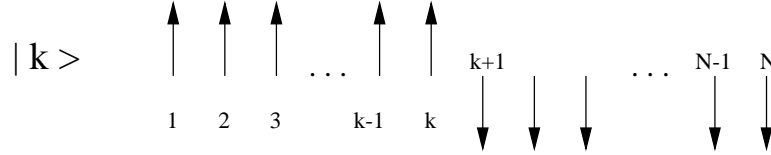


Figure 2.6: Arrangements of spins in configuration $|k\rangle$ when $D = \infty$.

The Hamiltonian (2.25) becomes

$$\mathcal{H}(\{\sigma_i\}) = E_I + \mathcal{H}_0 + V_{\parallel} + V_{\parallel\!/\!} + V_4, \quad (2.32)$$

where

$$E_I = -J \sum_{i=1}^{N-1} \sigma_i \sigma_{i+1} + H \sum_{i=2}^{N-1} \sigma_i - K[\sigma_1 - \sigma_N] \quad (2.33)$$

$$\mathcal{H}_0 = \sum_{i=2}^{N-1} \left[2D + J\sigma_i(\sigma_{i-1} + \sigma_{i+1}) - H\sigma_i \right] S^{-1} a_i^+ a_i, \quad (2.34)$$

V_4 represents the four operator terms proportional to $1/S^2$, and V_{\parallel} ($V_{\parallel\!/\!}$) is the interaction between spins which are parallel (antiparallel)

$$V_{\parallel} = - \sum_{i=2; i \neq k}^{N-1} JS^{-1}(a_i^+ a_{i+1} + a_{i+1}^+ a_i), \quad (2.35)$$

$$V_{\parallel\!/\!} = -JS^{-1}(a_k^+ a_{k+1}^+ + a_{k+1} a_k). \quad (2.36)$$

We work to lowest order in $1/S$ and therefore neglect terms like V_4 which are higher order than quadratic in the boson operators.

We will regard \mathcal{H}_0 as the unperturbed Hamiltonian, since it is diagonal in a_i^\dagger and a_i . The role of the perturbative terms V_{\parallel} is to create or destroy a pair of excitations (i.e., spin-deviations) at the sides of the interface, while V_{\perp} has the effect of hopping these excitations to nearest-neighbouring sites (though they can never be hopped past an interface, to ensure conservation of the total magnetization of the chain). The energies E_k will be calculated at $H = 0$ using standard perturbation techniques [31]

$$E_k = {}_k\langle 0|(V_{\parallel} + V_{\perp})|0\rangle_k - {}_k\langle 0|(V_{\parallel} + V_{\perp})\frac{Q_0}{\mathcal{H}_0 - E_0}(V_{\parallel} + V_{\perp})|0\rangle_k + \dots \quad (2.37)$$

where the vector $|0\rangle_k$ corresponds to the configuration with the interface at position k and no excitation present and $Q_0 = 1 - |0\rangle_k {}_k\langle 0|$. All the vectors $|0\rangle_k$ are eigenstates of \mathcal{H}_0 with the same eigenvalue E_0 . However, the perturbative term $(V_{\parallel} + V_{\perp})$ conserves $\sum_i S_i^z$ and thus it can never cause a transition between two different ground states. Therefore we may use non-degenerate perturbation theory to check whether the excitations can lift the degeneracy of the interface states.

At this stage it is important to point out that in equation (2.37) there might be terms where a physical state $|P\rangle$, with $-S \leq S_i^z \leq S$ for all i 's, is connected to an unphysical one, $|U\rangle$, as shown below,

$$\langle U|V|P\rangle, \quad (2.38)$$

However, the Dyson-Maleev transformation (2.26), which is non-Hermitian, guarantees that

$$\langle P'|V|U\rangle = 0 \quad (2.39)$$

where $\langle P'|$ is an arbitrary physical state. In other words it will never be possible to connect two physical states through unphysical intermediate ones. Therefore, the effect of spurious states in (2.37) is automatically eliminated without having to impose from the outside the constraint that only physical states can appear.

Contributions to the energies E_k arise from spin deviations at the interface created by V_{\perp} which are propagated away from and then back to the interface by V_{\parallel} and subsequently destroyed by V_{\perp} . However only such processes which are k -dependent are of interest to us. Amongst all the k -dependent processes, the ones that will give the leading order contribution to $\Delta E_k = E_k - E_{k+1}$ are those involving the least number V 's since, for each V , the energy denominators in (2.37) introduce a factor of order $1/D$.

The lowest order term which contributes to ΔE_k corresponds to an excitation which is created at the interface at position k and propagates to the surface and back before being destroyed. This graph is illustrated in Fig. 2.7. (This process contributes to E_k , but does not occur for E_{k-1} .) It has a contribution which follows immediately from $(2k)^{\text{th}}$ order perturbation theory as

$$\Delta E_k = -\frac{J^{2k}}{S(4D)^{2k-1}} + \mathcal{O}\left(\frac{1}{D^{2k}}\right) \quad (2.40)$$

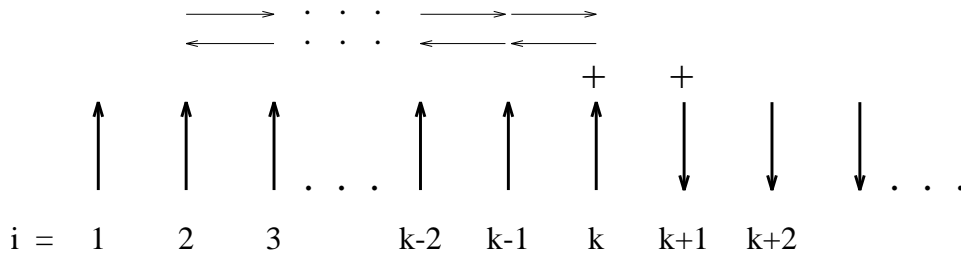


Figure 2.7: The process which gives the lowest order contribution to the energy difference $\Delta E_k \equiv E_k - E_{k-1}$ between the interface at positions k and $k-1$. $+$ ($-$) denotes the creation (destruction) of a spin excitation by V_{\parallel} . An arrow is used to denote a hop mediated by V_{\parallel} . The process shown contributes to E_k but not to E_{k-1} because the $i=1$ spin can not be flipped when $H \rightarrow \infty$.

where the terms in J and H in the denominator contribute only to higher order in $1/D$. ΔE_k is negative corresponding to a repulsive interaction between the interface and the surface and hence as $H \rightarrow 0^+$ the interface unbinds through an infinite series of first order phase transitions with boundaries between the phases at

$$H_{k:k-1} = \frac{J^{2k}}{S(4D)^{2k-1}}. \quad (2.41)$$

It is important to point out that these conclusions are based on a leading order calculation of ΔE_k for very large k . However, as we argued at the end of section 2.5, given the absence of competing interactions in the Hamiltonian (2.25), it seems unreasonable to expect that higher-order corrections could change the sign of ΔE_k , thus truncating the layering series.

2.9 Conclusions

To summarise we have shown that the softening of spins with p -fold anisotropy, for $p \geq 3$, can remove the multidegeneracy in a spin model with short range interactions in the presence of a magnetic field. We have given evidence for a sequence of first order layering transitions which is probably infinite.

The additional symmetry present in the model for $p=2$ is responsible for the persistence of degeneracy observed in the ground state for high values of the spin anisotropy. We have shown that, for the quantum version of the two-fold anisotropic classical model, zero-temperature quantum fluctuations are sufficient to break the degeneracy and stabilize a sequence of layering transitions.

Chapter 3

Quantum fluctuations in the transverse Ising model

3.1 Introduction

The transverse Ising model [32] was first introduced by de Gennes [33] in connection with hydrogen-bonded ferro-electrics. For this class of materials [34, 35, 36] the bonding proton can occupy one of the two minima of a double well potential. Within the pseudo-spin description of the system, the two equivalent positions of the proton are associated with spin up or spin down, while the transverse magnetic field controls the tunnelling of the proton between the two wells.

Although the model can be used as a pseudo-spin description for several other materials [37, 38] it also used in connection with genuine magnetic systems, like some compounds of Tb with group-V elements, where the ground state, stabilized by the crystal field splitting, is a singlet [39, 40].

In this Chapter we will focus on the behaviour of a domain wall in a semi-infinite three-dimensional version of the model. This study has been stimulated by the work of Henkel *et al.* [41] who have discussed the effect of quantum fluctuations on a domain wall in the system. Their work considers one dimension, where the interface is rough [4, 42]. Very different behaviour can be expected for a smooth interface, as in the case presented here.

We find that, for zero transverse field, the short range nature of the spin interactions is responsible for the appearance of a multidegeneracy with respect to the position of the flat domain wall. For a non-zero transverse field, the multidegeneracy can be split by quantum fluctuations and an infinite sequence of layering transitions is stabilized [43].

3.2 The model

The Hamiltonian of the classical three-dimensional transverse Ising model we shall consider is

$$\begin{aligned} \mathcal{H} = & -J_0 \sum_{i=1,L} \sum_{\langle j,j' \rangle} S_z(i,j)S_z(i,j') - J_1 \sum_{i=0,L} \sum_j S_z(i,j)S_z(i+1,j) \\ & - \sum_{i=1,L} \sum_j \left[hS_x(i,j) + HS_z(i,j) \right] - K \sum_j \left(S_z(0,j) - S_z(L+1,j) \right), \end{aligned} \quad (3.1)$$

where i labels two-dimensional planes and $\langle j,j' \rangle$ pairs of nearest neighbours within a plane.

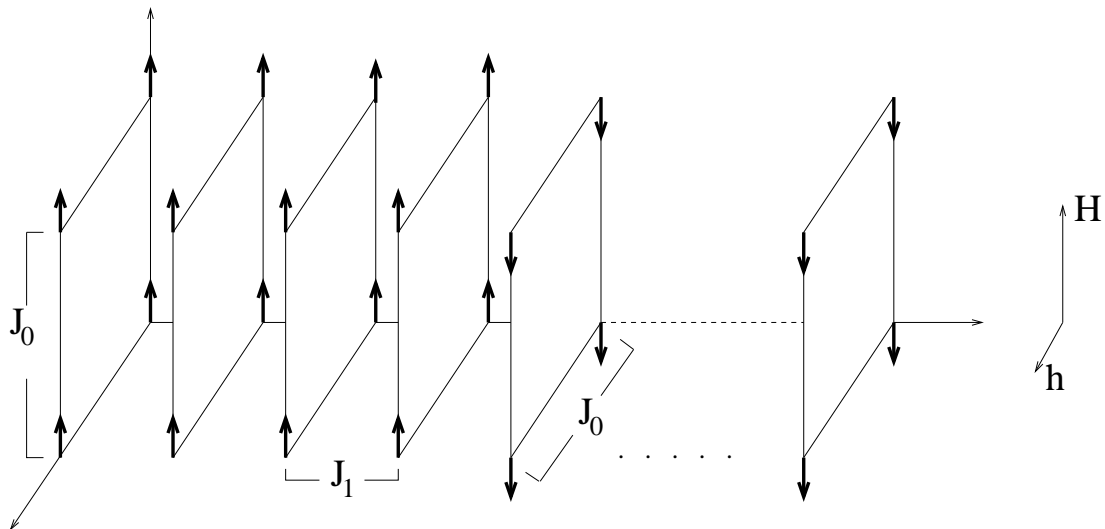


Figure 3.1: Schematic representation of the model introduced in Eq. (3.1). The leftmost plane is labeled $i = 0$ and the rightmost $i = L + 1$. The surface field K is not shown.

The parameter $K \rightarrow \infty$ is used to impose appropriate boundary conditions, namely to fix the spins at the surface ($i = 0$) to be up and those in the last layer ($i = L + 1$) to be down. These boundary conditions will create a domain wall, or interface, in the system separating layers of up and down spins (see Fig. 3.1).

As shown in Fig. 3.2a we will say that the interface is at position k if

$$\begin{aligned} S_z(i,j) &= +1/2 & \text{for } i \leq k \\ S_z(i,j) &= -1/2 & \text{for } i > k \end{aligned}$$

Although, strictly speaking, this definition applies only when $h = 0$, it can also be used for finite, though small enough values of h , as long as a sharp interface can still be identified (despite the presence of some disorder).

Our aim is to construct the phase diagram which gives the position, k , of the interface as a function of the uniform field H and the transverse field h .

As for the interface unbinding problem addressed in Chapter 2 we consider the case $T = 0$, where the interface is flat, and we shall work in the limit $L \rightarrow \infty$.

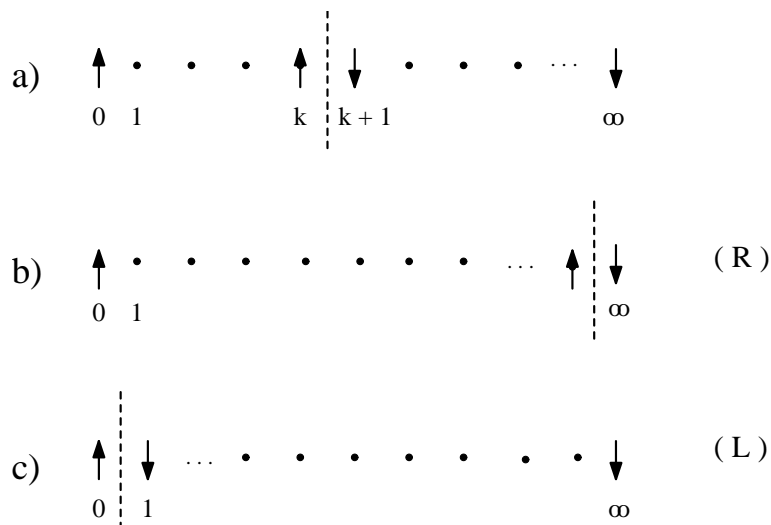


Figure 3.2: a) Configuration of the spins when the interface is at position k . Layer 0 is constrained to be up and the layer at infinity is constrained to be down. In panels (b) and (c) we have represented the configurations R and L.

3.3 Qualitative remarks

As a first step in understanding the phase diagram we consider the situation for $h = 0$. In this case it is clear that for positive H , $k = \infty$ while, for negative H , $k = 0$. We shall call these phases, which are illustrated in Fig. 3.2, R and L respectively. For $H=0$ the energy is independent of k , so that all interface positions are degenerate.

As we discussed in the previous Chapter, the perturbations introduced by thermal or quantum fluctuations can produce an effective coupling between the interface and the wall which raises the multidegeneracy (this phenomenon has been referred to as ground-state selection by Henley and others [44, 45]). The qualitative aspect of the resulting phase diagram will differ according to whether the wall-wall interaction is repulsive or has an attractive part. Since we are interested in studying the phase diagram at zero temperature, here we will consider the effect of quantum fluctuations. Our results show that the effective interaction between surface and interface introduced by quantum fluctuations is repulsive and is responsible for the appearance of a sequence of layering transitions which is probably infinite.

First of all we notice that, even when h is nonzero, the R phase is stable whenever H is positive. As we will show, the stability of the L phase requires that $H < -Ch^2 J_1/J_0^2$, where C is a constant. To determine the interface position for intermediate values of H , we shall calculate the energy of different interface states by applying quantum perturbation theory and assuming perfectly flat interfaces. If we were dealing with a finite system, then perturbation theory would introduce coupling in finite order between states when the interface is at different positions. However, this tunnelling effect disappears in the thermodynamic limit ($L \rightarrow \infty$) and this justifies our use of non-degenerate perturbation theory. Our perturbative calculations are valid for $h \ll J_0$ and $h \ll J_1$. We also

impose the condition $J_1 \ll J_0$ although, as long as we remain in the regime where the interfaces are flat, this restriction is probably inessential.

Since we will need to compare the energy of different interface states, it is convenient, at this stage, to write the energy per layer spin $e(k)$ of the state when the interface is at position k as

$$e(k) = e_0 - kH + E_k, \quad (3.2)$$

where e_0 is the energy per layer spin for the $k = 0$ phase and E_k is the k -dependent energy correction due to quantum fluctuations. Hence, the critical field, H_k^* separating the phase k from $k + 1$ is given by

$$-H_k^* = E_k - E_{k+1} \equiv \Delta E_k. \quad (3.3)$$

In the next section we will use quantum perturbation theory to calculate ΔE_k to leading order in $1/J_0$. To this purpose it is helpful to notice that ΔE_k in (3.3) can be safely evaluated for $H = 0$. In fact, E_k depends on H through the energy denominators that appear in perturbation theory, which are typically of the form $2J_0 + J_1 + H$. However, perturbative contributions to E_k , when expanded in powers of H , lead to corrections which are of relative order H/J_0 or smaller. But since we will only be interested in H in the range $-Ch^2/J_0 < H < 0$, these corrections are smaller than of relative order $(h^2/J_0^2) \ll 1$, which we may ignore. Therefore, in equation (3.3), we may evaluate ΔE_k at $H = 0$.

3.4 Calculation of ΔE_k

From equation (3.3) it is clear that we only need to keep track of terms in the ground-state energy which depend on k . In other words we need to ascertain how the corrections to the ground-state energy which are perturbative in h depend on the location of the interface. For convenience we now transform to occupation number operators. For spins that are up (down) we write $S_z(i, j) = 1/2 - n_{i,j}$ [$S_z(i, j) = -1/2 + n_{i,j}$]. Also $S_x(i, j) = (a_{i,j}^\dagger + a_{i,j})/2$, where the operator $a_{i,j}^\dagger$ ($a_{i,j}$) creates [destroys] a Bose excitation at site i in the j th layer and $n_{i,j} = a_{i,j}^\dagger a_{i,j}$. To enforce the restriction that no more than one excitation can exist on a single site, we include a term of the form $\Lambda \sum_{i,j} a_{i,j}^\dagger a_{i,j}^\dagger a_{i,j} a_{i,j}$, where $\Lambda \rightarrow \infty$. Although normally, it is difficult to take full account of such a hard-core interaction we will be able to accommodate this constraint by never involving matrix elements connecting to a state in which there is more than one excitation at any site. Therefore, when the interface is at position k we are led to the following bosonic Hamiltonian,

$$\begin{aligned} \mathcal{H}_B = & E_0 + \sum_{i=1}^{\infty} \sum_j \left(2J_0 n_{i,j} - (h/2)[a_{i,j}^\dagger + a_{i,j}] \right) - \sum_{i=1}^{\infty} \sum_{\langle j,j' \rangle} J_0 n_{i,j} n_{i,j'} \\ & + \Lambda \sum_{i=1}^{\infty} \sum_j a_{i,j}^\dagger a_{i,j}^\dagger a_{i,j} a_{i,j} - J_1 \sum_{i=0}^{\infty} \sum_j [-(1/2)(n_{i,j} + n_{i+1,j}) + n_{i,j} n_{i+1,j}] \end{aligned}$$

$$+J_1 \sum_j [-n_{k,j} - n_{k+1,j} + 2n_{k,j}n_{k+1,j}] , \quad (3.4)$$

where E_0 is the unperturbed energy of the $k = 0$ phase and $\Lambda \rightarrow \infty$. In (3.4) we set $H = 0$ for the reasons explained before and we also omitted the term proportional to K in (3.1) since, for $K \rightarrow \infty$, $n_{0,j}$ must be set equal to zero. We write this Hamiltonian as

$$\mathcal{H}_B = E_0 + \mathcal{H}_0 + V_1 + V_2 + V_3 + V_4 , \quad (3.5)$$

where

$$\mathcal{H}_0 = \Delta \sum_i \sum_j n_{i,j} , \quad (3.6)$$

with $\Delta = 2J_0 + J_1$, and

$$V_1 = - \sum_i \sum_j J_{i,i+1} n_{i,j} n_{i+1,j} - J_0 \sum_i \sum_{\langle j,j' \rangle} n_{i,j} n_{i,j'} \quad (3.7)$$

$$V_2 = -(h/2) \sum_i \sum_j [a_{i,j}^\dagger + a_{i,j}] , \quad (3.8)$$

$$V_3 = -J_1 \sum_j (n_{k,j} + n_{k+1,j}) , \quad (3.9)$$

where

$$J_{i,i+1} = \begin{cases} J_1 & \text{for } i \neq k \\ -J_1 & \text{for } i = k \end{cases} \quad (3.10)$$

and (with $\Lambda \rightarrow \infty$)

$$V_4 = \Lambda \sum_i \sum_j a_{i,j}^\dagger a_{i,j}^\dagger a_{i,j} a_{i,j} . \quad (3.11)$$

We now consider how the perturbative contributions to the energy depend on the various coupling constants. To carry out this discussion it is convenient to introduce a diagrammatic representation of the contributions to the perturbation expansion. Each term of V_1 proportional to $J_{rs}n_rn_s$, where r (and similarly s) denotes a position label of the form i, j , is represented by a line joining the two interacting sites r and s and $J_{rs} = J_0$ or $J_{rs} = J_1$ depending on whether sites r and s are in the same plane or are in adjacent planes. The perturbation in V_2 proportional to a_r (a_r^\dagger) is represented by a minus (plus) sign at the site r . However, for simplicity, since each site involved with any of the other interactions must be excited (i. e. must have both a "+" and a "-" associated with it), we have not explicitly shown "+"'s and "-"'s in Fig. 3.3. The term in the perturbation V_3 proportional to $n_{k,j}$ ($n_{k+1,j}$) is represented by a circle attached to the site k, j ($k+1, j$). Any term in perturbation theory which does not involve V_4 can be constructed from these elements. Some simple examples are shown in Fig. 3.3.

At this stage it is convenient to introduce the definition of connected terms. Any term which involves only a single site is connected. Terms which involve more than one site are connected only if all such sites are connected with respect to lines representing terms of V_1 . If this is not the case,

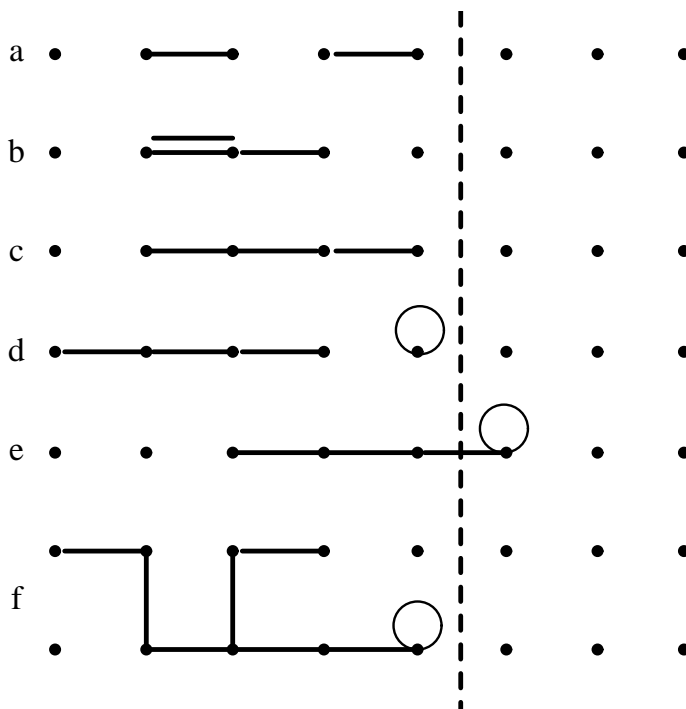


Figure 3.3: Representation of perturbative contributions to the ground-state energy. The dashed line corresponds to the location of the interface. Contributions which involve J_1 and h for four sites (a) and (c) and for three sites (b) with one of the J_1 's taken to second order. (d-f) Terms which involve factors of V_3 . Diagram (f) represents a term which involves the J_0 interaction. Diagrams (a) and (d) are disconnected and therefore give zero contribution to the ground state energy, as discussed in the text.

the term will be called disconnected. Thus diagrams (a) and (d) of Fig. 3.3 are disconnected. It is useful to distinguish between connected and disconnected diagrams since the latter do not contribute to the energy. This can be established by considering a disconnected diagram Γ which consists of two disjoint components, Γ_A and Γ_B . The contribution of this diagram is unchanged if we were to treat perturbatively the system $S(\Gamma_A + \Gamma_B)$ in which all coupling constants J_{rs} not in Γ_A or Γ_B are set to zero. But because Γ_A and Γ_B are disjoint systems, we have $E(\Gamma_A + \Gamma_B) = E(\Gamma_A) + E(\Gamma_B)$. This result indicates that there are no disconnected terms in the ground state energy which involve simultaneously an exchange constant from one component Γ_A and an exchange constant from the other component Γ_B . Thus disconnected diagrams can be omitted from further consideration.

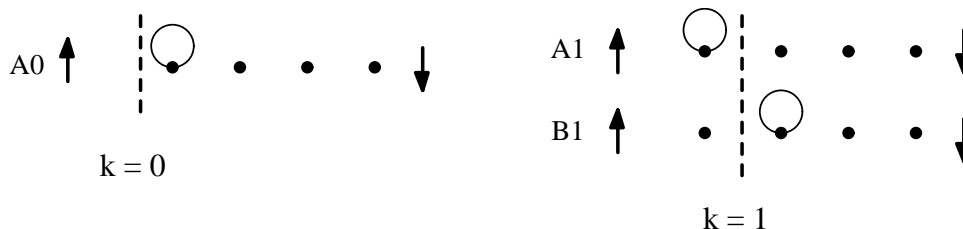


Figure 3.4: Perturbative contributions to the ground-state energy used to evaluate $\Delta E_0 = E_0 - E_1$. Panel A0 corresponds to the case when the interface is at $k = 0$; panels A1 and B1 to the case $k = 1$.

To evaluate ΔE_k it is apparent from the definition of equation (3.3) that we only need to keep

connected contributions which appear when the interface is at position $k + 1$ but *not* when it is at position k . To identify the contributions which are lowest order in (J_1/Δ) and in (h/Δ) , it is convenient to refer to Figs. 3.4 and 3.5, where typical contributions to the ground state energy are shown. In particular consider contributions to ΔE_1 , some of which are shown in Fig. 3.5. It is important to notice that we did not include diagrams like those of Fig. 3.4 which involve no lines representing V_1 and one circle representing V_3 , because such diagrams occur equally for E_1 and E_2 . Similarly, one can see from the system of five layers shown in Fig. 3.5, that contributions which are first order in V_1 and zeroth order in V_2 occur identically in E_1 and E_2 . For both E_1 and E_2 there is one way to take V_1 spanning the wall, and three ways to take a V_1 which does not span the wall. Next in order of smallness, we consider contributions which involve one J_1 line (i.e. one power of V_1) and one circle (i.e. one power of V_3). In this case for E_2 one has the extra term labeled E2 in Fig. 3.5. The rule is thus: the leading contribution in (J_1/Δ) to ΔE_k arises from the contribution to E_{k+1} coming from a diagrams which involves k lines (each carrying a factor J_1) which connect the surface to the interface and one circle representing V_3 .

Furthermore, we now show that it is only minimal length chains which give the dominant contribution to ΔE_k . As we shall see, taking additional factors of V_1 involving J_0 leads to contributions which are higher order in (h/Δ) than those from diagrams involving only J_1 .

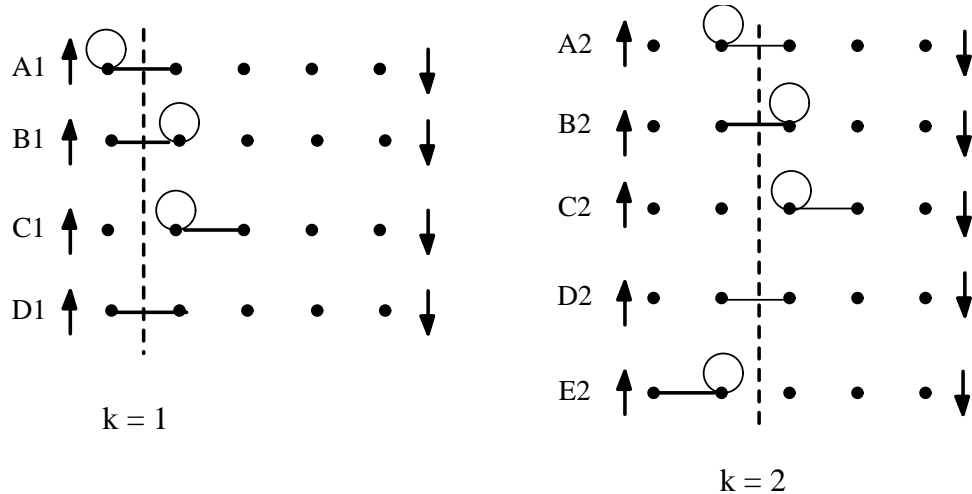


Figure 3.5: Perturbative contributions to the ground-state energy used to evaluate $\Delta E_1 = E_1 - E_2$. Panels A1 – D1 are for the case when the interface is at $k = 1$. Panels A2 – E2 correspond to $k = 2$. The dashed line represents the position of the interface. Contributions from diagrams A1, B1, C1, and D1 are equal to those from diagrams A2, B2, C2, and D2, respectively. So ΔE_1 is determined by E2.

To see this we give a more detailed analysis of the contribution of a diagram involving, say, p different lines representing V_1 and, as we explained, necessarily involving at least one interface potential term V_3 . Note that both these perturbations, V_1 and V_3 , involve occupation numbers n_r , which vanish when there is no excitation at site r . For every site r involved in a V_1 or V_3 interaction, it is necessary to create an excitation so that n_r can be evaluated in a virtual state in which $n_r = 1$. Subsequently,

in order to get back into the ground state, we must destroy the excitation on the site r . Thus in all a diagram involving p different lines will involve $p + 1$ sites and therefore give rise to a perturbative contribution to the energy which is of order $\delta_p E$, where

$$\delta_p E = h^{(2p+2)} J_1^{p_1} J_0^{p_2} (J_1/\Delta) / \Delta^{2p+1+p_1+p_2} , \quad (3.12)$$

where of the p lines, p_1 are associated with J_1 and p_2 with J_0 [see Eq. (3.7)]. In writing this equation we included the factor (J_1/Δ) to take account of the necessary factor of V_3 . At this point, it is clear that to have a diagram which occurs for position $k + 1$ but not for k it is best to invoke a linear diagram, and not one which reaches more than one row perpendicular to the interface. Unnecessary factors of J_0 in V_1 will give rise to additional factor of $J_0 h^2 / \Delta^3 \ll 1$. So, we conclude that to leading order

$$\Delta E_k = C_k J_0^2 (J_1 h_0^2 / J_0^3)^{k+1} , \quad (3.13)$$

where C_k is a constant which must be determined by an explicit calculation and, to leading order, we set $\Delta = 2J_0$.

Now we carry out a detailed calculation of ΔE_k for small values of k . We first start with the simplest case, namely $k = 0$. From Fig. 3.4 we obtain

$$\Delta E_0 = -E(A1) , \quad (3.14)$$

where $E(A1)$ is the contribution to the energy in diagram $A1$ of Fig. 3.4. Thus [31]

$$\begin{aligned} \Delta E_0 &= -\langle 0 | V_2 \frac{1}{\mathcal{E}} V_3 \frac{1}{\mathcal{E}} V_2 | 0 \rangle \\ &= -\langle 0 | (-h/2) a_1 \frac{1}{\mathcal{E}} (-J_1 a_1^\dagger a_1) \frac{1}{\mathcal{E}} (-h/2) a_1^\dagger | 0 \rangle \\ &= (h^2/4) (J_1/\Delta^2) = J_1 h^2 / (16J_0^2) . \end{aligned} \quad (3.15)$$

Here and below the excitation energies \mathcal{E} will be $-r\Delta = -2rJ_0$, where r is the number of excitations in the virtual state.

Next we calculate $\Delta E_1 = -E(E2)$ from diagram $E2$ of Fig. 3.5. Here we have to sum over the different orderings of the perturbations,

$$\begin{aligned} \Delta E_1 &= \\ &-\langle 0 | \left[(-h/2) a_1 \frac{1}{\mathcal{E}} (-h/2) a_2 + (-h/2) a_2 \frac{1}{\mathcal{E}} (-h/2) a_1 \right] \frac{1}{\mathcal{E}} \left[(-J_1 n_1 n_2) \frac{1}{\mathcal{E}} (-J_1 n_2) + (-J_1 n_2) \frac{1}{\mathcal{E}} (-J_1 n_1 n_2) \right] \\ &\quad \times \frac{1}{\mathcal{E}} \left[(-h/2) a_1^\dagger \frac{1}{\mathcal{E}} (-h/2) a_2^\dagger + (-h/2) a_2^\dagger \frac{1}{\mathcal{E}} (-h/2) a_1^\dagger \right] | 0 \rangle \\ &-\langle 0 | \left[(-h/2) a_1 \frac{1}{\mathcal{E}} (-h/2) a_2 + (-h/2) a_2 \frac{1}{\mathcal{E}} (-h/2) a_1 \right] \frac{1}{\mathcal{E}} (-J_1 n_1 n_2) \frac{1}{\mathcal{E}} (-h/2) a_1^\dagger \frac{1}{\mathcal{E}} (-J_1 n_2) \frac{1}{\mathcal{E}} (-h/2) a_2^\dagger | 0 \rangle \\ &-\langle 0 | (-h/2) a_2 \frac{1}{\mathcal{E}} (-J_1 n_2) \frac{1}{\mathcal{E}} (-h/2) a_1 \frac{1}{\mathcal{E}} (-J_1 n_1 n_2) \frac{1}{\mathcal{E}} \left[(-h/2) a_1^\dagger \frac{1}{\mathcal{E}} (-h/2) a_2^\dagger + (-h/2) a_2^\dagger \frac{1}{\mathcal{E}} (-h/2) a_1^\dagger \right] | 0 \rangle . \end{aligned} \quad (3.16)$$

When simplified this yields

$$\Delta E_1 = 2(h/2)^4 J_1^2 / \Delta^5 = (1/256) J_1^2 h^4 / J_0^5 . \quad (3.17)$$

This calculation is hard to extend to ΔE_k for larger k using the Schrödinger-Rayleigh perturbation theory. In fact, as suggested by A.B. Harris [46], it is more convenient to adopt the Matsubara formalism [47]. In the Matsubara perturbative scheme one has diagrams constructed from the following elements. The perturbations V_1 , V_2 , and V_3 are represented by vertices as shown in Fig. 3.6. Each such vertex carries the appropriate factor $(-h/2)$, $-J_1\delta_{r,k}$, and $-J_1$, respectively, where $\delta_{r,k}$

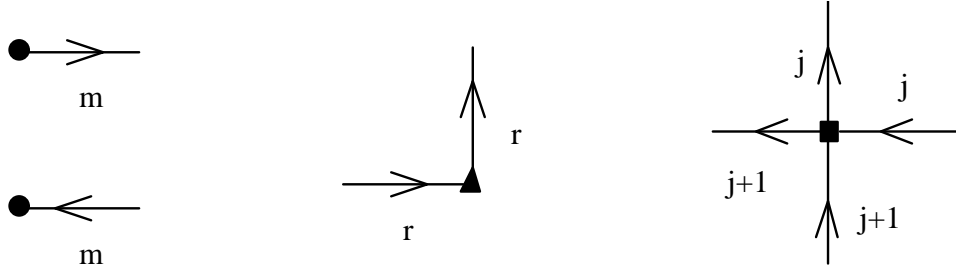


Figure 3.6: Vertices for Matsubara diagrams: (a) transverse field vertex $-(h/2)(a_m^\dagger)$ (top) and $-(h/2)a_m$ (bottom); (b) $-J_1\delta_{r,k}a_r^\dagger a_r$; (c) $-J_1n_j n_{j+1} = J_1a_j^\dagger a_{j+1}^\dagger a_{j+1} a_j$.

is the Kronecker delta. Since the leading order expressions for ΔE_k never involve $J_{k,k+1}$, we can set $J_{i,i+1} = J_1$.

In the Matsubara diagrams each line represents a Green's function $(z_\nu - \Delta)^{-1}$, and lines which carry the same label are joined. The contribution to the energy is obtained by summing over all topologically inequivalent connected diagrams. A sum is also taken over the Matsubara frequencies, $z_\nu = 2\nu\pi i/(k_B T)$ (where ν runs over all integers positive and negative), that appear in the Green's functions. One also needs to enforce the conservation of z_ν , that is for each vertex the sum of all incoming z 's minus the sum of all outgoing z 's must equal zero. For the present case, this conservation law means that at any vertex which has only one line entering or leaving the corresponding z must be zero. One can quickly see that the z_ν 's for all lines have to be zero. So, in fact, there is no sum over z_ν to be done.

The only Matsubara diagram contributing to ΔE_0 is shown in Fig. 3.7a, for which we have the contribution

$$\Delta E_0 = -(-h/2)(-J_1)(-h/2)(-\Delta)^{-2} = h^2 J_1 / (4\Delta^2) = h^2 J_1 / (16J_0^2), \quad (3.18)$$

as before. To obtain this result, note that diagram (a) has two filled circle vertices (each carrying a factor $-h/2$), one triangle (carrying a factor $-J_1$), and two lines, each of which carries a factor $(z - E_i)^{-1} = -\Delta^{-1}$. Similarly we can calculate ΔE_1 which is given by

$$\Delta E_1 = -(E_b + E_c) = -2E_b. \quad (3.19)$$

where E_b and E_c are the energies of diagrams b and c in Fig. 3.7 respectively (an analogous notation for the energy of other diagrams will be used below.) Since diagram b has four h vertices, two J_1

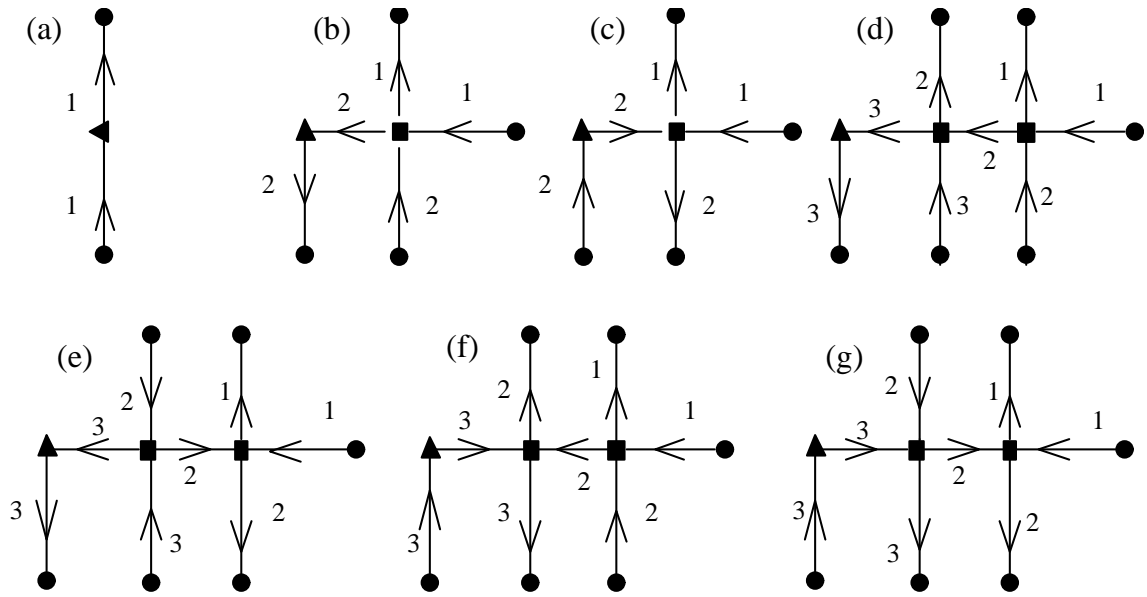


Figure 3.7: Matsubara diagrams. The vertices are explained in the preceding figure. The lines are labeled by an index i to represent the Green's function $(z - \Delta)^{-1}$. This calculation is for a linear system with sites labeled 1, 2, These diagrams give $-\Delta E_m$ following the reasoning of Figs. 4 and 5. Diagram (a) is for $m = 0$, diagrams (b) and (c) are for $m = 1$ and diagrams (d)–(g) are for $m = 2$. No new topology is obtained by reversing the direction of the line labeled "1". However, one may independently reverse the direction of all other lines giving rise to a degeneracy 2^m .

vertices, and five lines, we have that

$$\Delta E_1 = -2(-h/2)^4(-J_1)(-J_1)(-\Delta)^{-5} = h^4 J_1^2 / (8\Delta^5) = h^4 J_1^2 / (256J_0^5). \quad (3.20)$$

Finally, from Fig. 3.7 we have

$$\Delta E_2 = -(E_d + E_e + E_f + E_g) = -4E_d. \quad (3.21)$$

Since diagram (d) has six h vertices, three J_1 vertices, and eight lines

$$\Delta E_2 = -4(-h/2)^6(-J_1)(-J_1)^2(-\Delta)^{-8} = h^6 J_1^3 / (16\Delta^8) = h^6 J_1^3 / (4096J_0^8). \quad (3.22)$$

An analysis of the structure of the diagrams contributing to ΔE_k for general k shows that the general expression is

$$\Delta E_k = J_0 (J_1 h^2 / 16J_0^3)^{k+1}. \quad (3.23)$$

3.5 The phase diagram

Since the sign of ΔE_k is positive, we can conclude that an infinite sequence of layering transitions is observed as the field, H , is increased from zero. Equation (3.23) indicates that the boundary between phases with $k = p$ and $k = p + 1$ is given, to leading order by $H_p^* = -J_0 (J_1 h^2 / 16J_0^3)^{p+1}$. The resulting phase diagram is shown schematically in Fig. 3.8.

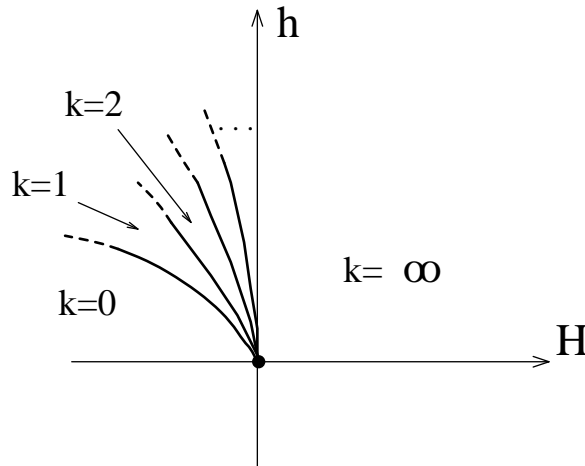


Figure 3.8: Schematic representation of the phase diagram for interface unbinding transitions in the transverse Ising model.

The analysis presented above was based on retaining only the leading-order (in h/J_0 and J_1/J_0) term in the surface–interface interaction. Although we cannot rule out the possibility that the neglected higher-order interactions could become dominant for very large k (for fixed h and J_0), we do not expect to observe any qualitative corrections to the phase diagram in this limit. This is because there are no competing interactions which would make correlation functions oscillatory at large distance and therefore it seems implausible that the positive sign of ΔE_p can be changed by the neglected higher-order terms [10].

3.6 The (3+1)-dimensional classical model

In this section we show how the correspondence between the $(d + 1)$ -dimensional classical Ising model and the d -dimensional quantum transverse Ising model [48, 49, 50, 51] can be used, at least in principle, as an alternative route for obtaining the expressions for ΔE_k . To do this we shall follow Kogut [48] and use the transfer matrix formalism to build a τ -continuum version of the classical Hamiltonian and then identify the Hamiltonian for the associated quantum model.

Consider a four-dimensional square lattice with Ising spins on the sites. We will denote the ferromagnetic spin coupling in the $[1, 0, 0, 0]$ and $[0, 1, 0, 0]$ directions as J_t and J respectively, while with J_0 we will refer to the interaction of spins in planes orthogonal to the J_t and J directions; all couplings, J , J_t and J_0 are assumed to be positive (i.e. ferromagnetic).

In view of the quantum mechanical correspondence it is useful to write the Hamiltonian for the classical problem in operator form,

$$\hat{H} = -J_0 \sum_{\langle j, j' \rangle}^{\perp} \hat{S}_z(i, j, t) \hat{S}_z(i, j', t) - J \sum_i^{\parallel} \hat{S}_z(i, j, t) \hat{S}_z(i + 1, j, t) - J_t \sum_t \hat{S}_z(i, j, t) \hat{S}_z(i, j, t) \quad (3.24)$$

where i , t and j label respectively sites along the J direction, J_t direction and in J_0 planes. The \hat{S}_z operators are the familiar 2x2 matrices

$$\hat{S}_z = \begin{pmatrix} 1/2 & 0 \\ 0 & -1/2 \end{pmatrix}, \quad (3.25)$$

and the vector states corresponding to spin up and down are, respectively,

$$\text{up: } \begin{pmatrix} 1 \\ 0 \end{pmatrix} \quad \text{down: } \begin{pmatrix} 0 \\ 1 \end{pmatrix}. \quad (3.26)$$

We can implicitly define the transfer operator in the J_t direction (which we will often refer to as the “time direction”) \hat{T} so that the partition function

$$\mathcal{Z} = \text{Tr} e^{-\hat{H}} \quad (3.27)$$

can be written as

$$\mathcal{Z} = \text{Tr} \hat{T}^N \quad (3.28)$$

where N , the number of layers in the time direction (see Fig. 3.9), is very large, the Boltzmann factor $1/k_B T$ is equal to unity, and Tr denotes the trace taken over all possible spin states.

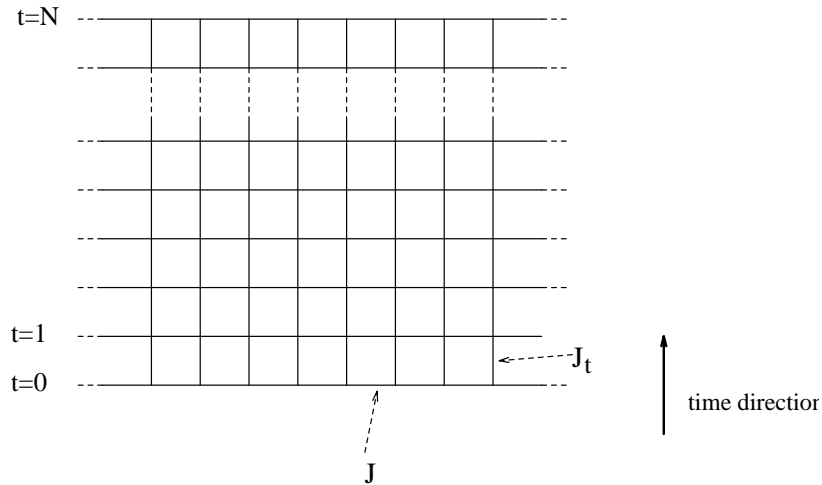


Figure 3.9: Section of the four-dimensional lattice along the $J - J_t$ plane.

The diagonal elements of \hat{T} connect two identical “hyper-rows”; therefore they have the form

$$\hat{T}_{diagonal} = A \exp \left[J_0 \sum_{\perp} \hat{S}_z(i, j, t) \hat{S}_z(i, j', t) + J \sum_{\parallel} \hat{S}_z(i, j, t) \hat{S}_z(i + 1, j, t) \right], \quad (3.29)$$

where

$$A = \exp \sum_t \hat{S}_z(i, j, t) \hat{S}_z(i, j, t + 1). \quad (3.30)$$

Now consider matrix elements that connect two rows that differ by one flipped spin, \hat{T}_{1-flip} . Making use of the fact that the matrix $2\hat{S}_x$, where \hat{S}_x is

$$\hat{S}_x = \begin{pmatrix} 0 & 1/2 \\ 1/2 & 0 \end{pmatrix}, \quad (3.31)$$

acts as a spin flipping operator we have

$$\hat{T}_{1-flip} = A \exp \left[-J_t/2 + J_0 \sum_{\perp} \hat{S}_z(i, j, t) \hat{S}_z(i, j', t) + J \sum_{\parallel} \hat{S}_z(i, j, t) \hat{S}_z(i+1, j, t) \right] 2\hat{S}_x \quad (3.32)$$

More in general, matrix elements connecting states that differ by n flipped spins will be proportional to $\exp(-nJ_t/2)$. Now we take the extreme anisotropic limit

$$\begin{aligned} J_t &\rightarrow \infty, \\ \lim_{J_t \rightarrow \infty} J_0 e^{J_t/2} &= \lambda_0, \\ \lim_{J_t \rightarrow \infty} J e^{J_t/2} &= \lambda, \end{aligned} \quad (3.33)$$

so that T can be expanded as follows (for convenience we drop the site labels of the \hat{S}_z matrices)

$$\begin{aligned} \hat{T} &= (1 + J_0 \sum_{\perp} \hat{S}_z \hat{S}_z + J \sum_{\parallel} \hat{S}_z \hat{S}_z + \dots) (1 + e^{-J_t/2} \sum 2\hat{S}_x + \dots) \\ &\approx 1 + e^{-J_t/2} (\lambda_0 \sum_{\perp} \hat{S}_z \hat{S}_z + \lambda \sum_{\parallel} \hat{S}_z \hat{S}_z + \sum 2\hat{S}_x) \\ &\approx e^{-\tau \mathcal{H}} \end{aligned} \quad (3.34)$$

If we regard τ as an infinitesimal time-step, expression (3.34) defines the generator of time translation, i.e. the Hamiltonian for the 3-dimensional transverse Ising model

$$\mathcal{H} = \lambda_0 \sum_{\perp} \hat{S}_z \hat{S}_z + \lambda \sum_{\parallel} \hat{S}_z \hat{S}_z + \sum \hat{S}_x. \quad (3.35)$$

Setting the surface field term, K , to zero in Eq. (3.1) we can establish a correspondence between (3.35) and (3.1) provided we make the substitution

$$\begin{aligned} \lambda_0 &\rightarrow 2J_0/h, \\ \lambda &\rightarrow 2J_1/h, \end{aligned} \quad (3.36)$$

and multiply (3.36) by $h/2$. In order to keep the derivation of the quantum Hamiltonian (3.35) as simple as possible, we did not include the infinite surface field which will be accounted for by fixing the spins at the boundary appropriately.

3.7 Calculation of ΔE_0

In this section we will show how to make use of the mapping described above to rederive the expression for ΔE_0 which followed from standard quantum perturbation theory (see equation 3.15).

In the classical picture we need to use an expansion in powers of e^{-2J_t} to calculate the difference in reduced free energy associated with different distances of the interface from the surface.

Since the reduced free energy, f , is defined as

$$f = -\frac{1}{N} \ln \mathcal{Z} \approx \tau \mathcal{H} \quad (3.37)$$

it follows that the corresponding energy for the quantum case E_q can be obtained from f by taking the limit

$$E_q = -\lim_{J_t \rightarrow \infty} e^{J_t/2} f. \quad (3.38)$$

Now we consider the two spin configurations represented in Figs. 3.10a and 3.10b, where all the spins with index i greater than 0 and 1, respectively, are pointing down, while the rest point up. Using (3.38) we can express ΔE_0 as

$$\Delta E_0 = -\lim_{J_t \rightarrow \infty} e^{J_t/2} [f_a - f_b] \quad (3.39)$$

where f_a and f_b are the classical free energies of the configurations a and b in Fig. 3.10, and the limits (3.33) are understood.

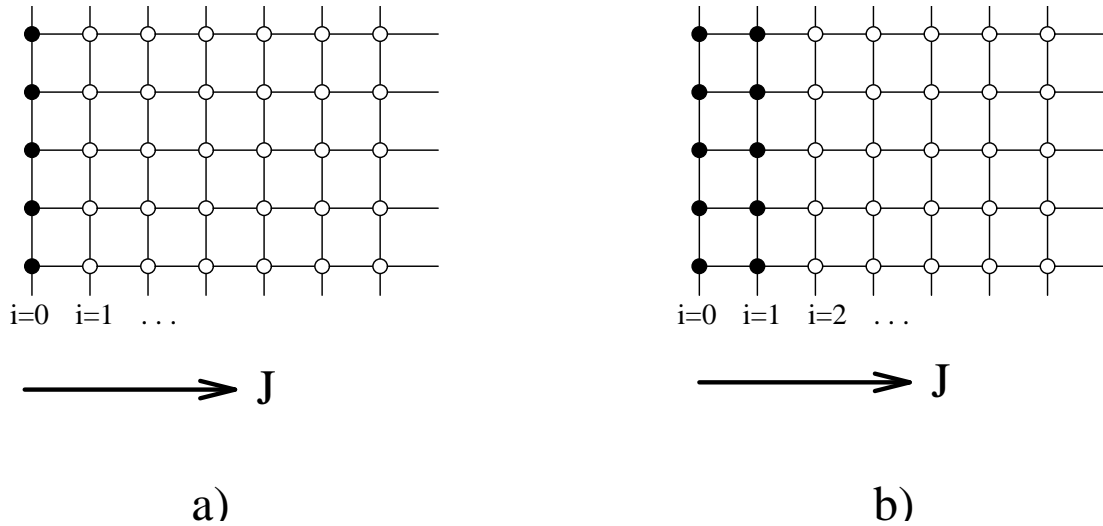


Figure 3.10: Two dimensional section of the classical 4-dimensional lattice when the interface is: a) at position $i = 1$, b) at position $i = 2$. A filled (empty) circle indicates a spin pointing up (down).

Now we calculate f_b and f_a to lowest order in e^{-2J_t} . To this purpose it is convenient to define the quantities

$$x = e^{-J/2}, \quad (3.40)$$

$$w = e^{-J_0/2}. \quad (3.41)$$

Flipping one spin on the immediate left of the interface in configuration b, the contribution to the free energy will be

$$e^{-J_t \omega^4}, \quad (3.42)$$

such a contribution does not exist for configuration a . However, this is not the only term of order e^{-Jt} that is present in b and absent in a . In fact, the increment in free energy associated with the flipping of a string of neighbouring spins along the time direction, as shown in Fig. 3.11b, is still proportional to e^{-Jt} .

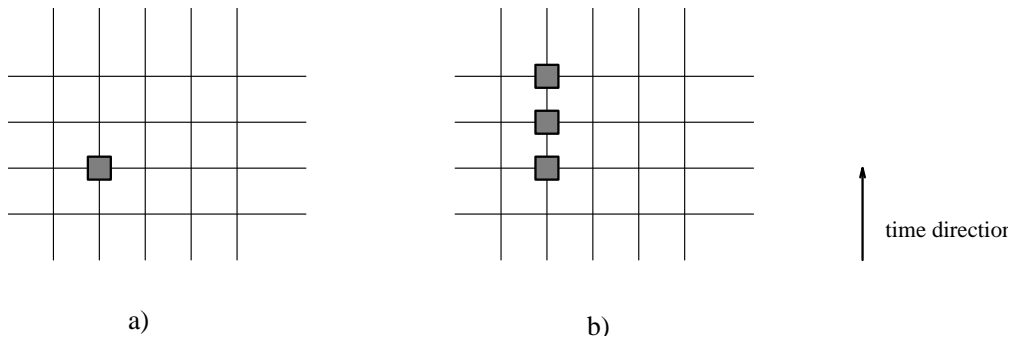


Figure 3.11: Section of the lattice showing some of the diagrams contributing to the free energy to order e^{-Jt} . A box indicates a flipped spin.

Summing all the contributions proportional to e^{-Jt} gives

$$e^{-Jt} \left(\omega^4 + \omega^8 + \omega^{10} + \dots \right) = -e^{-Jt} \frac{\omega^4}{1 - \omega^4} \quad (3.43)$$

On the other hand, in configuration a there is one extra layer of spins which points down with respect to configuration b . Hence, flipping any number of neighbouring spins in this extra layer will give rise to a contribution of order e^{-Jt} which is not present in f_b , namely

$$e^{-Jt} \left(\omega^4 x^2 + \omega^8 x^4 + \omega^{10} x^6 + \dots \right) = -e^{-Jt} \frac{\omega^4 x^2}{1 - \omega^4 x^2} \quad (3.44)$$

Therefore

$$f_a - f_b \approx e^{-Jt} \left(\frac{\omega^4 x^2}{1 - \omega^4 x^2} - \frac{\omega^4}{1 - \omega^4} \right) \quad (3.45)$$

giving finally

$$\begin{aligned} \Delta E_0 &= - \lim_{Jt \rightarrow \infty} e^{Jt/2} e^{-Jt} \left(\frac{\omega^4 x^2}{1 - \omega^4 x^2} - \frac{\omega^4}{1 - \omega^4} \right) \\ &\approx - \lim_{Jt \rightarrow \infty} e^{-Jt/2} \left(\frac{1}{J + 2J_0} - \frac{1}{J/2 + 2J_0} \right) \\ &\approx \frac{-1}{\lambda + 2\lambda_0} - \frac{-1}{2\lambda_0} \end{aligned} \quad (3.46)$$

In the limit $\lambda_0 \gg \lambda$ the expression for ΔE_0 simplifies further to

$$\Delta E_0 \approx \frac{\lambda}{4\lambda_0^2} \quad (3.47)$$

which is the same result as (3.15) as can be checked by making the substitutions (3.38) and multiplying the result by $h/2$.

Unfortunately, although this alternative derivation of ΔE_0 is an interesting and instructive exercise, the method used here is not easily generalised to calculate ΔE_k for large values of k . Therefore the use of the Matsubara formalism still provides the most efficient route for calculating the leading term in ΔE_k .

3.8 Conclusions

We considered the behaviour of an interface in a semi-infinite three-dimensional transverse Ising model. For zero transverse field the ground state of the system is degenerate with respect to the position of the interface. Using the Matsubara perturbative scheme we have shown that quantum fluctuations can introduce an effective coupling between the interface and the surface that removes the multidegeneracy. As a result a sequence of layering transitions which is probably infinite is stabilized.

We have also shown how the results obtained using the Matsubara formalism can be obtained, at least in principle, using an alternative route based on the correspondence between the three-dimensional transverse Ising model and the four-dimensional classical Ising model with anisotropic interactions.

Chapter 4

Layering transitions in an anisotropic antiferromagnet

4.1 Introduction

Recent experimental results on $Fe/Cr(211)$ superlattices [52, 53] (extensively studied in connection with the giant magnetoresistance effect [54, 55]) have stimulated theoretical and numerical work aimed at explaining the occurrence of series of phase transitions in samples with an even number of Fe blocks [52, 53, 56].

If the thickness of the layers is chosen appropriately, the blocks of Fe can be coupled antiferromagnetically [57]. At sufficiently low temperatures the system can be described phenomenologically by a chain of XY spins (each spin representing a Fe block) with antiferromagnetic interactions and uniaxial anisotropy, D . It is known that, as the external magnetic field acting on an infinitely extended antiferromagnet is increased, a first order transition occurs. The transition separates the antiferromagnetic phase from the so-called bulk spin-flop state, where neighbouring spins are symmetrically canted with respect to the field direction [58].

However, experimental investigations on finite samples of Fe/Cr have revealed that the phase diagram is much richer than the one expected for an infinite system. This has been correctly interpreted as due to surface effects [52]. In fact, following the seminal work of Mills, Keffer and Chow [59, 60], several authors have shown that, as the field H is increased, the transition between the antiferromagnetic and the bulk spin-flop phases occurs through a series of surface spin-flop transitions [52, 53, 60]. They argue that the surface spin-flop state expands continuously to give the bulk spin-flop state but give no explicit mechanism for this to occur. Recently Trallori *et al.* [56] have identified the surface spin-flop transitions for moderate values of the anisotropy $D \approx 1$ but have shown that they do not exist for low $D \approx 1/100$ [61].

Unfortunately the methods used so far for investigating the problem (which either rely on molecular field calculations [55] or on the study of chaotic iterative maps [62]) are not very efficient and, therefore they cannot be used to study the ground state of the model for all values of the anisotropy.

In this Chapter we shall adopt a novel approach to the problem by using the inverse anisotropy expansion technique (introduced in Chapter 2) together with a very efficient numerical strategy, based on the Chou-Griffiths algorithm [63]. By using these techniques we shall study the phase diagram of infinite, semi-infinite and finite antiferromagnetically coupled XY chains in a magnetic field for all values of the uniaxial anisotropy D . For semi-infinite chains of even length we prove analytically that there is a surface multiphase point from which the series of surface spin-flop (SSF) transitions originate. This sequence of transitions is associated with the nucleation of a discommensuration at the surface of the chain. For increasing values of the external magnetic field the discommensuration is pushed further and further away from the surface. We also show that the SSF transition lines terminate in critical points, thus explaining the disappearance of the surface phase transitions for very low D [61].

Finally we clarify the mechanism by which the bulk spin-flop phase evolves from the surface spin-flop state by proving the existence of a series of bulk transitions associated with a discontinuous increase of the discommensuration width. When the discommensuration length diverges the bulk spin-flop phase is accomplished [64].

4.2 Infinite Chain

We first consider an infinite chain of spins described by the Hamiltonian

$$\mathcal{H} = \sum_{i=-\infty}^{\infty} \left\{ \cos(\theta_i - \theta_{i+1}) - h \cos \theta_i + \frac{D}{4} [1 - \cos(2\theta_i)] \right\} \quad (4.1)$$

where θ_i is the angle between the i th spin and the direction of the field h and D is the spin anisotropy. It is convenient to describe first the case $D = \infty$ where the spins are Ising-like with the θ_i 's being restricted to the values $\{0, \pi\}$. For $0 < h < 2$ the ground state is given by the antiferromagnetic (AF) configuration $\dots 0, \pi, 0, \pi, \dots$ while, for $h > 2$, all the spins are aligned along the field direction in a ferromagnetic configuration (F). For $h = 2$ there is an infinitely-degenerate multiphase point where it is possible to flip any number of non-adjacent spins in the F phase with no increase in energy; the phase diagram of Fig. 4.1 summarizes the situation.

In general, for finite values of the anisotropy, D , the spins may move from the Ising positions and the ground state must be found by solving the equilibrium equations

$$\frac{\partial \mathcal{H}}{\partial \theta_i} = 0. \quad (4.2)$$

To solve equations (4.2) for the infinite chain it is helpful to note that the ground state will be at most of period 2. Therefore any ground state can be completely described by giving the values of

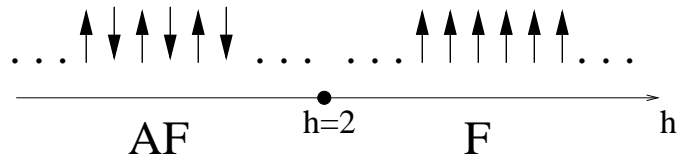


Figure 4.1: Schematic representation of the phase diagram for $D = \infty$. the F and AF labels denote the ferromagnetic and antiferromagnetic phases respectively. The point $(D = \infty, h = 2)$ is a multiphase point.

two consecutive spin angles: $\{\theta_1, \theta_2\}$. For $D > 2$ equations (4.2) can be satisfied only if

$$\{\theta_1, \theta_2\} = \{0, \pi\}, \quad h < 2, \quad (4.3)$$

$$\{0, 0\}, \quad h > 2 \quad (4.4)$$

exactly as for $D = \infty$. In other words there is a finite region of the phase diagram where the spins stay locked in their Ising positions. The occurrence of the spin locking is a common feature in models with two-fold spin anisotropy [65, 20]; here it implies that the degeneracy for $h = 2$ persists for all values of $D \in [2, \infty)$.

For $D < 2$ however, the softening of the spins stabilizes a third phase. Solving (4.2), we have

$$\{\theta_1, \theta_2\} = \{0, \pi\}, \quad h < \sqrt{D(4-D)}, \quad (4.5)$$

$$\{\bar{\theta}, -\bar{\theta}\}, \quad \sqrt{D(4-D)} < h < 4-D, \quad (4.6)$$

$$\{0, 0\}, \quad h > 4-D, \quad (4.7)$$

where $\cos \bar{\theta} = h/(4-D)$. The phase boundaries are represented in Fig. 4.2. Phase (4.6), where consecutive spins are symmetrically canted with respect to the field direction, is called the bulk spin-flop phase, SF .

4.2.1 Discommensuration phase diagram

To complete the study of the infinite chain we shall study the behaviour of a kink (or discommensuration) in the chain. This is important because the minimal energy discommensurations can provide information about the way a chain can distort under the effect of perturbations such as surface effects, thermal fluctuations etc. . We can enforce the presence of a discommensuration by choosing the following boundary conditions

$$\begin{cases} \lim_{n \rightarrow -\infty} \theta_{2n+1} = \theta_1 \\ \lim_{n \rightarrow -\infty} \theta_{2n} = \theta_2 \end{cases} \quad \begin{cases} \lim_{n \rightarrow +\infty} \theta_{2n+1} = \theta_2 \\ \lim_{n \rightarrow +\infty} \theta_{2n} = \theta_1 \end{cases} \quad (4.8)$$

As before it is useful to start the analysis of the discommensuration phase diagram by considering the case $D = \infty$.

For $0 < h < 2$ a discommensuration appears in the middle of the chain in the form of two successive spins pointing along the field, h , (we label this phase as AF'). Due to the absence of

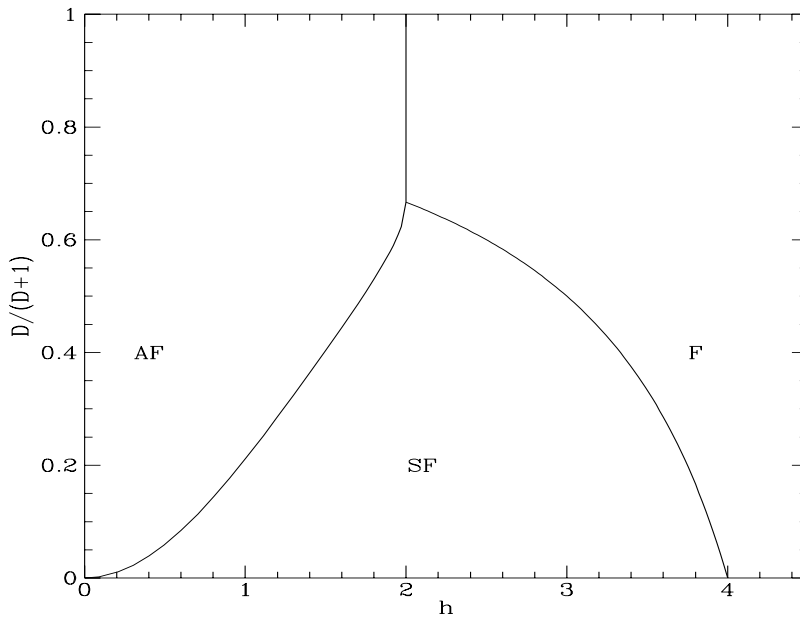


Figure 4.2: Phase diagram for an infinite chain. The *AF*, *F* and *SF* regions are occupied by the antiferromagnetic, ferromagnetic and spin-flop phases.

further-than-nearest-neighbours interactions, when $h = 2$ the ground state comprises configurations where the discommensuration is not limited to a pair of spins but can involve an arbitrary even number of them. On the other hand, for $h > 2$, the ground state corresponds to the ferromagnetic phase, where no discommensurations are present. The resulting discommensuration phase diagram for $D = \infty$ is summarised in Fig. 4.3.

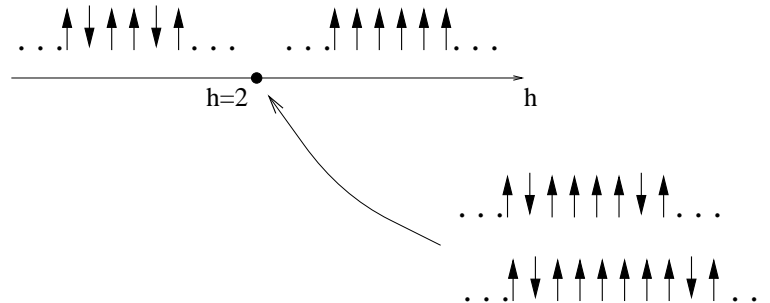


Figure 4.3: Schematic representation of the minimal-energy discommensuration phase diagram of an infinite chain for $D = \infty$.

Due to the lack of periodicity of a chain with a discommensuration, it is very difficult to find analytical solutions to the equilibrium equations (4.2) and one has to rely on numerical methods. The numerical procedure that we adopted is based on the Chou-Griffiths algorithm [63] which is very efficient for obtaining the ground state of models with short range interactions and discretized variables (we chose to discretize our spins with a step of $2\pi/1400$). The Chou-Griffiths algorithm is based on an energy minimization procedure which can always correctly identify the ground state

of the system except very close to phase boundaries, when it can yield metastable states which are mixtures of the phases coexisting at the boundaries. To overcome this potential problem we always used the Chou-Griffiths algorithm to identify the different phases sufficiently far away from any phase boundaries. Then the resulting minimal energy configurations for the discretized problem were used as starting points for the solution of the continuous recursion equations (4.2) and the phase boundaries followed from a comparison of the energies of neighbouring phases. Using the procedure outlined above we identified the minimal energy discommensurations by finding the ground state of a ring of spins of odd length, L with suitable boundary conditions. For large enough L (we used $L \leq 31$) this is practically equivalent to studying the minimal energy discommensuration in an infinite chain.

The numerical results, summarised in Fig. 4.4, reveal that in regions AF' and F , the spins stay locked in their $D = \infty$ positions.

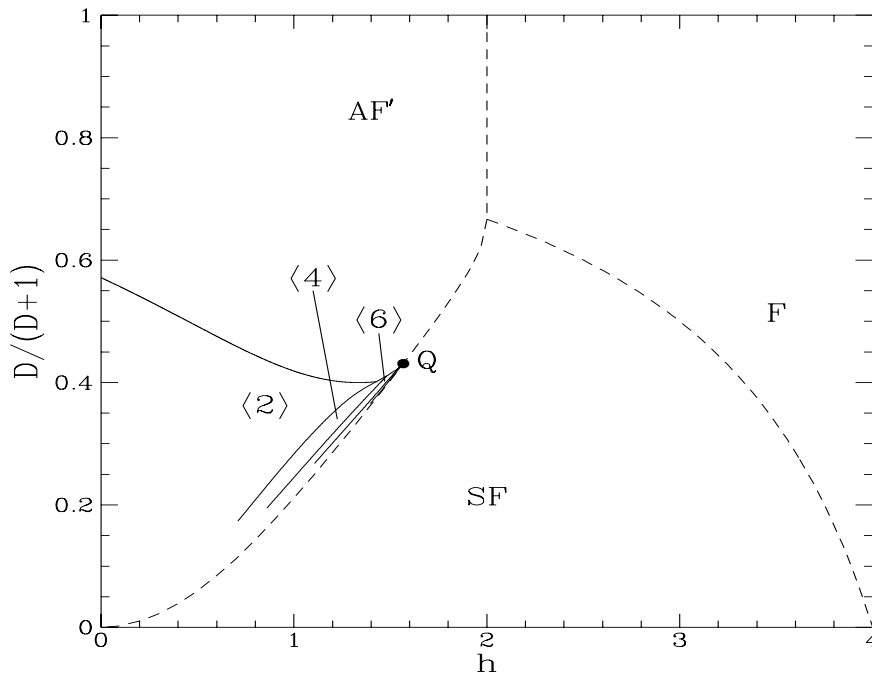


Figure 4.4: Discommensuration phase diagram for an infinite chain. The dashed phase boundaries corresponds to phase transitions in the discommensuration-free chain.

However, when D is sufficiently low, the spins cant from their Ising positions, θ_i^0 . The canting angle of the discommensuration spins from the field direction never exceeds $\pi/2$ and it oscillates with decreasing amplitude around zero when moving from the centre to the edge of the discommensuration.

The phases labelled $\langle 2m \rangle$ in Fig. 4.4 correspond to configurations of *softened* spins with a discommensuration of length $2m$ in the middle of the chain. For all phases the canting angle, defined

as

$$\tilde{\theta}_i = \theta_i - \theta_i^0, \quad (4.9)$$

decreases continuously to zero as the AF' boundary is approached from below. For sufficiently low D , for increasing values of the field, one observes a series of first order transitions $\langle 2m \rangle \rightarrow \langle 2m + 2 \rangle$. This sequence is probably infinite, although numerically we could only check that all phases $\langle 2m \rangle$ with m up to 7 enter. The point Q in Fig. 4.4 shows the location of the extrapolated accumulation point for the $\langle 2m \rangle \rightarrow \langle 2m + 2 \rangle$ transition at the boundary with phase AF' .

Some physical insight into the occurrence of this sequence of transitions can be gained by regarding the discommensuration in the $\langle 2m \rangle$ phases as resulting from inserting a segment of the spin-flop phase in the middle of an antiferromagnetic chain, as shown in Fig. 4.5.

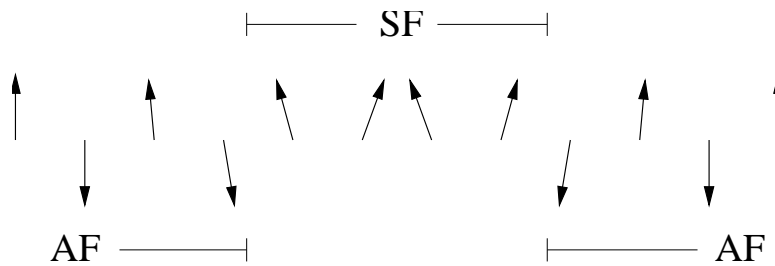


Figure 4.5: Schematic representation of phase $\langle 4 \rangle$. The phase can be regarded as resulting from merging a portion of the spin-flop phase (SF) with two semi-infinite antiferromagnetic chains (AF). The spins nearest the $AF - SF$ and $SF - AF$ interfaces are expected to relax from their ideal AF or SF angles.

Accordingly the discommensuration phase diagram of Fig. 4.4 can be conveniently explained by assuming that the two interfaces, $AF - SF$ and $SF - AF$ created by the introduction of the insertion, repel each other with a strength that decays rapidly with their separation. As the excess energy per spin of the metastable spin-flop phase decreases (i.e., moving towards the SF phase boundary) the ground state is attained for larger and larger interface separations. This is in agreement with the fact that the $\langle 2m \rangle : \langle 2m + 2 \rangle$ boundary is consistent for $m \rightarrow \infty$, with the bulk $AF - SF$ transition line. Finally, we notice that the introduction of a discommensuration in the bulk spin-flop phase, does not lead to the appearance of new phase transitions. We also note that limitations on numerical accuracy prevented us from following the phase boundaries for very low values of D . However, since the pinning energy of the discommensurations is not expected to vanish for $D > 0$, we believe that the boundaries persist all the way down to $D = 0$.

4.2.2 Analytical results for the $AF' - \langle 2 \rangle$ boundary

It is possible to obtain an analytic expression for the second-order boundary $AF' - \langle 2 \rangle$ in Fig. 4.4 by solving approximate equilibrium equations. In fact, close to the boundary the equilibrium equations (4.2) may be linearized to give

$$c_i(\tilde{\theta}_i - \tilde{\theta}_{i-1}) + c_{i+1}(\tilde{\theta}_i - \tilde{\theta}_{i+1}) = (hc_i^0 + D)\tilde{\theta}_i, \quad (4.10)$$

where $c_i = \cos(\theta_i^0 - \theta_{i-1}^0)$ and $c_i^0 = \cos(\theta_i^0)$.

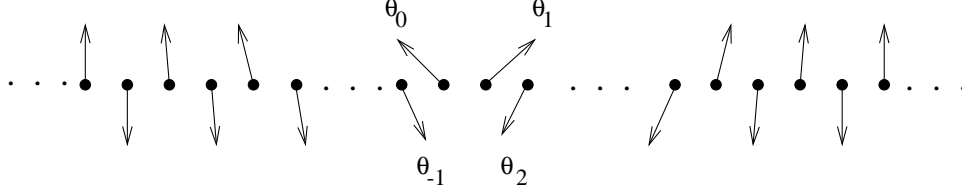


Figure 4.6: Schematic representation of the canted phase (2)

Now consider phase (2) with the spin labelling as in Fig. 4.6. If we introduce the quantity

$$x_i = \frac{\tilde{\theta}_i}{\tilde{\theta}_{i-1}}, \quad (4.11)$$

the equilibrium equations (4.10) can be written as

$$\frac{1}{x_{2j}} + x_{2j+1} = 2 + D + h; \quad j \leq -1, \quad (4.12)$$

$$\frac{1}{x_{2j+1}} + x_{2j+2} = 2 + D - h; \quad j \leq -1, \quad (4.13)$$

$$\frac{1}{x_0} - x_1 = D + h, \quad (4.14)$$

$$-\frac{1}{x_1} + x_2 = D + h, \quad (4.15)$$

$$\frac{1}{x_{2j}} + x_{2j+1} = 2 + D - h; \quad j \geq 1, \quad (4.16)$$

$$\frac{1}{x_{2j+1}} + x_{2j+2} = 2 + D + h; \quad j \geq 1. \quad (4.17)$$

Substituting (4.16) and (4.17) recursively into one another gives

$$\frac{1}{x_{2j}} = 2 + D - h - \frac{1}{2 + D + h - \frac{1}{2 - D - h - \frac{1}{2 + D + h - \dots}}} \equiv \frac{1}{s_2}; \quad j \geq 1, \quad (4.18)$$

$$\frac{1}{x_{2j+1}} = 2 + D + h - \frac{1}{2 + D - h - \frac{1}{2 - D + h - \frac{1}{2 + D - h - \dots}}} \equiv \frac{1}{s_1}; \quad j \geq 1. \quad (4.19)$$

where s_2 and s_1 satisfy

$$\begin{cases} \frac{1}{s_1} + s_2 = 2 + D + h \\ \frac{1}{s_2} + s_1 = 2 + D - h. \end{cases} \quad (4.20)$$

Similarly, from equations (4.12) and (4.13),

$$x_{2j+2} = \frac{1}{s_2}; \quad j \leq -1, \quad (4.21)$$

$$x_{2j+1} = \frac{1}{s_1}; \quad j \leq -1. \quad (4.22)$$

The quantities s_1 and s_2 which appear in (4.18)-(4.22) can be written explicitly in terms of D and h as

$$\begin{cases} s_1 = \frac{2(2+D-h)}{(2+D+h)(2+D-h) + \sqrt{(2+D+h)^2(2+D-h)^2 - 4(2+D+h)(2+D-h)}} , \\ s_2 = \frac{(2+D+h)}{2} + \frac{\sqrt{(2+D+h)^2(2+D-h)^2 - 4(2+D+h)(2+D-h)}}{2(2+D-h)} . \end{cases} \quad (4.23)$$

When equations (4.21) and (4.22) are substituted into (4.14) and (4.15) we obtain

$$\begin{aligned} s_2 - x_1 &= D + h \\ -\frac{1}{x_1} + s_2 &= D + h \end{aligned} \quad (4.24)$$

Comparing (4.24) with (4.20) and invoking the requirement that the modulus of s_1 and s_2 cannot exceed 1 (so that the spin deviations decay to zero infinitely far from the discommensuration) gives

$$\frac{1}{D+h-1} = 5/3 + D - h \quad (4.25)$$

Equation (4.25) identifies the locus of points where the spin deviations for phase $\langle 2 \rangle$ are vanishingly small, that is the second-order boundary $AF' - \langle 2 \rangle$. The strategy outlined above can, in principle, be extended to calculating the general $AF' - \langle 2m \rangle$ phase boundary. However, for $m > 2$, the phase boundaries $AF' - \langle 2m \rangle$ do not have a simple expression and therefore we will not pursue the calculation any further.

4.3 Semi-infinite chains

Now we move on to study the case of semi-infinite chains. Consider a point (D, h) that does not lie on a phase boundary of the Hamiltonian (4.1), so that the ground state of the infinite chain is unique. Cutting the chain in two without allowing the spins to move will give two semi-infinite chains that we shall term unreconstructed. If the spins of the unreconstructed chains are then allowed to relax, a rearrangement of the spins near the surface may take place.

The phenomenon of surface reconstruction is rather common in nature, and can be observed in a variety of contexts ranging from rearrangements of atoms near the surface of a crystal [66, 67, 68], to the transitions of materials from solid to liquid [69, 70]. In this section we will show how the occurrence of a surface reconstruction can remove the multidegeneracy present for large values of D by stabilizing discommensurations at different distances from the surface.

First of all we notice that, since the surface reconstruction usually occurs only over a finite portion of the chain the spins angles sufficiently far away from the surface will be, essentially, those pertaining to the infinite chain.

We start by considering a point (D, h) that lies in the ferromagnetic phase of Fig. 4.2. In this case one can check that the surface does not reconstruct, since the spins prefer to stay locked along the field direction. However, if (D, h) lies in the antiferromagnetic region for the infinite

chain the situation is more complicated. As before it is helpful to consider $D = \infty$ first. Since the antiferromagnetic ground state of the infinite chain has period 2 there will be two different classes of reconstructed ground states, A and B , whose underlying unreconstructed structures are, respectively,

$$A_u = \{0, \pi, 0, \pi, 0, \pi, \dots\}, \quad (4.26)$$

$$B_u = \{\pi, 0, \pi, 0, \pi, 0, \dots\}. \quad (4.27)$$

The ground state of class A remains unreconstructed throughout the region $0 < h < 2$. However, for class B a reconstruction occurs for $1 < h < 2$, because it becomes energetically favourable to introduce a discommensuration into the chain in the form of two successive spins pointing along the field, h

$$B_r = \{0, 0, \pi, 0, \pi, 0, \pi, \dots\}. \quad (4.28)$$

The discommensuration can be moved away from the surface by an even number of steps without changing the energy. This leads to a multidegeneracy in the interval $1 < h < 2$. At this stage it is convenient to introduce a notation to distinguish between the degenerate configurations. We shall use $[2n]$ to denote the ground state belonging to class B with a discommensuration of length 2 whose first spin is at a distance $2n$ from the surface.

For ($D > 2, h = 2$), there is an additional increase in degeneracy since here class B also includes ground states where the discommensuration is not limited to a pair of spins but can involve an arbitrary even number of them (for example $\{0, 0, 0, 0, \pi, 0, \pi, \dots\}$ or $\{0, \pi, 0, \pi, 0, 0, 0, 0, 0, \pi, 0, \pi, \dots\}$).

To study the phase transition of the chain of class B for finite values of D we used the following numerical procedure. We first started by considering the case of discretized spins (the step was typically chosen to be $2\pi/1400$). Since the θ_i 's are constrained to take on only discrete values, after a finite distance, d , from the surface (which we will refer to as reconstruction penetration depth) the spins will be *exactly* in the discretized positions for the unreconstructed chain. These were found by using the Floria-Griffiths algorithm [71, 72] which, within the limits of the discretization, yields the exact ground state for an infinite chain of spins.

For a fixed value of the penetration length, d , and for each class of ground states we used the Chou-Griffiths algorithm [63, 72] to generate all the reconstructed surface configurations $\{\theta_0, \theta_1, \dots, \theta_d\}$ satisfying the recursion equations (4.2). In principle the ground state is chosen by comparing the energies of the semi-infinite chains with all the generated reconstructed surfaces of any penetration length, d . From a practical point of view we had to restrict d to be $\leq d_{max} = 50$, so that this numerical scheme will lead the correct ground state only if its penetration depth does not exceed d_{max} .

Once the ground state structure was identified, the continuous recursion equations (4.2) were solved for the corresponding phase to give the $\{\theta_i\}$'s and the energy calculated from the Hamiltonian

$$\mathcal{H} = \sum_{i=0}^{\infty} \left\{ \cos(\theta_i - \theta_{i+1}) - h \cos \theta_i + \frac{D}{4} [1 - \cos(2\theta_i)] \right\} \quad (4.29)$$

Phase boundaries followed from a comparison of the energies of neighbouring states. The resulting phase diagram is shown in Fig. 4.7.

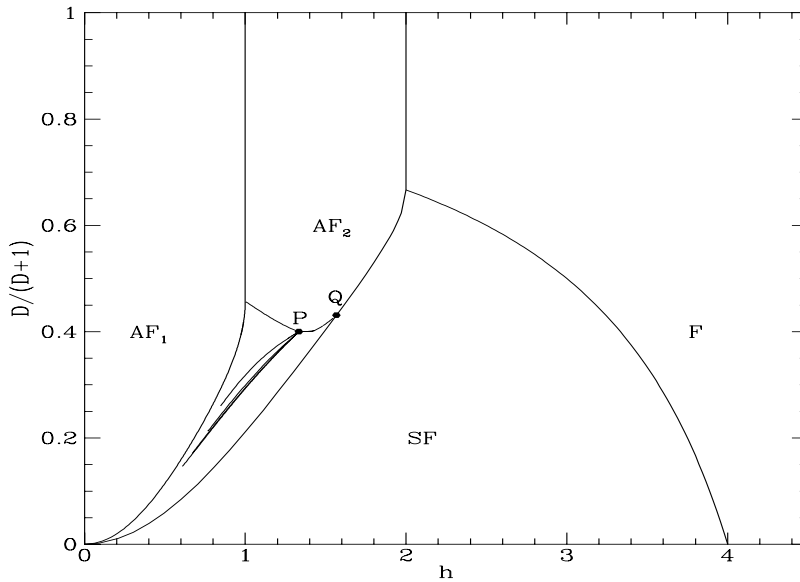


Figure 4.7: Phase diagram for the semi-infinite chain.

In region AF_1 in Fig. 4.7 the chain is unreconstructed, while region AF_2 is occupied by the locked $[2m]$ phases. As a result of the spin locking the multidegeneracy encountered for $D = \infty$ persists throughout the AF_2 region. However, outside the AF_1 and AF_2 domains the spins of configuration $[2n]$ appear to soften with their canting angles from the Ising positions decreasing continuously to zero as the point P of Fig. 4.8 is approached from below.

As a consequence of the softening the multidegeneracy of phase AF_2 is removed and, as found by Trallori *et al.* [56] the surface spin flop sequence of transitions $[2m] \rightarrow [2m+2]$ is stabilized as h is increased. The sequence is probably infinite, although this could not be confirmed by analytical calculations. Numerically we have checked that all phases $[2m]$ with $m \leq 7$ enter. Moreover numerical results show that the boundaries between the different interface phases end in critical points which were identified as the point where both the energy and the energy derivative with respect to h of two neighbouring phases vanishes, as shown in Fig. 4.9.

The sequence of surface phase transitions can be described in terms of an effective interaction between the surface and the discommensuration of length 2. Upon increasing the field h the attractive interaction energy between the discommensuration and the surface becomes weaker and phases $[2n]$ with larger n are stabilized. In the region between the accumulation boundary of the surfaces spin-flop transitions and the SF boundary, the penetration depth of the reconstructed surface diverges,

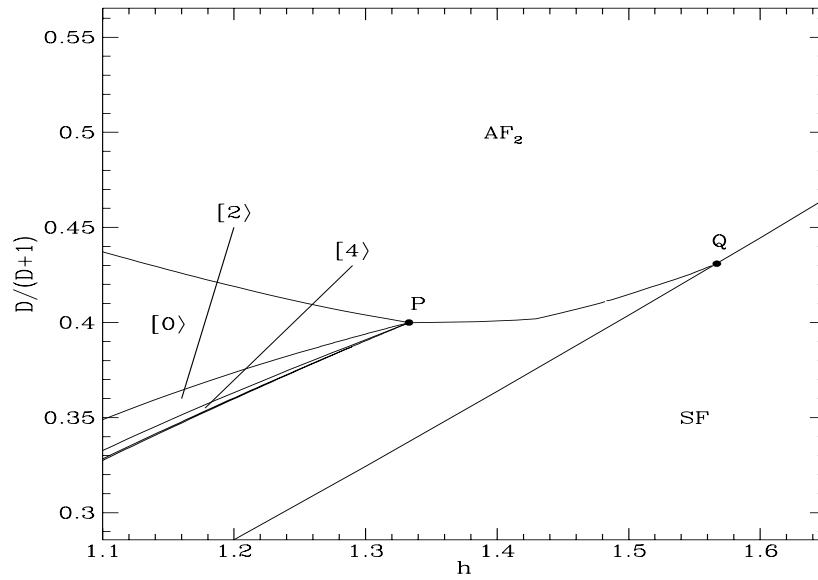


Figure 4.8: Close up of the phase diagram of Fig. 4.7 near the multiphase point, P .

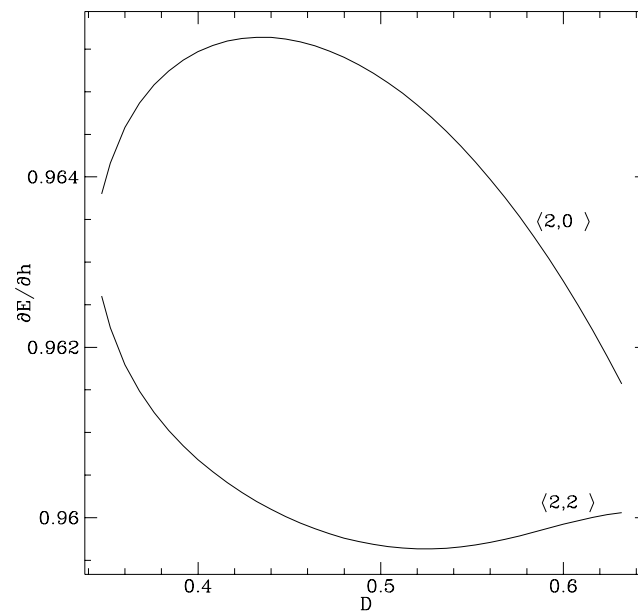


Figure 4.9: Plot of energy derivatives along the $\langle 2,0 \rangle - \langle 2,2 \rangle$ boundary.

and it is not appropriate to speak of the existence of a surface of class B .

We conclude the description of the phase diagram by noting that both classes of chains undergo a surface reconstruction when (D, h) is in the spin-flop region of the infinite chain. In fact, the spins nearest the surface tend to deviate from the bulk spin-flop positions to align along the field. However, as the parameters (D, h) are varied, the surface spins' deviations change smoothly, and no phase transition is observed. This explains why Trallori *et al.* did not observe the SSF transitions for very low values of the spin anisotropy [61].

We can summarize schematically the results for the semi-infinite chain in the following way:

ground state of class A

- No surface reconstruction occurs in the AF and F regions of Fig. 4.2.
- Although a surface reconstruction occurs in the SF region this does not lead to any new phase being stabilized.
- The phase boundaries are the same as for the infinite chain.

ground state of class B

- No surface reconstruction in F region of Fig. 4.2.
- The surface reconstruction in the SF region does not stabilize any new phase.
- In the AF region of Fig. 4.2 we can identify four regions where the chain has different behaviour

region 1 (labelled AF_1 in Fig. 4.7) The surface is unreconstructed.

region 2 (labelled AF_2 in Fig. 4.7) The surface reconstructs by introducing a discommensuration of even length in the chain. The discommensurations can be placed at arbitrary even distance from the surface and the spins are locked in the Ising positions.

region 3 is occupied by the sequence of softened $[2m]$ phases. This corresponds to the surface spin-flop (SSF) region.

region 4 is the region on the right of the accumulation boundary of the SSF sequence. Here the surface reconstruction length is divergent.

In the following section we show analytically that the multiphase point exists and identify its co-ordinates.

4.4 Analytical results

4.4.1 The multiphase point

Using a self-consistent analytical calculation analogous to the one used in section 4.2.2 it is possible to identify the co-ordinates of P . Guided by numerical calculations we assume the existence of a point P such that as $(D, h) \rightarrow P$ the spin deviations, $\{\tilde{\theta}_i\}$, of all phases $[2n)$ tend continuously to zero. Sufficiently close to P the recursion equations (4.2) may be linearised to give

$$\begin{aligned} c_i(\tilde{\theta}_i - \tilde{\theta}_{i-1}) + c_{i+1}(\tilde{\theta}_i - \tilde{\theta}_{i+1}) &= (hc_i^0 + D)\tilde{\theta}_i ; \quad i > 0, \\ c_1(\tilde{\theta}_0 - \tilde{\theta}_1) &= (hc_0^0 + D)\tilde{\theta}_0 , \end{aligned} \quad (4.30)$$

where $c_i = \cos(\theta_i^0 - \theta_{i-1}^0)$ and $c_i^0 = \cos(\theta_i^0)$.

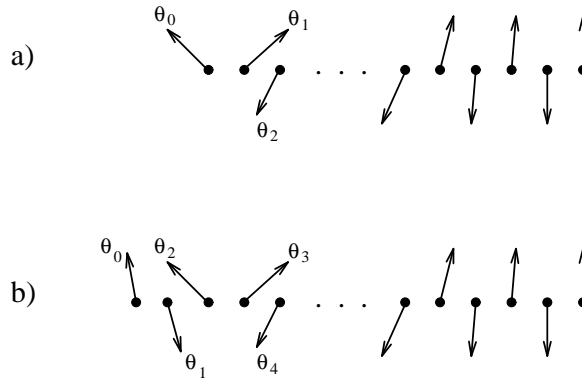


Figure 4.10: Schematic representation of phases $[0)$ and $[2)$.

Now consider phase $[0)$, as represented in Fig. 4.10a. Using the recursion equations (4.30) for $i = \{0, 1\}$ and adopting the notation introduced in section 4.2.2 one has

$$x_1 = 1 - h - D , \quad (4.31)$$

$$-\frac{1}{x_1} + s_2 = h + D . \quad (4.32)$$

Solving (4.31) and (4.32) explicitly for s_2 gives

$$s_2 = h + D + \frac{1}{1 - h - D} . \quad (4.33)$$

The second equation in (4.23) also provides another relation for s_2 which can be satisfied simultaneously with (4.33) only on the locus of points, Γ , defined by the equation

$$\frac{1}{2 + D - h - 1/a} = 2 + D + h - a \quad (4.34)$$

where $a = h + D + 1/(1 - h - D)$. Γ corresponds to the locus where the spin deviations for phase $[0)$ are vanishingly small. In other words equation (4.34) defines the second order phase boundary $[0) - AF_2$.

Now we carry on our analysis assuming that, in agreement with the initial assumption, for some point(s) P on Γ the angular deviations $\tilde{\theta}_i$'s for phase $[2]$ (see Fig. 4.10b) are vanishingly small so that we may linearize the recursion equations (4.30). The explicit relations (4.30) for $i = \{0, 1, 2, 3\}$ are

$$-\frac{1}{x_3} + s_2 = h + D, \quad (4.35)$$

$$\frac{1}{x_2} - x_3 = h + D, \quad (4.36)$$

$$\frac{1}{x_1} + x_2 = 2 + D - h \quad (4.37)$$

$$x_1 = 1 + D + h \quad (4.38)$$

Some algebra shows that equations (4.35)-(4.38) can be solved consistently with (4.33) only if

$$1 + D + h = \frac{1}{1 + D - h} . \quad (4.39)$$

The only point where equations (4.39) and (4.34) hold simultaneously is $P \equiv (h = 4/3, D = 2/3)$. Moreover, near the point $(h = 4/3, D = 2/3)$, the spin deviations for all the remaining phases, $[2n]$, $n \geq 2$, are also vanishingly small. Therefore we can conclude this self-consistent analysis by saying that $P = (h = 4/3, D = 2/3)$ is a multiphase point. The result is in agreement with the numerical co-ordinates for P , $(D = 0.6666, h = 1.333)$.

4.4.2 Layering transitions

Unlike the case discussed in Chapter 2, the quadratic approximation of the Hamiltonian (4.29) is not sufficient to yield the leading order expressions for the spin deviations (although it gives us information about the ratio of successive spin deviations). Nevertheless, numerical results show that, close to P , the spin deviations at the discommensurations are the same for all phases $[2m]$. If we assume that this numerical picture is correct, we can use a scheme analogous to the one adopted in Chapter 2 to find the leading order energy difference of neighbouring phases, $\Delta E_n = E_{[2n]} - E_{[2n+2]}$, near the multiphase point. Within the quadratic approximation one obtains

$$\Delta E_n \approx \frac{1}{2}(\tilde{\theta}_1 - \tilde{\theta}_0)^2 + \frac{1}{2}(\tilde{\theta}_2 - \tilde{\theta}_1)^2 + \frac{1}{2}D(\tilde{\theta}_1^2 + \tilde{\theta}_0^2) - \frac{1}{2}h(\tilde{\theta}_1^2 - \tilde{\theta}_0^2) \quad (4.40)$$

where the $\tilde{\theta}_i$'s are the spin deviations of phase $[2n+2]$. The expression for ΔE_n can be somewhat simplified by using relations (4.10) for $i = \{0, 1\}$ to express $\tilde{\theta}_1$ and $\tilde{\theta}_2$ in terms of $\tilde{\theta}_0$. By substituting

$$\begin{aligned} \tilde{\theta}_1 &\approx (1 + D + h)\tilde{\theta}_0 , \\ \tilde{\theta}_2 &\approx \left(2 + D - h - \frac{1}{1 + D + h}\right)\tilde{\theta}_1 , \end{aligned} \quad (4.41)$$

into (4.40) one has

$$\Delta E_n = \left(\frac{2D + 7D^2 + 5D^3 + D^4 + 2Dh}{2} + \frac{D^2h - h^2 - 5Dh^2 - 2D^2h^2 - h^3 + h^4}{2} \right) \tilde{\theta}_0^2 + \mathcal{O}(\tilde{\theta}_0^3) \quad (4.42)$$

It is important to stress that, for general n , expression (4.42) is valid *only* close to the multiphase point. In fact, near P , the deviations of all the spins in the chain are vanishingly small. However, it can be noticed that the surface-spin deviations of phases with very large surface-discommensuration separation will be small throughout the surface-spin flop (SSF) region. In other words the energy difference of phases $[2n\rangle$ and $[2n+2\rangle$, in the limit $n \rightarrow \infty$, is given by (4.42) for *all* values of D and h in the SSF region. This observation has an important consequence since the expression for ΔE_n can be used to determine the accumulation boundary of the SSF series.

In fact, when crossing this boundary, the discommensuration, which is infinitely far away from the surface, changes from being attracted to being repelled by the surface. The change of sign of the surface-kink interaction is, in turn, related to the change of sign of ΔE_n . Despite the complicated form of equation (4.42), the set of physically meaningful roots of the equation $\Delta E_{n \rightarrow \infty} = 0$ has a simple expression,

$$D = \sqrt{1 + h^2} - 1. \quad (4.43)$$

Near the multiphase point, P , equation (4.43) can be linearised in $\epsilon_D \equiv D - 2/3$ and $\epsilon_h \equiv h - 4/3$ to give

$$\epsilon_h = 5/4\epsilon_D. \quad (4.44)$$

This result is in agreement with the equation for the accumulation boundary extrapolated from our numerical calculations. On the other hand, near the point ($D = 0, h = 0$), the asymptotic equation for the boundary becomes

$$D = \frac{h^2}{2}, \quad (4.45)$$

which, in turn, is in agreement with the numerical results obtained by Trallori *et al.* for $D \approx 1/100$ [61].

4.5 Finite chain

For a finite chain of length L , the surface reconstruction can occur at both ends. If L is sufficiently large that we can neglect the interaction between the two ends of the chain the total energy of the chain can be written as

$$E = L\epsilon + E_s^L + E_s^R + E_d \quad (4.46)$$

where ϵ is the bulk energy per spin, E_s^L and E_s^R are the energies of the left and right surfaces respectively, and E_d is the energy of a discommensuration in the chain (if present). If L is sufficiently large, the energy minimization problem consists finding the spin configuration that minimizes $E_s^L + E_s^R + E_d$.

Except for very large D , when spin locking occurs, the minimization of (4.46) cannot be done analytically and, therefore, we relied on the Chou-Griffiths algorithm to find the minimal energy configurations of the chain (we used L up to 31).

Since the detailed behaviour of the ground state depends explicitly on the length of the chain, L , we cannot present the phase diagram for a chain of arbitrary finite length. Nevertheless, it is possible to identify regions of the (h, D) plane where the qualitative behaviour of finite chains is the same. A description of the behaviour of the system in the different regions is summarised below.

In the spin-flop and ferromagnetic regions the minimization is obtained with two surfaces of type A (no discommensuration). In the AF region the situation is more complex and we need to treat separately the cases of a chain of even and odd length.

Chain of odd length

- The ground state has two surfaces of type A, no phase transition is observed as D and h are varied.

Chain of even length The behaviour of the chain differs according to which of the regions introduced on page 52 we consider.

- **region 1** One surface is of type A, the other of type B. The spins are locked in the Ising positions.
- **region 2** Due to the spin locking, all states with a discommensuration of even length are degenerate.
- **region 3** The ground state exhibits a softened discommensuration of length 2 that nucleates from the surface and, for increasing values of the field, migrates to the middle of the chain with discontinuous jumps. This is the finite-size analogue of the layering transition observed in the semi-infinite chain.
- **region 4** The discommensuration, lying in the middle of the chain, increases its size discontinuously. This second sequence of first order transitions, which can be regarded as a truncated version of the $\langle 2m \rangle \rightarrow \langle 2m + 2 \rangle$ transitions of Fig. 4.4, has not been identified before.

The very rich behaviour of a chain of spins of even length is clearly illustrated by the plot of Fig. 4.11 which portrays the behaviour of the magnetic susceptibility $\chi = dm/dh$ for a chain of 22 spins when $D = 1/2$. The spikes appearing in Fig. 4.11 should be Dirac delta functions. Here they appear to have a finite height because of the finite incremental step δh chosen for the numerical calculation.

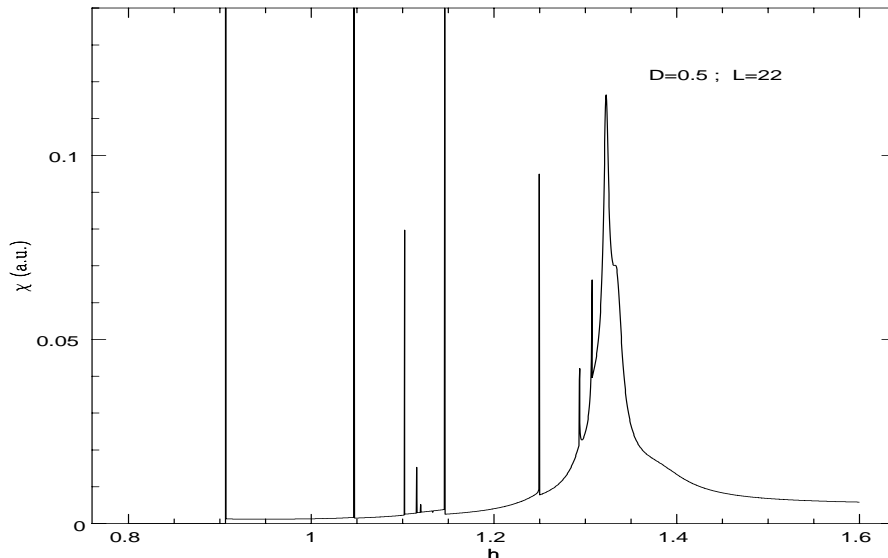


Figure 4.11: Plot of the susceptibility (in arbitrary units) for a chain of 22 spins for $D = 0.5$.

The first spike in Fig. 4.11 (for $h \approx 0.9$) signals the transition from the locked AF_1 phase (where χ is exactly equal to zero) into the surface spin-flop region, more precisely into phase $[0]$. The first series of spikes, encountered in the interval $h \in (0.9, 1.13)$ is associated with the truncated surface spin-flop transitions while the second one, for $h \in (1.13, 1.32)$, reflects the discontinuous increase of the discommensuration width.

For sufficiently low values of D one expects to observe fewer phases, because of the presence of the critical points. This is precisely what happens as shown in the plot of χ for $D=0.3$ in Fig. 4.12.

4.6 Conclusions

To summarize, we have presented numerical and analytical evidence that, for the semi-infinite, antiferromagnetic, classical XY chain, the surface spin-flop transition comprises a sequence of phases springing from a single multiphase point with associated phase boundaries that end in critical points. We have also clarified the mechanism of the crossover between the surface spin-flop and the bulk spin-flop states by identifying a new sequence of first-order transitions associated with discontinuous rearrangements of the spins in the middle of the chain.

It would be very interesting to try to detect the new sequence of transitions in $Fe/Cr(211)$ superlattices. However, the susceptibility measurements performed nowadays with Kerr techniques (usually adopted in these circumstances [52, 53]) are plagued by a relatively high noise to signal ratio and, therefore the achievable resolution might not be sufficient to study the second type of transitions. In addition, since Kerr-based investigation methods are especially sensitive to surface magnetization,

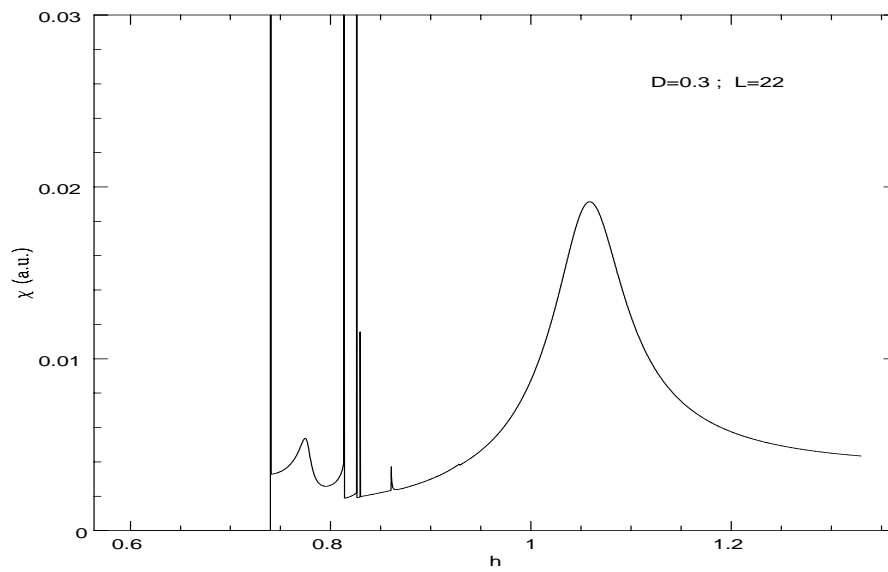


Figure 4.12: Plot of the susceptibility (in arbitrary units) for a chain of 22 spins for $D = 0.3$.

they may not be optimal to reveal the discontinuous increase in size of the discommensuration in the middle of the chain.

Chapter 5

Quantum fluctuations in the ANNNI model

5.1 Introduction

There are many naturally occurring examples of uniaxially modulated structures. For instance, the spatial modulation observed in polytypic materials is associated with the stacking of one or more structural units. In the case of *SiC*, the closed packed layers of the material can be stacked in three different ways to give rise to a multitude of different structures with period up to 100 layers [73]. Other examples include samples of binary alloys [74, 75] like *TiAl₃* where experiments have revealed the presence of periodically spaced two-dimensional flat antiphase boundaries. As the temperature is varied in the range 600 – 1200 *K*, the periodic arrangement of the antiphase boundaries changes discontinuously and up to 15 modulated phases have been identified [76].

The variety of modulated structures observed in polytypes, binary alloys, magnetic systems etc. can all be successfully explained in terms of arrays of interacting domain walls or, depending on context, antiphase boundaries, defects, solitons etc. [5, 77, 78]. When the domain-wall energy is small, wall–wall interactions become important in determining the spacing of the walls and small changes in the external parameters can stabilise many different modulated phases.

A model which has proved very useful for understanding this process is the axial next-nearest neighbour Ising or ANNNI model which is an Ising system with first- and second-neighbour competing interactions along one lattice direction [3, 79, 80, 81]. At zero temperature the ANNNI model has a multiphase point where an infinite number of phases are degenerate, corresponding to zero domain wall energy. At low temperature entropic fluctuations cause domain wall interactions which stabilize a sequence of modulated structures [7, 9]. A slightly modified version of the model, which was originally introduced by R. Elliott in connection with rare-earth magnetism [3, 21], has been

used by Uimin and Pokrovsky [82, 83, 84] to explain the periodic magnetic structures observed in cerium monopnictides like *CeSb* and *CeBi* [1, 2, 85, 86].

However, one of the reasons for the popularity of the ANNNI model lies in the fact that it can be mapped onto a one-dimensional system of interacting domain walls. This allows the use of the model to describe, in terms of pseudospins, the uniaxially modulated structures observed in a variety of materials like *TiAl₃*, *Cu₃Pd*, *SiC* and spinelloids [87, 79, 88, 89, 90].

In this Chapter we will use a formalism similar to the one adopted in Chapter 3 to approach a more complicated problem: the effect of quantum fluctuations in a generalised ANNNI model, where the multiphase point is a point of infinite degeneracy for bulk rather than interface phases. We show that quantum fluctuations, like thermal ones, do indeed remove the infinite degeneracy near the multiphase point of the classical model. A sequence of first order transitions is stabilized in a way qualitatively similar to the finite temperature behaviour but involving a different sequence of phases. However, we will show that, for long-period phases, entropic and quantum fluctuations behave in a subtly different way.

5.2 The model

The Hamiltonian we consider is

$$\mathcal{H} = -\frac{J_0}{S^2} \sum_{i\langle jj' \rangle} \mathbf{S}_{i,j} \cdot \mathbf{S}_{i,j'} - \frac{J_1}{S^2} \sum_{i,j} \mathbf{S}_{i,j} \cdot \mathbf{S}_{i+1,j} + \frac{J_2}{S^2} \sum_{i,j} \mathbf{S}_{i,j} \cdot \mathbf{S}_{i+2,j} - \frac{D}{S^2} \sum_{i,j} ([S_{i,j}^z]^2 - S^2), \quad (5.1)$$

where i labels the planes of a cubic lattice perpendicular to the z -direction and j the position within the plane. Also $\langle jj' \rangle$ indicates a sum over pairs of nearest neighbours in the same plane and $\mathbf{S}_{i,j}$ is a quantum spin of magnitude S at site (i, j) . All the spin interactions, J_i in (5.1) are assumed positive, so that the inter-plane coupling for nearest and second-nearest neighbours is ferromagnetic and antiferromagnetic respectively, while the in-plane coupling is ferromagnetic (see Fig. 5.1). The parameter, D , in (5.1) controls the strength of the two-fold anisotropy of the spins.

For $D = \infty$, only the states $S_i^z = \sigma_i S$, where $\sigma_i = \pm 1$ are allowed and \mathcal{H} reduces to the standard ANNNI model [3, 79].

$$\mathcal{H}_A = -J_0 \sum_{i\langle jj' \rangle} \sigma_{i,j} \sigma_{i,j'} - J_1 \sum_{i,j} \sigma_{i,j} \sigma_{i+1,j} + J_2 \sum_{i,j} \sigma_{i,j} \sigma_{i+2,j}. \quad (5.2)$$

The ground state of the ANNNI model is ferromagnetic for $\kappa \equiv J_2/J_1 < 1/2$ while, for $\kappa > 1/2$, the ground state displays an antiphase structure with layers ordering in the sequence $\{\sigma_i\} = \{\dots 1, 1, -1, -1, 1, 1, -1, -1 \dots\}$. $\kappa = 1/2$ is a multiphase point [6, 7, 91]. In fact, it turns out that all phases consisting of a sequence of domains of 2 or more parallel spins with alternate orientation are degenerate at the point $\kappa = 1/2$.

At this stage it is useful to introduce a notation to distinguish between the degenerate phases. We will use the notation $\langle n_1, n_2, \dots, n_m \rangle$ to denote a state consisting of domains of parallel spins

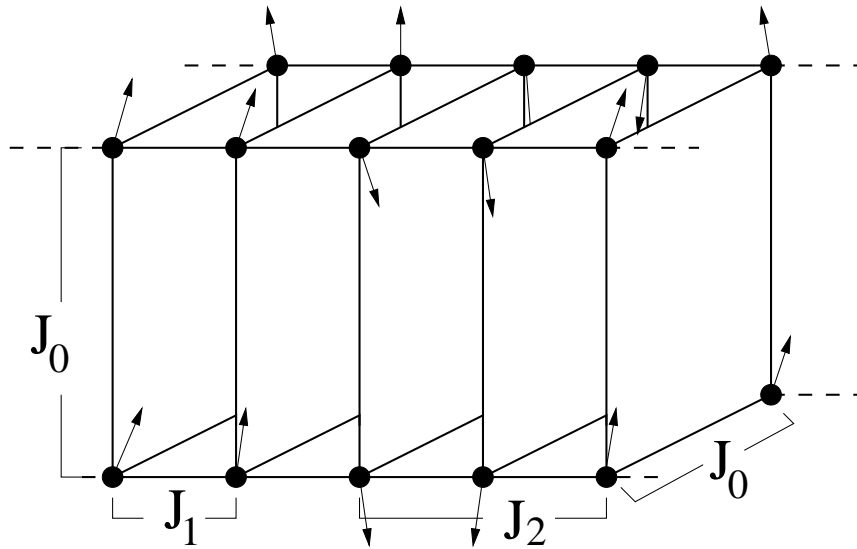


Figure 5.1: Schematic representation of the model (5.1).

Figure 5.2: Schematic representation of the phase diagram of the model (5.1) for $D = \infty$. The region $J_2/J_1 < 1/2$ is occupied by the homogeneous phases: all spins up or all spins down. For $J_2/J_1 > 1/2$ the ground state has period 4. At the point $J_2/J_1 = 1/2$ an infinite degeneracy is encountered.

with alternate orientation whose widths repeat periodically the sequence $\{n_1, n_2, \dots, n_m\}$ so that, for $\kappa > 1/2$ the ground state is $\langle 2 \rangle$, while the labelling $\langle \infty \rangle$ is consistently used to denote the homogeneous ground state (all spins up or all down) for $\kappa < 1/2$. Although this definition applies to the $D = \infty$ case, it can be used also for lower values of D , provided the spins deviations from the Ising positions are sufficiently small. The phase diagram, for $D = \infty$ is sketched in Fig. 5.2. In 1980 Fisher and Selke [6, 91] showed that thermal fluctuations can raise the degeneracy at the multiphase point. However, it was not until the introduction of the wall-wall interaction formalism by Fisher and Szpilka (in this context a wall separates two opposite domains of parallel spins) that the qualitative features of the phase diagram were fully understood. Fisher and Szpilka showed that, for a given (low) temperature, only a finite sequence of phases is stabilized by thermal fluctuations. For lower values of temperature, more phases are observed, as shown in Fig. 5.3.

For classical spins, $S = \infty$, at zero temperature one expects that spin softening controlled by an anisotropy parameter, D , can remove the multidegeneracy in a way similar to thermal fluctuations. However, for other models with two-fold spin anisotropy (see Chapters 2, 4), for large enough values of D the spins remain locked in their Ising positions, which implies a persistence of multidegeneracy as D is reduced from ∞ . As shown in the numerical phase diagram of Fig. 5.4 the multidegeneracy is removed only for D lower than 0.36. The interesting question is then whether for quantum spins (finite S) the persistence of multidegeneracy is not observed. Indeed we will show that quantum fluctuations remove the multidegeneracy as soon as D is reduced from infinity.

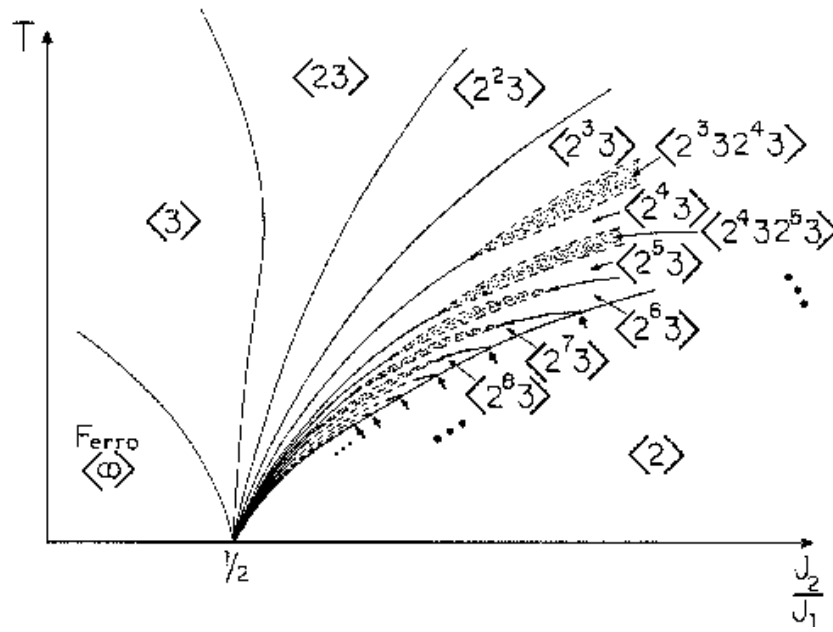


Figure 5.3: In the classical ANNNI model the multidegeneracy at the point $\kappa = 1/2$ is lifted by thermal fluctuations (after A. M. Szpilka [5]).

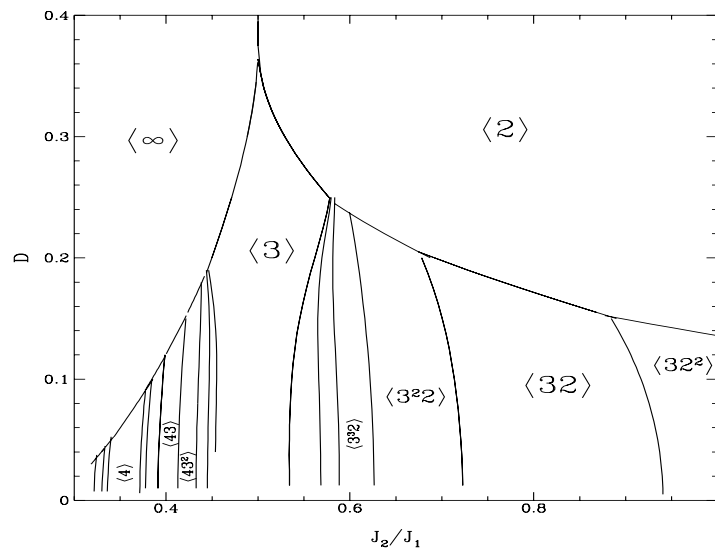


Figure 5.4: Phase diagram from the *classical* version of Hamiltonian (5.1) at zero temperature the multidegeneracy for $J_2/J_1 = 1/2$ is lifted only for $D \lesssim 0.36$ (after F. Hadrović [92]).

5.3 Perturbation expansion

To study the effect of quantum fluctuations near the multiphase point ($D = \infty, \kappa = 1/2$) we use the Dyson-Maleev [26, 27] transformation (introduced in Chapter 2) to recast the Hamiltonian (5.1) into bosonic form (working to lowest order in $1/S$) with the result

$$\mathcal{H}(\{\sigma_i\}) = E_0 + \mathcal{H}_0 + V_{\parallel} + V_{\parallel\!}, \quad (5.3)$$

where $E_0 \equiv \mathcal{H}_A$,

$$\begin{aligned} \mathcal{H}_0 &= \sum_{i,j} \left[2\tilde{D} + J_1 \sigma_{i,j} (\sigma_{i-1,j} + \sigma_{i+1,j}) - J_2 \sigma_{i,j} (\sigma_{i-2,j} + \sigma_{i+2,j}) \right] S^{-1} a_{i,j}^+ a_{i,j} \\ &\equiv \sum_{i,j} E_{i,j} S^{-1} a_{i,j}^+ a_{i,j}, \end{aligned} \quad (5.4)$$

with $\tilde{D} = D + 2J_0$ and V_{\parallel} ($V_{\parallel\!}$) is the interactions between spins which are parallel (antiparallel)

$$V_{\parallel} = \frac{1}{S} \sum_{i,j} \left[-J_1 X(i, i+1; j) (a_{i,j}^+ a_{i+1,j} + a_{i+1,j}^+ a_{i,j}) + J_2 X(i, i+2; j) (a_{i,j}^+ a_{i+2,j} + a_{i+2,j}^+ a_{i,j}) \right] \quad (5.5)$$

$$V_{\parallel\!} = \frac{1}{S} \sum_{i,j} \left[-J_1 Y(i, i+1; j) (a_{i,j}^+ a_{i+1,j}^+ + a_{i+1,j} a_{i,j}) + J_2 Y(i, i+2; j) (a_{i,j}^+ a_{i+2,j}^+ + a_{i+2,j} a_{i,j}) \right], \quad (5.6)$$

where $X(i, i'; j)$ [$Y(i, i'; j)$] is unity if spins (i, j) and (i', j) are parallel [antiparallel] and is zero otherwise. In other words $V_{\parallel\!}$ creates/destroys a pair of excitations on either sides of a wall, while V_{\parallel} hops the excitation within a domain of parallel spins. The impossibility of creating two excitations in the same domain or hopping an excitation past a domain wall is a consequence of the conservation of the total magnetization.

We do not consider quantum fluctuations within a plane, since the phase diagram is determined by the interplanar quantum couplings. Moreover we shall work to leading order in $1/S$, in which case four-operator terms can be neglected. As for the models considered in Chapters 2 and 3 we shall use non-degenerate perturbation theory, since the perturbative term ($V_{\parallel} + V_{\parallel\!}$) cannot connect states in which the wall is at different locations, since such states have different values of $\sum_i S_i^z$.

5.4 The wall-wall interaction formalism

Using the wall-wall interaction formalism we will construct the phase diagram by considering in turn E_w , the energy of an isolated domain wall, $V_2(n)$, the interaction energy of two walls separated by n sites, and generally $V_k(n_1, n_2, \dots, n_{k-1})$, the interaction energy of k walls with successive separations n_1, n_2, \dots, n_{k-1} . In terms of these quantities one may write the total energy of the system, when there are N_w walls with separation $\{n_1, n_2, \dots, n_{N_w-1}\}$, as [77, 78]

$$E = E_0 + N_w E_w + \sum_i V_2(n_i) + \sum_i V_3(n_i, n_{i+1})$$

$$+ \sum_i V_4(n_i, n_{i+1}, n_{i+2}) + \dots, \quad (5.7)$$

where E_0 is the energy with no walls present.

5.4.1 Two-wall interactions

Typically, for models with short range interactions, the wall-wall interactions decay very rapidly (usually exponentially) as a function of the separation of the walls [5, 10]. For this reason one usually starts the analysis of the phase diagram neglecting interactions that involve more than two walls. Higher order interactions can be included later on to resolve the finer details of the phase diagram. In the two domain-wall interaction approximation, equation (5.7) simplifies to

$$E = E_0 + N_w E_w + \sum_i V_2(n_i). \quad (5.8)$$

Because we are considering only $V_2(x)$, the walls must be equispaced in the ground state [12]. For a given wall equispacing, n , the energy per spin is

$$e_n = e_0 + \frac{E_w + V_2(n)}{n} \quad (5.9)$$

where e_0 is the energy per spin with no walls in the system. To identify which wall equispacing is observed in the ground state for given values of J_2 , J_1 and \tilde{D} we need to find the wall separation, n^* , which minimizes e_n . n^* can be conveniently found using the simple geometrical construction described below [5, 10].

Given the value of E_w (determined by the value of J_2 , J_1 and \tilde{D}), consider the line of minimal slope that passes through the point $(0, -E_w)$ and touches the (discrete) curve $V_2(x)$. The abscissa of the intersection point, P , between V_2 and the line gives the value n^* , as sketched in Fig. 5.5a.

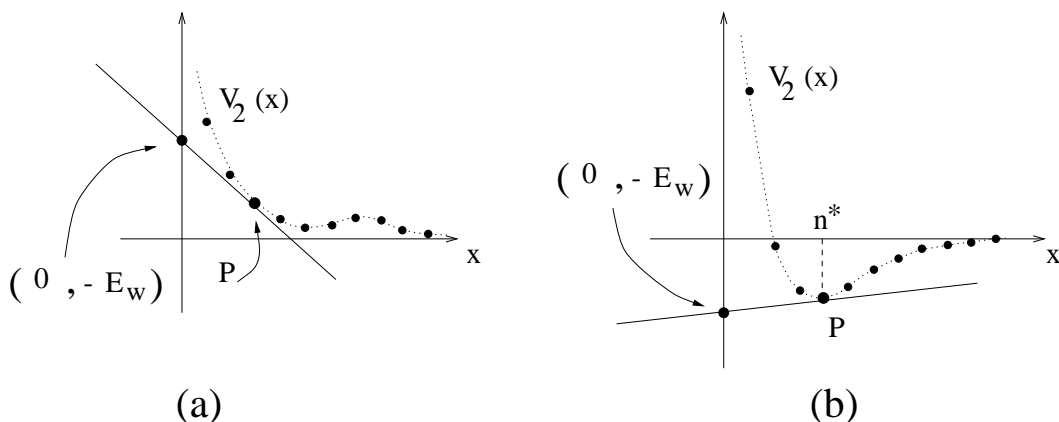


Figure 5.5: Examples of the use of the lowest tangent construction to find the wall equispacing in the case where a) $V_2(x)$ is always positive, b) $V_2(x)$ has a negative minimum.

Naturally, a variation of E_w (i.e. a variation of the parameters of the model) can cause a discontinuous change in the value of n^* . The precise sequence of phases observed as a function

of E_w will depend on the form of $V_2(n)$. First of all we notice that, in the absence of long-range interactions (as in our case) the wall-wall interactions, V_k , must go to zero as the spacing of the walls goes to infinity. When $D = \infty$, it is not difficult to check that the V_k 's are identically zero for all values of the wall separations. In particular

$$V_2(n) = 0 \quad \forall n. \quad (5.10)$$

In this case, when $E_w = 0$ (which occurs for $J_2/J_1 = 1/2$) all values of n minimize (5.9), in agreement with the fact that ($D = \infty, J_2/J_1 = 1/2$) is a multiphase point.

When D is relaxed from infinity we expect that $V_2(n)$ acquires a dependence on n since quantum fluctuations are likely to introduce a weak coupling between walls. The effective coupling can be either repulsive for all n (so that $V_2(n)$ is positive definite, as in Fig. 5.5a) or have one or more attractive parts, as in Fig. 5.5b. It is important to distinguish between the sign of $V_2(n)$ as this dramatically affects the sequence of phases observed as E_w is varied.

In fact, if $V_2(x)$ is always positive (see Fig. 5.5a), one realizes that, as E_w is increased from negative to positive, one passes through an infinite sequence of states

$$\langle n_1 \rangle \rightarrow \langle n_2 \rangle \rightarrow \langle n_3 \rangle \rightarrow \dots \langle \infty \rangle \quad (5.11)$$

where the n_i 's increase monotonically. In principle, one cannot expect the wall spacing to increase by one lattice unit at a time in the sequence (5.11). This will occur only if $V_2(x)$ is convex. On the other hand, if the two-wall potential is not convex, some of the points of $V_2(x)$ will never be touched by the geometrical construction, as is the case for some of the points lying on the "bump" of $V_2(x)$ in Fig. 5.5a. Consequently the wall spacing associated with the points "in shade" will never be observed in the ground state.

The situation is very different if $V_2(x)$ becomes negative for some values of x , as in Fig. 5.5b. In this case all the points of $V_2(x)$ that lie on the right of the negative minimum, $V_2(n^*)$, cannot be reached by the construction of the lower tangent. Hence, as E_w is varied, the infinite sequence of phases in (5.11) is replaced by a finite one that ends with a first order transition from $\langle n^* \rangle$ to the homogeneous phase $\langle \infty \rangle$.

It is important to mention that, for models with short range interactions, as in this case, the rapid decay (usually exponential) of $V_2(x)$ as a function of x , ensures that phases with larger domain-wall spacing will occupy smaller regions of the phase diagram. In fact, using equation (5.9) it is possible to calculate the width of the region of stability of phase $\langle n \rangle$ in terms of variation of the wall energy

$$\Delta E_w = n \left[V_2(n-1) - 2V_2(n) - V_2(n+1) \right]. \quad (5.12)$$

5.4.2 Three-wall interactions

We have shown that if for finite D the wall-wall interaction $V_2(n)$ is not identically zero for all values of n , then some of the phases that were degenerate at the multiphase point will occupy a finite region of the phase diagram. However, the original multidegeneracy present at the multiphase point is not entirely lifted by $V_2(n)$. To see this consider two neighbouring phases $A = \langle n_1 \rangle$ and $B = \langle n_2 \rangle$. Using (5.8) it is easy to check that, on the phase boundary $A|B$, all mixed phases (i.e. phases where the walls can be separated by distances n_1 or n_2) are degenerate. This is illustrated in Fig. 5.6a for the case of the mixed phase $AB = \langle n_1, n_2 \rangle$. If we switch on the three-wall interaction V_3 , the excess energy per spin phase $\langle n_1, n_2 \rangle$ on the $A|B$ boundary is given by

$$\Delta e = \frac{V_3(n_1, n_2) + V_3(n_2, n_1) - V_3(n_1, n_1) - V_3(n_2, n_2)}{n_1 + n_2} \quad (5.13)$$

Depending on the form of V_3 , the expression (5.13) can be positive or negative. In the first case the energy curve of the mixed phase, E_{AB} is shifted to higher energies with respect to E_A and E_B , as in Fig. 5.6b, so that a first-order line separates A from B . The inclusion of higher-order interactions, V_n , provided they decay sufficiently rapidly as a function of n , cannot possibly modify the first-order nature of the transition. Therefore the residual multidegeneracy is completely lifted and the analysis can stop.

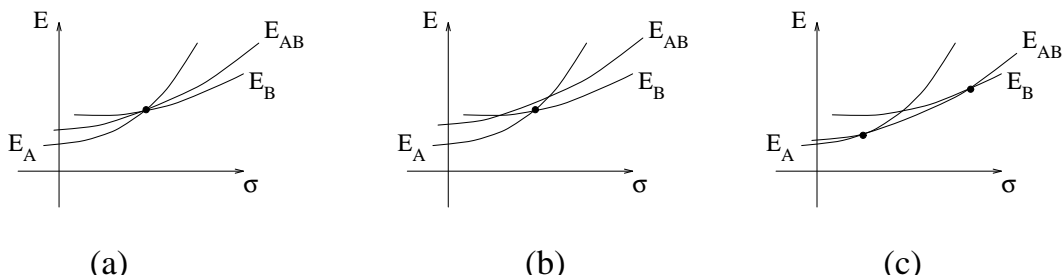


Figure 5.6: (a) In the two wall-interaction approximation, the $A|B$ boundary is multidegenerate (E_x denotes the energy of phase x). The introduction of three walls interaction can remove partially the degeneracy shifting the energy curve of the mixed phase AB (b) above or (c) below the energy curves for the A and B phases.

On the other hand, if E_{AB} is shifted to lower energies, as in Fig. 5.6c then the mixed phase will occupy a finite portion of the phase diagram

$$\langle n_1 \rangle | \langle n_1, n_2 \rangle | \langle n_2 \rangle . \quad (5.14)$$

In this case, a residual multidegeneracy is still present on the two new boundaries $\langle n_1 \rangle | \langle n_1, n_2 \rangle$ and $\langle n_1, n_2 \rangle | \langle n_2 \rangle$. The stability of the new boundaries with respect to the mixed phases on must be studied by including V_4 and so forth.

5.4.3 The reconnection formulae

The applicability of the analysis of the phase diagram based on the domain wall interactions is ultimately limited by the feasibility of the calculation of the general k -wall interaction term, V_k . Such a calculation can be performed, at least in principle, using the powerful and elegant reconnection formulae, introduced by Bassler *et al.* [12]. Now we illustrate the application of this method in the context of the spin model we are studying.

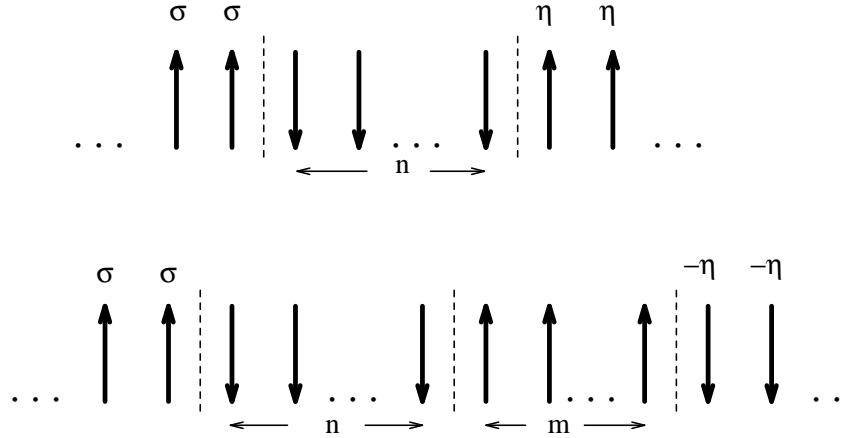


Figure 5.7: Configurations needed to calculate the interaction energy for two walls at separation n (top) and three walls at separation n and m (bottom). When $\sigma + 1$ ($\eta = +1$) the left-most (right-most) wall is positioned as shown. When $\sigma = -1$ ($\eta = -1$) the left-most (right-most) wall does not exist.

Let all spins to the left of the first wall have $\sigma_i = \sigma$ and those to the right of the last wall have $\sigma_i = \eta$ for k even and $\sigma_i = -\eta$ for k odd, as in the example of Fig. 5.7. We denote the energy of such a configuration as $E_k(\sigma, \eta)$. Noting that, if $\sigma = -1$ ($\eta = -1$) the left (right) wall is absent, we can write $E_k(\sigma, \eta)$ explicitly in terms of the V 's as follows

$$\begin{aligned}
 E_k(1, 1) &= E_0 + kE_w + \sum_{i=1}^{k-1} V_2(n_i) + \sum_{i=1}^{k-2} V_3(n_i, n_{i+1}) + \dots + V_k(n_1, \dots, n_{k-1}) \\
 E_k(1, -1) &= E_0 + (k-1)E_w + \sum_{i=1}^{k-2} V_2(n_i) + \sum_{i=1}^{k-3} V_3(n_i, n_{i+1}) + \dots + V_{k-1}(n_1, \dots, n_{k-2}) \\
 E_k(-1, 1) &= E_0 + (k-1)E_w + \sum_{i=2}^{k-1} V_2(n_i) + \sum_{i=2}^{k-2} V_3(n_i, n_{i+1}) + \dots + V_{k-1}(n_2, \dots, n_{k-1}) \\
 E_k(-1, -1) &= E_0 + (k-2)E_w + \sum_{i=2}^{k-2} V_2(n_i) + \sum_{i=2}^{k-3} V_3(n_i, n_{i+1}) + \dots + V_{k-2}(n_2, \dots, n_{k-2})
 \end{aligned} \tag{5.15}$$

Thus the energy ascribed to the interaction of k walls is given by the reconnection formula

$$V_k(n_1, n_2, \dots, n_{k-1}) = E_k(1, 1) - E_k(1, -1) - E_k(-1, 1) + E_k(-1, -1) = \sum_{\sigma, \eta = \pm 1} \sigma \eta E_k(\sigma, \eta) . \tag{5.16}$$

We note that terms in E_k which are independent of σ or η do not influence V_k . In our perturbative scheme we will calculate $E_k(\sigma, \eta)$ by developing the energy in powers of the perturbations V_{\parallel} which

allows creation (and annihilation) of a pair of excitations straddling a wall and $V_{||}$ which allows the excitations to hop within domains. In the following we shall consider contributions to the wall energy and to two- and three-wall interactions in turn.

5.5 Wall energy

Contributions to the wall energy to second order in perturbation theory arise from excitations which are created at a wall and then immediately destroyed as shown in Fig. 5.8. These effectively count the number of walls and therefore lead to a renormalization of the wall energy of

$$E_w = 2J_1 - 4J_2 - \frac{J_1^2 - 2J_2^2}{4\tilde{D}S} + \mathcal{O}\left(\frac{J^3}{\tilde{D}^2S}\right). \quad (5.17)$$

Expression (5.17) shows that when $J_2 \lesssim J_1/2 - J_1/(32\tilde{D}S)$, E_w is positive and therefore the stable phases is the homogeneous one, $\langle \infty \rangle$. Outside the region $J_2 \lesssim J_1/2 - J_1/(32\tilde{D}S)$ it is convenient to introduce domain walls in the system, and long-period modulated phases will be stabilized by wall-wall interactions, as we will see in the next sections. The width of the regions, in the phase diagram, where the modulated structures are stable will be estimated using expression (5.17).

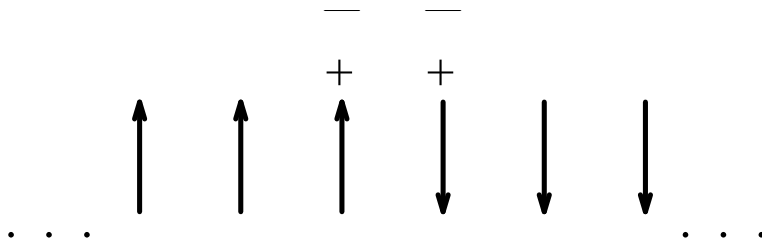


Figure 5.8: The contribution from second order perturbation theory which renormalizes the wall energy. + (−) denotes the creation (destruction) of a spin excitation by $V_{||}$.

5.6 Two-wall interactions

The lowest order contributions to $V_2(n)$ are obtained by creating an excitation at, say, the left wall using $V_{||}$ and then using $V_{||}$ for it to hop to the right wall and back. Because we assume the existence of the left wall, this contribution implicitly includes a factor $\delta_{\sigma,1}$ (see Fig. 5.7). Now we look for the lowest-order (in J/D) terms which also have a dependence on η (otherwise, according to equation (5.16), we will have a zero contribution to V_2). In analogy with the unbinding problem of Chapter 2, we might consider processes in which the excitation hops beyond the position of the wall. Since such a term can not occur when the wall is actually present, it will carry a factor $\delta_{\eta,-1}$. For n odd, we illustrate this process in Fig. 5.9, and see that it gives a contribution to $V_2(n)$ of order J_2^{n+1}/D^n .

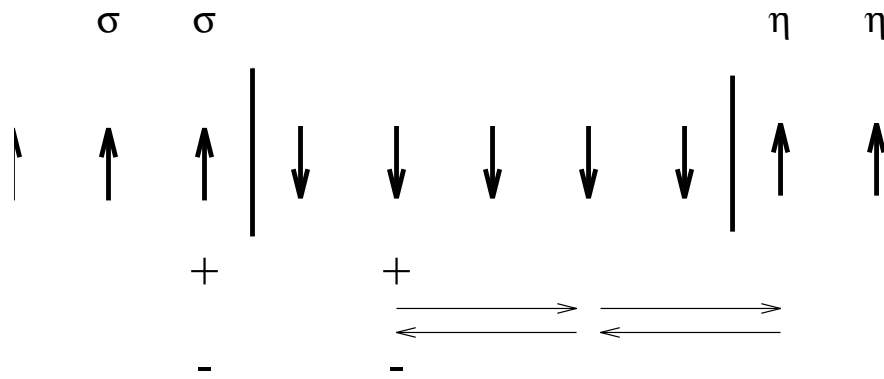


Figure 5.9: Contribution to the two-wall interaction $V_2(n)$ for $n = 5$ in analogy with the unbinding problem of Chapter 2. This process exists only when $\eta = -1$ and contributes to $V_2(5)$ at order J_2^6/D^5 .

As we shall see, there is actually a slightly different process which comes in at one order lower in J/D . To sense the presence of the right-hand wall, note that $E_{i,j}$ in equation (5.4) will depend on η if the i is within two sites of the wall. Therefore it is only necessary to hop to within two sites of the right wall, as shown in Fig. 5.10, for an energy denominator $(\mathcal{H}_0 - E_0)$ in the series expansion (2.37) to depend on η . This process is of lower order in J/D because it takes two interactions to

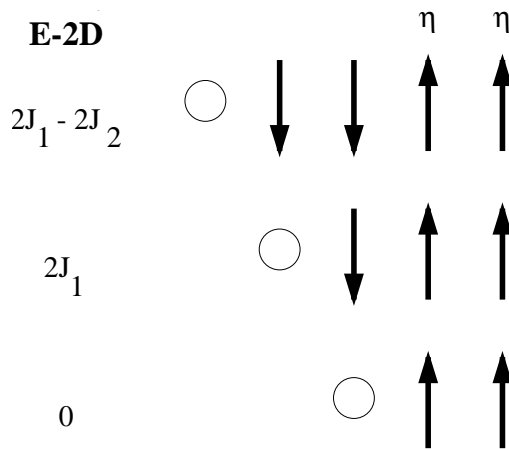


Figure 5.10: The energy, E , of an excitation as a function of position near a wall. We list $E - 2\tilde{D}$ when the excitation is created at the circled site. Thus, when the excitation is further-than-next-nearest-neighbouring to the domain wall, its energy is $E = 2\tilde{D} + 2J_1 - J_2$. If it lies on a site second-neighbouring to the wall one has $E = 2\tilde{D} + 2J_1 - J_2(1 - \eta)$ and, when nearest neighbouring, $E = 2\tilde{D} + (J_1 - J_2)(1 - \eta)$.

hop back and forth but only one to sense the potential via an energy denominator. Accordingly, in contrast to the interface unbinding considered in Chapter 2, it is necessary to retain the terms in the J 's in the energy denominators to obtain the leading order contribution to $V_2(n)$. We consider separately n odd and n even.

n odd

To lowest order the processes which contribute are those shown in Fig. 5.11a. For a domain of n

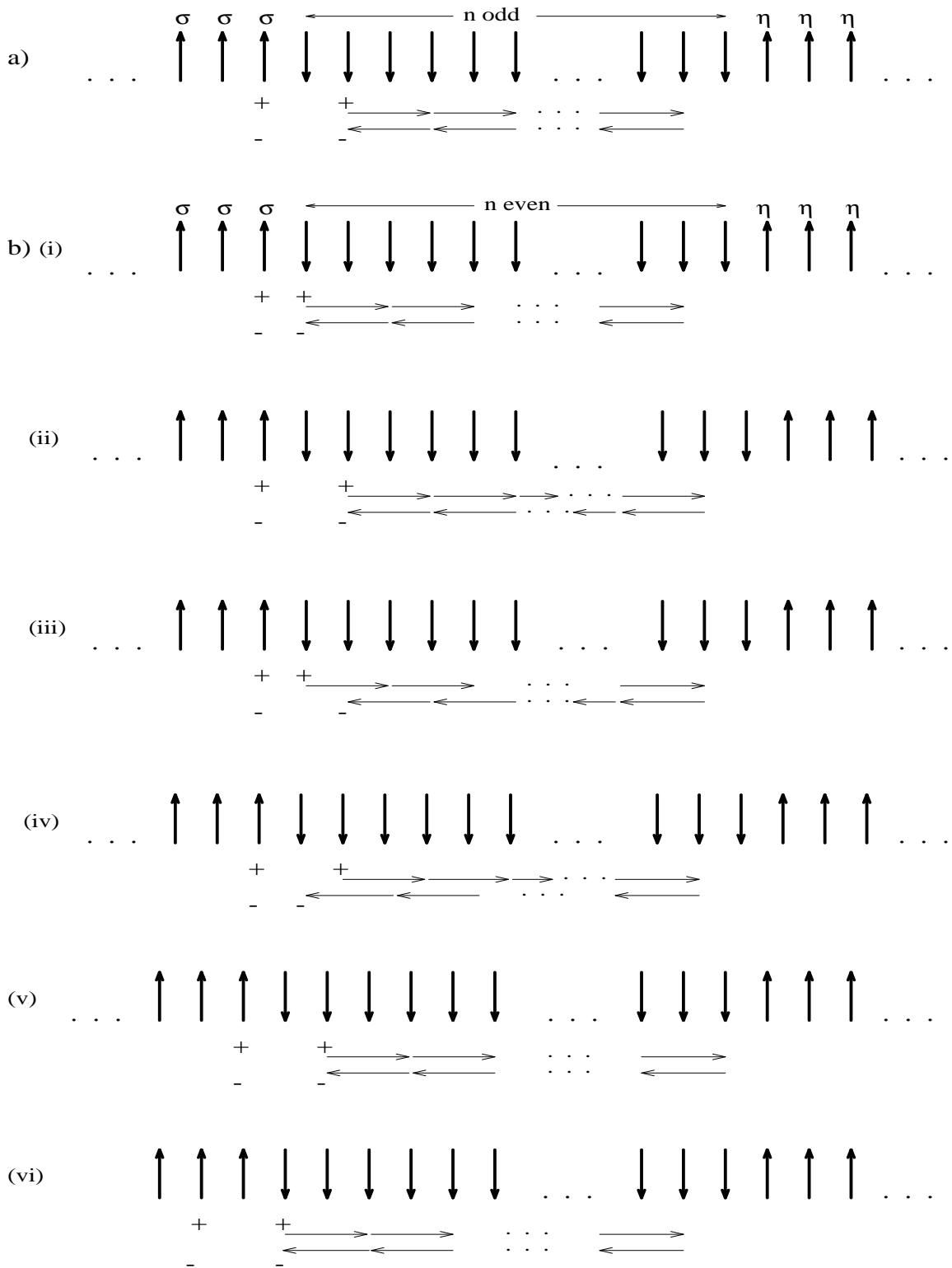


Figure 5.11: Excitations which contribute to the 2-wall interaction $V_2(n)$ for (a) n odd and (b) n even. + (-) denotes the creation (destruction) of a spin excitation by V_{\parallel} . An arrow denotes a hop mediated by V_{\parallel} .

spins with $\sigma_i = -1$, $(n-1)$ th order perturbation theory gives

$$E_2(\sigma, \eta) = 2\delta_{\sigma,1} J_2^{n-1} S^{-1} (-1)^{n-2} \{4\tilde{D} + 2J_1\}^{-2} \{4\tilde{D} + 2J_1 - 2J_2\}^{-(n-5)} \\ \times \{4\tilde{D} + 2J_1 - J_2(1-\eta)\}^{-1}. \quad (5.18)$$

In writing this result we dropped all lower-order terms because they do not depend on both σ and η . Here and below, the dependence on σ is contained in the factor $\delta_{\sigma,1}$ because we assume the existence of the left-hand wall. The energy denominators are constructed as follows. The left-hand excitation has energy $2\tilde{D}$ since it is next to a wall. The right-hand excitation has an energy which depends on its position as illustrated in Fig. 5.10. The prefactor of 2 arises because the initial excitation can be near either wall and the overall factor $(-1)^{n-2}$ arises from the (-1) associated with each energy denominator. Adding the contributions from (5.18) appropriately weighted as in (5.16) gives

$$V_2(n) = \frac{2J_2^{n-1} S^{-1} (-1)^{n-2}}{\{4\tilde{D} + 2J_1\}^2 \{4\tilde{D} + 2J_1 - 2J_2\}^{n-5}} \left\{ \frac{1}{4\tilde{D} + 2J_1} - \frac{1}{4\tilde{D} + 2J_1 - 2J_2} \right\} \quad (5.19)$$

$$= 4J_2^n S^{-1} / (4\tilde{D})^{n-1} + \mathcal{O}(1/\tilde{D}^n), \quad n \text{ odd}. \quad (5.20)$$

Note that there is no term $\mathcal{O}(1/\tilde{D}^{n-2})$. This is because to this order the energy denominators are independent of the J 's. Hence to this order $E_k(\sigma, \eta)$ is independent of η and the sum in equation (5.16) is zero. Similarly terms from n th order perturbation theory (in which one J_2 hop is replaced by two J_1 hops) do not contribute $\mathcal{O}(1/\tilde{D}^{n-1})$.

n even

For even n several diagrams contribute to leading order, i. e., at n th order perturbation theory. These are shown in Fig. 5.11b. As an example we give the contributions to the energy from the diagram (b)(iii). Again we drop all terms which do not depend on both σ and η . Thus

$$E_2^{(\text{iii})}(\sigma, \eta) = 2(-1)^{n-1} \delta_{\sigma,1} \left(\frac{n-2}{2} \right) J_1^2 J_2^{n-2} S^{-1} (4\tilde{D})^{-1} (4\tilde{D} + 2J_1)^{-1} \\ (4\tilde{D} + 2J_1 - 2J_2)^{-(n-4)} [4\tilde{D} + 2J_1 - J_2(1-\eta)]^{-1}, \quad (5.21)$$

where the superscript (iii) indicates a contribution from diagram (iii) of Fig. 5.11, the prefactor 2 comes from including the contribution of the mirror image diagram, the prefactor $(-1)^{n-1}$ is the sign of n th order perturbation theory, the factor $(n-2)/2$ is the number of places the single (J_1) hop can be put, and $\delta_{\sigma,1}$ indicates that this contribution assumes the existence of the left-hand wall. To leading order in \tilde{D} , the η -dependence is contained in

$$E_2^{(\text{iii})}(\sigma, \eta) = (-1)^{n-1} (n-2) \delta_{\sigma,1} J_1^2 J_2^{n-2} S^{-1} (4\tilde{D})^{-(n-2)} (4\tilde{D} + \eta J_2)^{-1} \\ \approx (-1)^n (n-2) \eta \delta_{\sigma,1} J_1^2 J_2^{n-2} S^{-1} (4\tilde{D})^{-n} J_2. \quad (5.22)$$

Using equation (5.16) we get

$$V_2^{(\text{iii})} = 2(n-2) J_1^2 J_2^{n-1} S^{-1} (4\tilde{D})^{-n}. \quad (5.23)$$

We treat the other diagrams of Fig. 5.11 similarly. Dropping terms which do not depend on both σ and η and working to lowest order in $(\tilde{D})^{-1}$, gives

$$E_2(\sigma, \eta) = \eta \delta_{\sigma,1} J_2^{n-2} S^{-1} (4\tilde{D})^{-n} \left[2J_1^2 J_2 + \frac{1}{2} J_1^2 (n-2)^2 J_2 \right. \\ \left. + (n-2) J_1^2 J_2 + (n-2) J_1^2 J_2 + 2J_2^2 (J_2 - J_1) + 2J_2^2 J_2 \right], \quad (5.24)$$

where the contributions are from each diagram of Fig. 5.11, written in the order in which they appear in the figure. Thus for n even gives

$$V_2(n) = S^{-1} (4\tilde{D})^{-n} J_2^{n-2} \left[4J_1^2 J_2 + J_1^2 J_2 (n-2)^2 + 4(n-2) J_1^2 J_2 + 4J_2^2 (J_2 - J_1) + 4J_2^3 \right] \\ = \frac{J_2^{n-1}}{(4\tilde{D})^n S} (n^2 J_1^2 - 4J_1 J_2 + 8J_2^2), \quad n \text{ even.} \quad (5.25)$$

As explained in section 5.2 it is possible to determine graphically the sequence of phases entering the phase diagram by constructing the lower convex envelope of $V_2(n)$ versus n [77, 78]. The points $(n, V_2(n))$ which lie on the envelope correspond to stable phases. The pair interactions defined by the expressions (5.20) and (5.25) correspond to a convex function for $n \ll (\tilde{D}/J)^{1/2}$. Hence, in this regime, we expect, within the two-wall approximation, a sequence of phases $\langle 2 \rangle, \langle 3 \rangle, \langle 4 \rangle, \dots$ as shown schematically in Fig. 5.12.

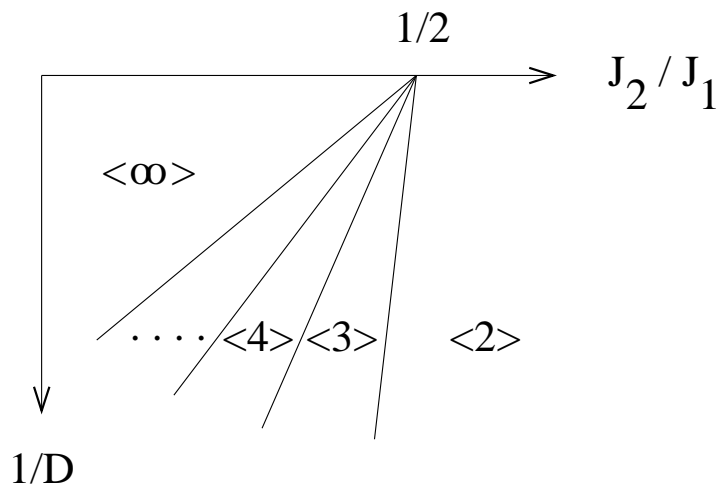


Figure 5.12: Schematic phase diagram of the generalised quantum ANNNI model (5.1) in the limit of strong uniaxial spin anisotropy D .

The widths of the phases $\langle n \rangle$ can be estimated using the fact that each phase is stable over an interval $\Delta E_w = n[V_2(n-1) - 2V_2(n) - V_2(n+1)]$ [77, 78]. Therefore, using (5.17) we find that the width $\Delta(J_2/J_1)$ occupied by the phase $\langle n \rangle$ in Fig. 5.12 is $\mathcal{O}((J_2/D)^{n-1})$ for n odd and $\mathcal{O}((J_2/D)^{n-2})$ for n even.

This sequence of layering through unitary steps $\langle n \rangle \rightarrow \langle n+1 \rangle$ will not be obeyed for large n , i. e., for $n \sim (\tilde{D}/J)^{1/2}$, because then $V_2(n)$ will suffer from strong even-odd oscillations that will alter

its convexity. Moreover, for large n , the entropy of more complicated perturbations may dominate the physics. The large n limit behaviour of $V_2(n)$ can be found using Green's function techniques [93]. Within this framework one is able to account for the entropic contributions of terms where the right-most excitation (see Fig. 5.11) is allowed to wander between domain walls, and the left-most one is held fixed (non-propagation limit). The detailed analysis, carried out by A. B. Harris, is too long to be reproduced here and can be found in ref. [20]. The resulting expression for $V_2(n)$ is

$$\begin{aligned} V_2(n) &= \frac{16D'}{S\lambda^n} \left(\sin^2[n\delta + 4\delta^3] - (3/8)(J_2/D')^3 \right), \quad n \text{ even}; \\ &= \frac{16D'}{S\lambda^n} \left(\cos^2[n\delta + 4\delta^3] - (3/8)(J_2/D')^3 \right), \quad n \text{ odd}; \end{aligned} \quad (5.26)$$

where, to leading order in $J_2/(4D')$, $\lambda^{-1} = \delta^2 = J_2/(4D')$. For small n these expressions reduce to our previous results (5.20) and (5.25) at leading order in J_2/D' . Equations (5.26) are, unfortunately, insufficient to ascertain whether $V_2(n)$ is positive definite or whether it has a negative minimum. In the latter case there will be a first-order transition from n_0 to $n = \infty$ where n_0 is the value of n for which $V_2(n)$ attains its most negative value. On the other hand, if $V_2(n)$ is positive for all n , then one has an infinite devil's staircase, with no bound on the allowed values of n .

Equation (5.26) suggests that $V_2(n)$ can become negative when $(n\delta + 4\delta^3)/(\pi)$ is sufficiently close to an integer. However, when one considers the leading order corrections to the non-propagation approximations (i.e., one allows the left excitation to move too) one can establish that the sign of $V_2(n)$ is always positive [20]. The result is unchanged if one allows both excitations to move also in the J_0 direction i.e., parallel to the domain walls [20]. Therefore we can establish that the sign of $V_2(n)$ is always positive. Hence an infinite sequence of phases is stabilized by quantum fluctuations in the large D limit.

In the next section we consider the effect of 3-wall interactions which can split the phase boundaries $\langle n \rangle : \langle n + 1 \rangle$ where there is still a multiphase degeneracy of all states comprising domains of length n and $n + 1$.

5.7 Three-wall interactions

Three-wall interactions are needed to analyze the stability of the $\langle n \rangle : \langle n + 1 \rangle$ phase boundary to mixed phases of $\langle n \rangle$ and $\langle n + 1 \rangle$. As discussed in section 5.2 the condition that the boundary be stable is

$$F(n, n + 1) \equiv V_3(n, n) - 2V_3(n, n + 1) + V_3(n + 1, n + 1) < 0. \quad (5.27)$$

Consider first the calculation of $F(2n - 1, 2n)$. The diagrams which contribute in leading order to $V_3(2n - 1, 2n - 1)$ and $V_3(2n, 2n - 1)$ are shown in Figs. 5.13a and 5.13b, respectively. To leading order in $1/\tilde{D}$, $V_3(n + 1, n + 1)$ does not contribute to $F(n, n + 1)$.

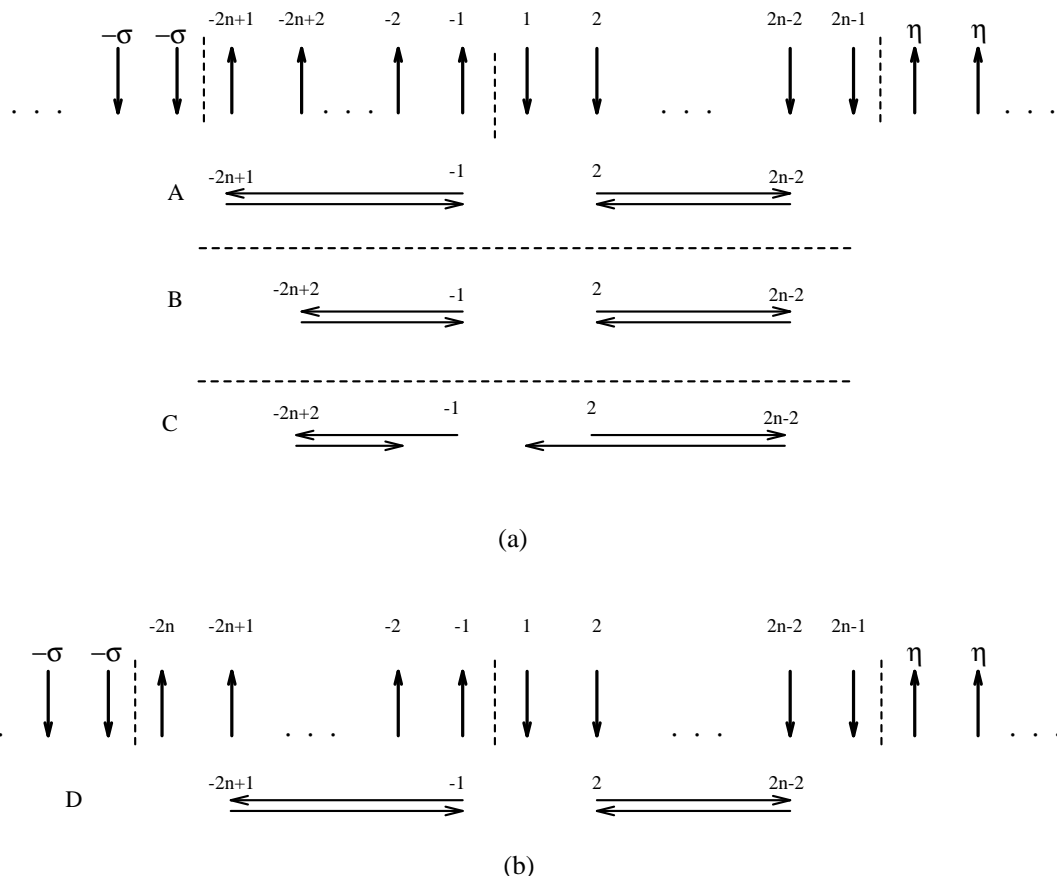


Figure 5.13: The diagrams needed to calculate $F(2n - 1, 2n)$ to leading order: contributions to (a) $V_3(2n - 1, 2n - 1)$ (b) $V_3(2n, 2n + 1)$.

Figure 5.13 aims to emphasize the positions of the initial excitation and the closest approaches to the neighbouring domain walls. One must also consider the position of the first neighbour hops in B and C and the sequence of the hops when calculating the contribution of the diagrams.

An explicit calculation of the contributions of the relevant diagrams would be tedious but, as we will show it is not required for estimating the sign of $F(2n-1, 2n)$. If N_i is the contribution to F of diagrams of type i in Fig. 5.13 ,

$$F(2n-1, 2n) = 2N_A + 2N_B + 2N_C - 2N_D, \quad (5.28)$$

where the factors of 2 multiplying N_A , N_B and N_C account for the mirror image diagrams and that multiplying N_D occurs because of the 2 in equation (5.27).

We shall now show that $F(2n-1, 2n) < 0$. Consider a diagram in which the hops occur in the same order in A, B, C and D and the J_1 hops in B and C are, say, nearest the outer walls. The matrix elements m_i of all types of diagram carry a negative common factor (the sign arising because we are considering even-order perturbation theory) and their ratios are $m_A/m_D = 1$ and $m_A/m_B = m_A/m_C = J_2^2/J_1^2$.

We must also expand the difference in the energy denominators in a way analogous to the step between equation (5.19) and (5.20), but here to second order in J/\tilde{D} (since the σ dependence of the perturbative terms is in the energy denominators). Using (5.16), the contribution of each diagram to the appropriate N_i may be written

$$\begin{aligned} & \sum_{\sigma, \eta} \sigma \eta \left[\frac{m_i}{(4\tilde{D})^{4n-5} S} \left(f_1 + \frac{f_2 + f_3\sigma + f_4\eta}{(4\tilde{D})} \right. \right. \\ & \left. \left. + \frac{f_5 + f_6\sigma + f_7\eta + f_8\sigma^2 + f_9\eta^2 + f_{10}\sigma\eta}{(4\tilde{D})^2} + \dots \right) \right] \\ & = \frac{4m_i f_{10}}{(4\tilde{D})^{4n-3} S} + \mathcal{O}\left(\frac{1}{(4\tilde{D})^{4n-2}}\right) \end{aligned} \quad (5.29)$$

where the coefficients f depend only on J_1 and J_2 . When the sum is taken only the term f_{10} multiplying $\sigma\eta$ survives. For diagrams of type A, f_{10} is $J_2(J_2 - J_1)$, while for B, C and D it is J_2^2 . Therefore these diagrams give a contribution to F proportional to

$$-J_2^2 J_1 (2J_1 - J_2) < 0. \quad (5.30)$$

The contributions to F of the other diagrams in B and C (which correspond to a different position of the first neighbour hop) is proportional to $-J_1^2 J_2^2$. Hence $F(2n-1, 2n) < 0$ and, consequently, the $\langle 2n-1 \rangle : \langle 2n \rangle$ boundaries are stable.

A similar argument holds for $F(2n, 2n+1)$ for $n > 1$. The relevant diagrams are shown in Fig. 5.14. They contribute

$$F(2n, 2n+1) = 2N_A + 2N_B + 2N_C + 2N_D + 2N_E - 2N_F. \quad (5.31)$$

Using the same argument as above

$$N_A + N_B - N_F \propto -J_2^2 J_1 (J_1 - J_2) < 0. \quad (5.32)$$

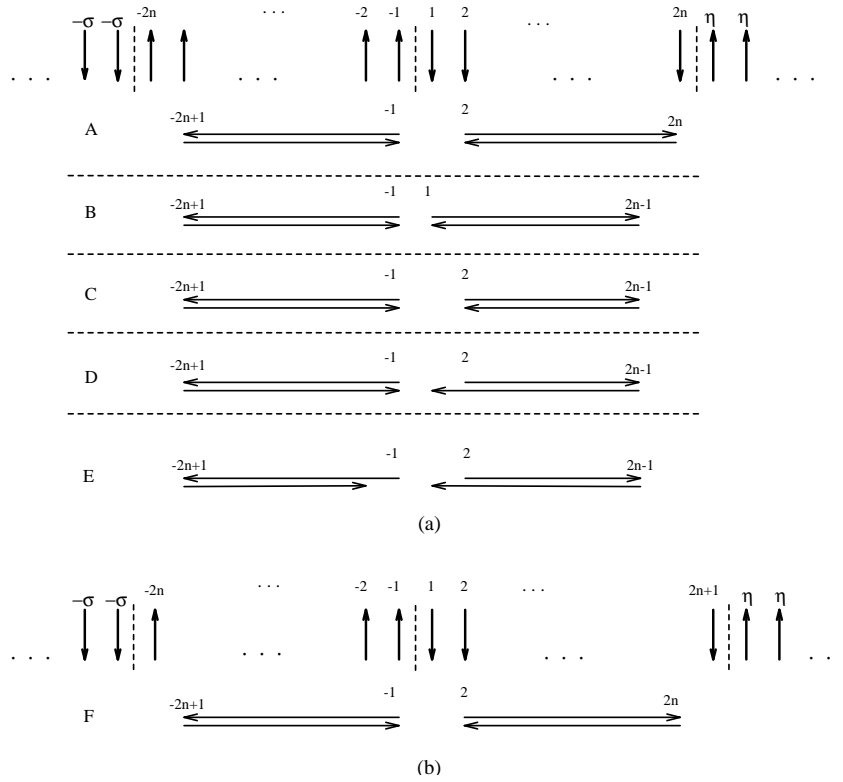


Figure 5.14: The diagrams needed to calculate $F(2n, 2n + 1)$ to leading order: contributions to (a) $V_3(2n, 2n)$ (b) $V_3(2n, 2n + 1)$.

N_C , N_D , N_E , and the other orderings of N_B are negative and hence $F(2n, 2n + 1) < 0$. Thus the phase boundaries $\langle 2n \rangle : \langle 2n + 1 \rangle$ are first order for $n > 1$.

For the $\langle 2 \rangle : \langle 3 \rangle$ boundary different diagrams contribute to $F(2, 3)$. Indeed the second order expansion of the energy denominators [as in equation (5.29)] gives a zero contribution. Accordingly, the calculation of $F(2, 3)$ requires going to higher order in (J_2/\tilde{D}) . This calculation is carried out in detail in Appendix A.1 and shows that the $\langle 2 \rangle : \langle 3 \rangle$ boundary is also stable.

5.8 Conclusions

We have described the behaviour of the Heisenberg model with first- and second-neighbour competing interactions and uniaxial anisotropy D near the ANNNI model limit, $D = \infty$. It was shown that, near the multiphase point, the classical multidegeneracy is removed by quantum effects. In fact, a perturbative calculation showed that quantum fluctuations stabilise a sequence of phases where the domain-wall equispacing increases by one lattice unit,

$$\langle 2 \rangle, \langle 3 \rangle, \langle 4 \rangle, \dots \langle n \rangle \dots \quad (5.33)$$

By using an energy expansion in $1/D$ it could be established that, for n not too large, a first-order line separates neighbouring phases of the sequence (5.33).

The series of transitions (5.33) is very different from the one that results from the thermal excitation of domain walls (see Fig. 5.3). In fact, the largest portion of the low-temperature phase diagram of the ANNNI model is occupied by the sequence

$$\langle 3 \rangle, \langle 23 \rangle, \langle 2^2 3 \rangle, \dots, \langle 2^k 3 \rangle \dots . \quad (5.34)$$

In addition, contrary to what happens in the quantum case, higher order corrections show that the boundary between neighbouring phases, $\langle 2^k 3 \rangle : \langle 2^{k+1} 3 \rangle$, is unstable with respect to the formation of mixed phases $\langle 2^k 3 2^{k+1} 3 \rangle$ [77, 78].

Another important qualitative difference between the quantum and thermal series of transitions is revealed only when long-period phases are considered. At a given low temperature, the thermal sequence (5.34) appears to be truncated, in the sense that a first-order transition separates phase $\langle 2^{k_{max}} 3 \rangle$ from $\langle 2 \rangle$. On the other hand, for the quantum series, (5.33), no cutoff is observed for large n .

The reason for this difference is an inherently quantum one. In the thermal case, for two domains to interact, an excitation has to propagate from one wall to the other while, in the quantum case, the excitation also has to go back to the wall where it started from. Therefore, in the quantum case, the domain-wall interaction is always positive (i.e. repulsive) since it is proportional to the square of an oscillatory Green's function. On the other hand, in the thermal ANNNI case, the analogous function appears linearly and so the wall-wall potential has a negative (attractive) part which is responsible for the differences in the phase diagrams.

Chapter 6

Complete devil's staircase in the Falicov-Kimball model

6.1 Introduction

In this Chapter we study the ground-state phase diagram of the one-dimensional Falicov-Kimball model. This model was proposed to describe metal-insulator transitions [94] and has since been investigated in connection with a variety of problems such as binary alloys [95], ordering in mixed-valence systems [96], and the formation of ionic crystals [97]. It is in the latter language we shall use here, considering a system of static positive ions and mobile spinless electrons.

The model comprises no electron-electron or ion-ion interactions (apart from the Pauli exclusion principle for electrons and a hard-core repulsion for ions) but takes into account an on-site electron-ion attraction, $-U$. The interesting question in the context of crystal formation is whether or not the interactions of the ions with the electrons is sufficient to yield a ground state where the ions are arranged periodically. Unfortunately, despite the simplicity of the Falicov-Kimball model the determination of the ground state is far from trivial, and most of the known properties of the model have been established through extensive numerical simulations.

In particular Gruber *et al.* [98] have shown that, for the neutral system, for small U the delocalisation of electrons favours the formation of segregated phases, where the ions cluster together on one side of the lattice. For large U , however, there are a large number of modulated ground states where the periodic arrangement of the ions obey the so-called most-homogeneity requirement [99].

In an interesting paper Gruber *et al.* [97] were able to prove rigorously the appearance of ground states with equispaced ions for large values of U . To do this they calculated the ion-ion interaction to leading order in $1/U$.

In this Chapter we show that a full determination of the ground state requires a calculation

of the general m -ion interactions, which we obtain to leading order in $1/U$ using Green's function techniques. Hence, using arguments first introduced by Fisher and Szpilka [100], we are able to prove the existence of a complete devil's staircase in the neutral Falicov-Kimball model [101], confirming a conjecture by Barma and Subrahmanyam [11].

6.2 The model

We write the Falicov-Kimball model in the form

$$\begin{aligned} \mathcal{H} = & t \sum_j (a_j^\dagger a_{j+1} + a_{j+1}^\dagger a_j) - 2U \sum_i (s_i a_i^\dagger a_i - 1/2) \\ & + (U - \mu_i) \sum_j (s_j - 1/2) + (U - \mu_e) \sum_j (a_j^\dagger a_j - 1/2) \end{aligned} \quad (6.1)$$

where a_i^\dagger (a_i) denotes the creation (destruction) operator for a spinless electron, s_i is equal to 1 (0) if site i is (un)occupied by an ion, t is the hopping integral for electrons, μ_i and μ_e are the chemical potentials for ions and electrons respectively and U is a positive constant corresponding to the ion-electron attractive energy. The choice of a positive U is not restrictive since the transformations $\{U \rightarrow -U; \mu_i \rightarrow -\mu_i; s_i \rightarrow 1 - s_i\}$ maps the Hamiltonian (6.1) onto the same system with U negative.

The ground state of the system is chosen by minimizing the total energy per site of the system over all ionic configurations. In other words, for each possible ionic configuration, the energy eigenvalues of the Hamiltonian (6.1) are calculated and the total energy of the system is computed by filling the electron levels up to the Fermi energy. The ionic arrangement corresponding to the ground state is then chosen by energy comparison.

As already pointed out by Falicov and Kimball, the structure of the ground states differs significantly depending on whether U is large or small compared to t . In the first case the electrons are essentially localized near the ions and the latter tend to be as far apart as possible. On the other hand, for large t/U , the delocalisation of electrons favours the gathering of ions in clusters [99]. In this Chapter we consider the case where U is very large compared to other parameters in (6.1), and we shall treat t/U as a perturbative parameter.

6.3 The phase diagram for $t = 0$

We first consider the case when the hopping integral for the electrons, t , is zero so that each electron will occupy the same site at all times. In this case the Hamiltonian (6.1) simplifies to

$$\mathcal{H} = -2U \sum_i (s_i n_i - 1/2) + (U - \mu_i) \sum_j (s_j - 1/2) + (U - \mu_e) \sum_j (n_j - 1/2) \quad (6.2)$$

where we have set $n_i = a_i^\dagger a_i$. Since ions (and electrons) at different sites do not interact with each other, it is relatively easy to find the ground state configurations of the system. The resulting phase diagram is summarized in Fig. 6.1.

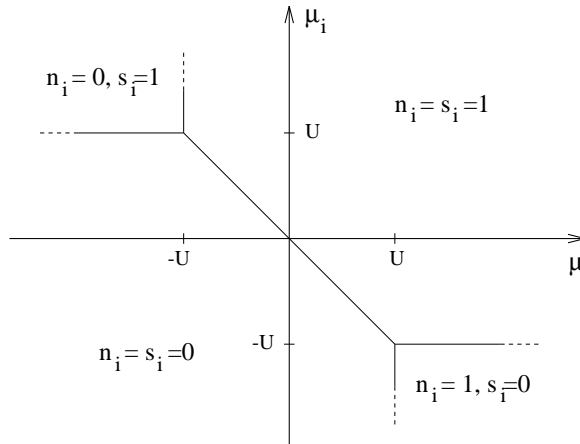


Figure 6.1: The phase diagram of the Falicov-Kimball model for $t = 0$.

All the phase boundaries in the figure are multidegenerate in that any phase obtained by mixing two neighbouring phases has the same energy on the boundary. Our aim is to study systematically how this multidegeneracy is lifted as t/U increases from zero.

Before doing this we discuss what constraints are imposed on the ground state by the assumption that U is very large. To do this it is convenient to introduce the quantities

$$h \equiv (\mu_i + \mu_e)/2, \quad (6.3)$$

$$\Delta \equiv (\mu_i - \mu_e)/2. \quad (6.4)$$

The physical interpretation of the auxiliary variables h and Δ is straightforward: h controls the total number of ions and electrons in the system, while Δ controls the excess number of ions with respect to electrons.

It can be argued that, since $\Delta/U \ll 1$ (we assume that U is much larger than any physical parameters in equation (6.1)), the total number of electrons and ions is the same. To see this consider the case when, for small t/U , the excess number of ions, $p \equiv \sum_j (s_j - n_j)$, is a large negative integer. If we add an electron to the system (i.e. increase p by one unit), the energy will be incremented by a quantity $\Delta E_p \approx -U$. Since t/U is assumed small, ΔE_p will remain approximately equal to $-U$ for all negative values of p . Conversely, when $p \geq 0$, ΔE_p will remain almost constant at $+U$, as shown in Fig. 6.2.

Now, for a given value of Δ , the excess number of ions observed in the ground state, p_Δ , is given by the largest integer p for which

$$\Delta E_{p+1} \leq \Delta. \quad (6.5)$$

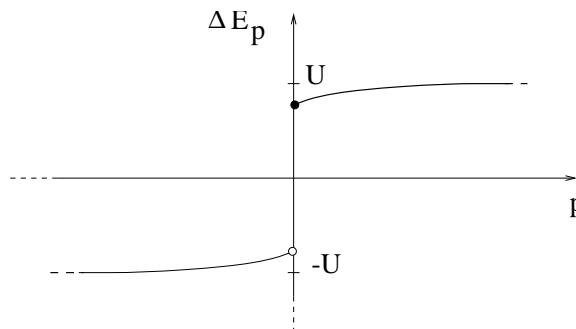


Figure 6.2: Schematic plot of ΔE_p when $t/U \ll 1$. Although, for simplicity, we have drawn ΔE_p as a continuous curve, it is actually defined only for integer values of p .

Since ΔE_p displays a gap roughly equal to $2U$ for $p = 0$ (see Fig. 6.2) we can conclude that, when $|\Delta| \ll U$, p_Δ will be equal to zero. For this reason throughout the rest of the Chapter, we will implicitly consider a neutral system, i.e. $\sum_i n_i = \sum_i s_i$.

6.4 The defect-defect interaction expansion

Since changing Δ in an interval of order $1/U$ will not modify the number of electrons and ions in the system, from now on we will set $\Delta = 0$. This amounts to exploring the phase diagram along the line $\mu_e = \mu_i$. Our aim is to discuss how the properties of the ground state change when moving along this line by varying h .

For negative values of h , the ground state corresponds to an empty lattice ($n_i = s_i = 0$). On the other hand, for h positive $n_i = s_i = 1$. The point $h = 0$ lies on the multi-degenerate phase boundary where all phases associated with an arbitrary spacing of the ions are degenerate. To distinguish between the different degenerate states it is convenient to introduce the labelling $\langle n_1, n_2, \dots, n_m \rangle$ to denote a phase consisting of ions whose separations (measured in lattice spacings) repeat periodically the sequence n_1, n_2, \dots, n_m . (Hence the phases $n_i = s_i = 1$ and $n_i = s_i = 0$ can be described as $\langle 1 \rangle$ and $\langle \infty \rangle$ respectively.)

The multidegeneracy encountered on the phase boundaries of Fig. 6.1 is due to the absence of interaction between the confined electrons. It is natural to expect that, for $t/U \neq 0$, the hopping of electrons will introduce an effective coupling between the ions, thus providing a mechanism for the removal of the degeneracy. By analogy with the approach in the previous Chapter, we will try to build systematically the phase diagram by using the defect-defect interaction formalism of Fisher and Szpilka [100] (in the present context, a defect corresponds to an ion). Following [100] we write the energy per lattice site of phase $\langle n_1, n_2, \dots, n_m \rangle$ as

$$E_{\langle n_i \rangle} = \frac{m\sigma + \sum_{i=1}^m V_2(n_i) + \sum_{i=1}^m V_3(n_i, n_{i+1}) + \dots}{\sum_i n_i} \quad (6.6)$$

where σ is the creation energy of an isolated ion, $V_2(x)$ denotes the effective interaction between two ions at a distance x , $V_3(x, y)$ the interaction of three ions with spacings x, y , and so on. Although,

for simplicity, we refer to the ion creation energy and ion–ion interactions, it must be borne in mind that each ion is associated with an electron.

In the rest of this section we will calculate the ion creation energy, σ , and the two-ion interaction potential, $V_2(n)$ and we will discuss how the multidegeneracy is raised in the two-ion interaction approximation.

6.4.1 The ion creation energy

We first consider the unperturbed case, $t = 0$, where the electrons are confined to the ions. In this case σ can be obtained by calculating the energy of the system when only one ion (and one electron) is present. One obtains $\sigma = -2h$. Switching on the perturbation term, t/U we expect each electron will be localized in a small region around the associated ion. The leading order correction in t/U to σ can be obtained by using standard perturbation theory (cf. section 5.3). In Fig. 6.3 we have represented the two diagrams that give the leading order contribution to σ ; each arrow represents an electron hopping. The total energy associated with the two diagrams is

$$E_t = -\langle n_i = 1, s_i = 1 | ta_i^\dagger a_{i+1} \frac{1}{\mathcal{E}} ta_{i+1}^\dagger a_i | n_i = 1, s_i = 1 \rangle - \langle n_i = 1, s_i = 1 | ta_i^\dagger a_{i-1} \frac{1}{\mathcal{E}} ta_{i-1}^\dagger a_i | n_i = 1, s_i = 1 \rangle \quad (6.7)$$

Since the energy denominators, \mathcal{E} are equal to U

$$E_t = -2t^2/U \quad (6.8)$$

so that

$$\sigma = -2h - 2t^2/U + \mathcal{O}(t^3/U^2) . \quad (6.9)$$

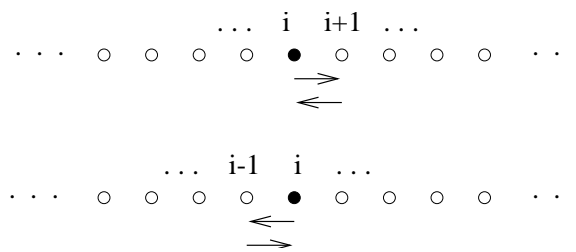


Figure 6.3: Lowest-order diagrams contributing to σ . A full circle represents an ion and an arrow denotes the hopping of an electron.

6.4.2 The two-ion interaction

The general ion–ion interaction term, $V_m(n_1, n_2, \dots, n_{m-1})$, can be obtained, at least in principle, through the reconnection formula [12]

$$V_m(n_1, n_2, \dots, n_{m-1}) = E_A - E_B - E_C + E_D \quad (6.10)$$

where E_X is the energy of configuration X , as in Fig. 6.4.

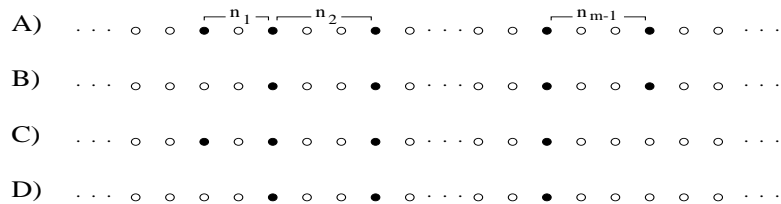


Figure 6.4: Ionic configurations needed to calculate the m -ion interaction $V_m(n_1, n_2, \dots, n_{m-1})$. In A there are m ions at sites $0, n_1, n_2, \dots, n_{m-1}$. In B the left-most ion is removed; in C the right-most ion is removed; and in D the left-most and right-most ions are missing.

In the absence of electron hopping, equation (6.10) gives $V_m = 0$ for all values of m . Our aim is to calculate V_m to leading order in t/U . As usual we will start our analysis of the phase diagram by neglecting interactions that involve more than two ions. Higher-order interactions will then be included successively to resolve the finer details of the phase structure.

There is a very simple way to obtain the leading-order contribution to the interaction between two ions occupying sites 0 and n . First note that diagrams involving fewer than $2n$ electron hops will not contribute to $V_2(n)$ because, as illustrated in Fig. 6.5a, the contribution of every such diagram in configuration A will be cancelled by a counter-diagram in configuration B (or C).

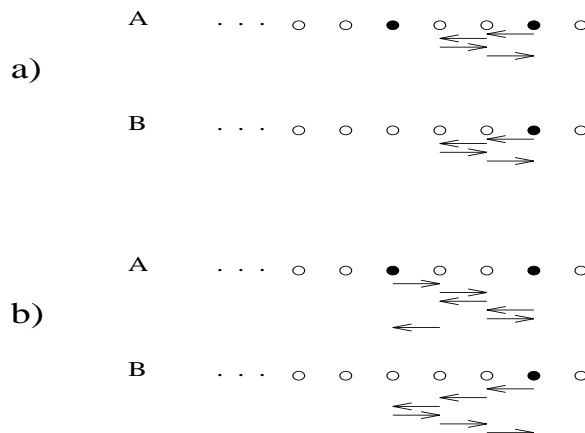


Figure 6.5: Examples of diagrams that, when the reconnection formula (6.10) is used, give a (a) zero (b) leading-order contribution to the two-ion interaction $V_2(3)$. A full circle represents an ion and an arrow denotes the hopping of an electron.

It is then apparent that the leading-order contribution to $V_2(n)$ is due to diagrams where the sites 0 and n are just connected by $2n$ hoppings, as in Fig. 6.5b, so that $V_2(n)$ will be proportional to t^{2n}/U^{2n-1} . The total contribution of all possible diagrams to $V_2(n)$ can be calculated inductively for increasing n , giving

$$V_2(n) = 2n \frac{t^{2n}}{U^{2n-1}} + \mathcal{O}\left(\frac{t^{2n+2}}{U^{2n+1}}\right). \quad (6.11)$$

Since $V_2(n)$ is always positive and convex, as h is varied from positive to negative, the ion-ion spacing in the ground state, \bar{n} , increases monotonically in steps of one lattice spacing, giving rise to

the infinite sequence of phases

$$\langle 1 \rangle \rightarrow \langle 2 \rangle \rightarrow \dots \rightarrow \langle \infty \rangle . \quad (6.12)$$

The phase $\langle n \rangle$ is stable over a region of width Δh_n given by (cf. equation 5.12)

$$\Delta h_n \approx \frac{n+1}{2} V_2(n-1) \approx (n^2-1) \frac{t^{2n-2}}{U^{2n-3}} + \mathcal{O}\left(\frac{t^{2n-1}}{U^{2n-2}}\right) . \quad (6.13)$$

As pointed out in section 5.4, the original multidegeneracy is not completely lifted by $V_2(n)$ because, on the boundary between two phases, $\langle n \rangle$ and $\langle n+1 \rangle$, all mixed phases where the ions can be separated by distances n or $n+1$ are still degenerate. To determine the finer structure of the phase diagram it is necessary to consider the effect of higher-order ion interactions. Unfortunately these are not easily obtained using the simple method outlined above but can still be calculated to leading order using Green's function techniques. In the next section we shall illustrate how this method can be used to reproduce the result for $V_2(n)$.

6.5 Calculation of $V_2(n)$ using Green's function methods

To calculate E_A in equation (6.10) we consider a system of $n+1$ sites with ions at sites 0 and n . The single-particle energies are determined by the eigenvalues of the the $(n+1)$ -dimensional tridiagonal matrix, \mathbf{M} , where

$$M_{ii} = -U(\delta_{i,0} + \delta_{i,n}) , \quad (6.14)$$

$$M_{i,i+1} = M_{i+1,i} = t \quad (6.15)$$

and the other matrix elements are zero. Two of these energies occur near $-U$, and these are the ones we want to sum over to get E_A . Introducing the resolvent operator for the matrix M , $(z\mathcal{I} - M)^{-1}$, where \mathcal{I} is the identity matrix, we can write E_A as

$$E_A = \frac{1}{2\pi i} \int_{\Gamma} \text{Tr} \left[\left(z\mathcal{I} - \mathbf{M} \right)^{-1} \right] z dz \quad (6.16)$$

The contour Γ in (6.16) encloses the region near $z = -U$. To evaluate the trace we need to expand the matrix inverse in equation (6.16) in powers of the t 's. To do this we define the perturbation matrix

$$V_{ij} = \begin{cases} t & \text{if } j = i \pm 1, \\ 0 & \text{otherwise,} \end{cases} \quad (6.17)$$

and expand the resolvent operator in powers of V ,

$$\begin{aligned} \left(z\mathcal{I} - \mathbf{M} \right)_{ii}^{-1} &= G_{ii} + G_{ii} V_{ij} G_{jj} V_{ji} G_{ii} + \\ &G_{ii} V_{ij} G_{jj} V_{jk} G_{kk} V_{kl} G_{ll} V_{li} G_{ii} + \dots \end{aligned} \quad (6.18)$$

where $G_{ii} = [z - M_{ii}]^{-1}$. It is important to notice that, in the expansion (6.18), terms of odd order cannot contribute to the trace. Since we are interested in finding the leading order expression of

$V_2(n)$ we will focus only on the terms in (6.18) which give a contribution to the resolvent operator for configuration A of order t^{2n} . (We have already argued that terms of lower order will not survive the summation in the reconnection formula (6.10).)

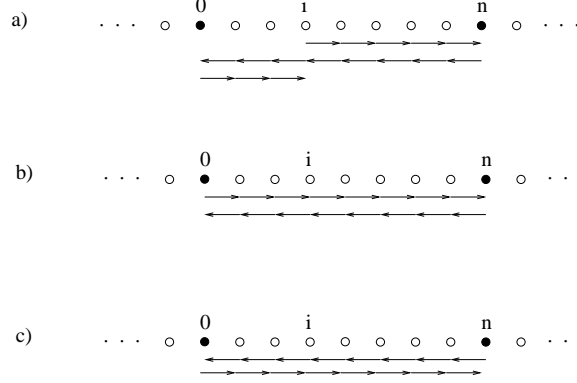


Figure 6.6: Examples of leading order diagrams contributing to E_A . Each arrow represents a matrix element, V_{ij} . The on-site interactions, g_{jj} are not shown.

In the expansion (6.18) one sees that, if i is not an end site, in order to involve $2n$ factors of t , the matrix elements must start at i , say, then increase to the highest number site (n), then decrease to the lowest number site (0) and finally increase back to the original value i , as shown in Fig. 6.6a. Alternatively, the matrix elements could initially decrease. However, if $i = \{0, n\}$, we note that the index can only initially increase or decrease respectively (see Fig. 6.6b and 6.6c). We can summarize the contribution of all the diagrams proportional to t^{2n} in the following compact form

$$\left(z\mathcal{I} - \mathbf{M} \right)_{ii}^{-1} \approx C_i G_{00} G_{ii} G_{n,n} \prod_{i=1}^{n-1} G_{ii}^2 \prod_{i=0}^{n-1} V_{i,i+1}^2, \quad (6.19)$$

where $C_i = 1$ if $i = 0$ or $i = n$ and $C_i = 2$ otherwise. The product over the G 's does not include the end sites, because these, in general, only appear once. The starting site appears an extra time and gives rise to the prefactor G_{ii} . Therefore the trace is

$$\text{Tr} (z\mathcal{I} - \mathbf{M})^{-1} \approx t^{2n} \left[\frac{2}{(z+U)^3 z^{2n-2}} + \frac{2n-2}{(z+U)^2 z^{2n-1}} \right]. \quad (6.20)$$

Here the first term includes C_1 and C_{n+1} , both of which are unity. The factor $2n-2$ comes from $\sum_{i=2}^n C_i$. Substituting (6.20) in (6.16) and calculating the integral using residues gives

$$\begin{aligned} E_A &\approx \frac{1}{2\pi i} \int_{\Gamma} t^{2n} \left[\frac{2}{(z+U)^3 z^{2n-3}} + \frac{2n-2}{(z+U)^2 z^{2n-2}} \right] dz \\ &= (2n-2) \frac{t^{2n}}{U^{2n-1}} + \mathcal{O}\left(\frac{t^{2n+2}}{U^{2n+1}}\right). \end{aligned} \quad (6.21)$$

In order to use the reconnection formula (6.10), we need to repeat the same calculation when one of the end ions is removed (corresponding to configurations B and C in Fig. 6.4). In this case we obtain

$$\text{Tr}(\mathcal{I} - \mathbf{M})^{-1} = t^{2n} \left[\frac{1}{(z+U)^2 z^{2n-1}} + \frac{2n-1}{(z+U)z^{2n}} \right] + \mathcal{O}\left(\frac{t^{2n+2}}{U^{2n+1}}\right). \quad (6.22)$$

Thus the perturbative contributions to V_2 , denoted E_B and E_C are

$$E_B = E_C = -\frac{t^{2n}}{U^{2n-1}} + \mathcal{O}\left(\frac{t^{2n+2}}{U^{2n+1}}\right). \quad (6.23)$$

Finally we note that when both ions are removed there are no longer any levels near $-U$ so that $E_D = 0$. The use of the reconnection formula (6.10) gives

$$V_2(n) = 2n \frac{t^{2n}}{U^{2n-1}}, \quad (6.24)$$

in agreement with the expression (6.11).

6.6 Calculation of the general V_m term

The Green's function method introduced in the previous section can be extended to calculate the m -ion interaction V_m for $m > 2$. As we shall explain below the general m -ion interaction term, $V_m(n_1, n_2, \dots, n_{m-1})$, depends, to leading order, only on the separation of the two outermost ions in configuration A , $n = \sum_{i=1}^{m-1} n_i$. We will show that the general leading order term for V_m is

$$V_m(n) = \frac{(2n)! t^{2n}}{(2m-3)!(2n-2m+3)! U^{2n-1}} + \mathcal{O}\left(\frac{t^{2n+2}}{U^{2n+1}}\right). \quad (6.25)$$

To obtain this result notice first that it is still possible to use equation (6.19) (originally introduced for calculating $V_2(n)$) to get the leading order expression for $V_m(n)$.

We first consider the case where the initial i corresponds to an ion, so that $G_{ii} = 1/(z+U)$. There will be $(2m-2)$ other factors of $1/(z+U)$ in the contribution to the diagonal elements of the resolvent operator for configuration A , two of them coming from G_{00} and G_{nn} and two for each of the $(m-2)$ interior ions (touched twice by leading order diagrams). Therefore, each leading order diagram for which the initial site is occupied by an ion, will give a contribution to $[z\mathcal{I} - M]_{ii}^{-1}$ equal to

$$C_i \frac{t^{2n}}{(z+U)^{2m-1} z^{2n-2m+2}}. \quad (6.26)$$

As before, the multiplicity factor, C_i is equal to 2 for interior ions and 1 for the outermost ones. Therefore the total contribution of diagrams where the initial site corresponds to an ion is

$$\text{Tr} \left[(z\mathcal{I} - \mathbf{M})^{-1} \right] = t^{2n} \frac{(2m-2)}{(z+U)^{2m-1} z^{2n-2m+2}}. \quad (6.27)$$

On the other hand, if i is not an ion site, then G_{00} will be simply equal to $1/z$ and the contribution from each of the diagrams is

$$C_i \frac{t^{2n}}{(z+U)^{2m-2} z^{2n-2m+3}}, \quad (6.28)$$

where the C_i 's are equal to 2 for all diagrams. Since there are $n - m + 1$ possible starting sites not occupied by ions, the total contribution of this type of diagrams is

$$\frac{2n - 2m + 2}{(z + U)^{2m-2} z^{2n-2m+3}} . \quad (6.29)$$

Thus, in all,

$$E_A = \frac{(2n - 2)!}{(2m - 3)!(2n - 2m + 1)!} \frac{t^{2n}}{U^{2n-1}} + \mathcal{O}\left(\frac{t^{2n+2}}{U^{2n+1}}\right) . \quad (6.30)$$

Similarly one obtains

$$E_B = E_C = -\frac{(2n - 2)!}{(2m - 4)!(2n - 2m + 2)!} \frac{t^{2n}}{U^{2n-1}} + \mathcal{O}\left(\frac{t^{2n+2}}{U^{2n+1}}\right) , \quad (6.31)$$

$$E_D = \frac{(2n - 2)!}{(2m - 5)!(2n - 2m + 3)!} \frac{t^{2n}}{U^{2n-1}} + \mathcal{O}\left(\frac{t^{2n+2}}{U^{2n+1}}\right) . \quad (6.32)$$

Finally the use of the reconnection formula (6.10) gives the result (6.25).

6.7 Hyperfine structure of the phase diagram

We now discuss how higher-order ion interactions modify the phase diagram obtained in the two-ion interaction approximation. Consider first V_3 . This has the effect of partially removing the multidegeneracy on the $\langle n \rangle | \langle n + 1 \rangle$ boundaries by stabilizing the mixed phases $\langle n, n + 1 \rangle$. This follows from noting that the energy difference

$$(2n + 1)E_{\langle n, n+1 \rangle} - nE_{\langle n \rangle} - (n + 1)E_{\langle n+1 \rangle} = \\ V_3(n, n + 1) + V_3(n + 1, n) - V_3(n, n) - V_3(n + 1, n + 1) \quad (6.33)$$

is negative.

The stability of the two new boundaries appearing at this stage of approximation, namely $\langle n \rangle | \langle n, n + 1 \rangle$ and $\langle n, n + 1 \rangle | \langle n + 1 \rangle$ can be determined similarly by considering four-ion interaction terms. Again they are unstable to the appearance of the mixed phases $\langle n, n, n + 1 \rangle$ and $\langle n, n + 1, n + 1 \rangle$ respectively. Indeed, since all interaction potentials are positive, convex and exponentially decaying with the separation of the outmost ions, we can conclude that, at every stage of the construction of the phase diagram, the introduction of neglected higher-order interactions will lead to the stabilization of mixed phases of increasingly long period which occupy smaller and smaller regions of the phase diagram [12]. Therefore the ion density has the behaviour characteristic of a devil's staircase.

6.8 Conclusions

To summarize we have constructed iteratively the phase diagram of the Falicov-Kimball model in the limit of large electron-ion coupling, U . The general ion-ion interaction term, V_m , was calculated, to leading order, using Green's function techniques. The determination of the sign, convexity and decay

properties of the V_m 's allowed us to conclude that an infinite sequence of phases appears in the phase diagram. As the ion and electron chemical potential are suitably varied, the ion density displays the behaviour characteristic of a devil's staircase, as conjectured by Barma and Subrahmanyam [11]. It is important to point out that these conclusions are based on a leading-order expansion of energy differences in powers of $1/U$. We cannot rule out the possibility that neglected higher-order corrections could dominate the interaction energies of very widely-spaced ions thus introducing modifications into the phase diagram.

Chapter 7

An epsilon point in a spin model

7.1 Introduction

In the previous Chapters we have shown that the onset of the appearances of modulated structures occurs when the energy creation of a domain wall or an interface, in a homogeneous, interface-free phase goes to zero. When this happens, the resulting ground states with complicated modulations can be conveniently analyzed in terms of interacting domain walls.

The domain-wall interaction formalism has been recently generalized by Bassler *et al.* [12] to study the phase diagram near a point where the surface tension between two phases that coexist at a first-order transition, $\langle\alpha\rangle$ and $\langle\beta\rangle$ goes to zero [12, 102, 103]. As shown schematically in Fig. 7.1 the resulting phase diagram can have a very complicated fan-like structure. Because the sides of the fan join at P in a cusp which is tangential to the $\langle\alpha\rangle|\langle\beta\rangle$ boundary, thus resembling the greek letter Υ , the multicritical point P has been termed epsilon-point (Υ -point). In many ways the Υ -point can be thought of as a two-dimensional generalisation of the behaviour customary near a multiphase point. While the behaviour near a single multiphase point can be analysed in terms of a unique type of interacting interfaces, there are three (or more, in case of degeneracy) different phases stable near an Υ -point, and hence several types of interface-interactions terms must be identified in the analysis.

The occurrence of an Υ -point in a spin model was recently suggested by the numeric work of Sasaki [25]. In an attempt to describe qualitatively the magnetism observed in samples of *Ho* [21, 104], Sasaki studied an *XY* model with first- and second-neighbour interactions and six-fold anisotropy in a magnetic field. In this model the Υ -points seemed to occur for large values of the spin anisotropy due to the removal of the degeneracy of two multiphase lines meeting at a first order boundary. Later Seno *et al.* [105, 106] devised an expansion in inverse spin anisotropy that allowed the systematic study of the phase diagram of the same model in zero magnetic field. However, due to the complication arising from the presence of second-neighbours interactions, the occurrence of

Υ -points in the model could not be confirmed analytically.

In this Chapter we consider the chiral XY model with six-fold spin anisotropy in a magnetic field [107]. Thanks to the absence of further-than-nearest-neighbour interactions we are able to prove that, as the spin anisotropy is reduced from infinity, the softening of the spins allows the formation of an Υ -point structure. This provides the first analytic evidence for the existence of an Υ -point in a spin model.

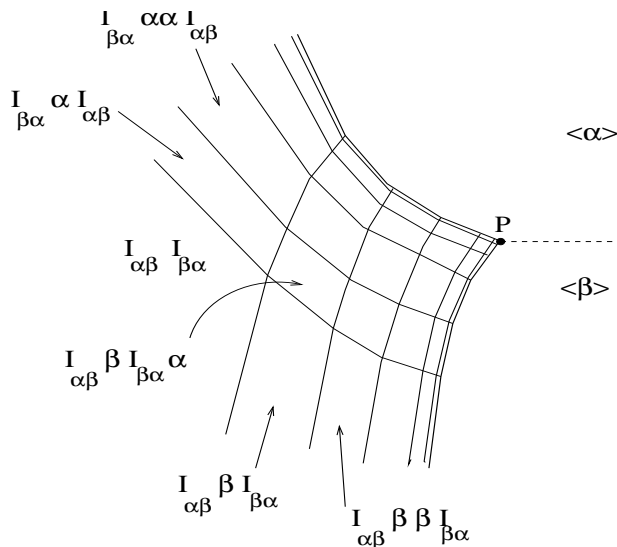


Figure 7.1: Schematic representation of an Υ -point. Finer details are not shown.

7.2 The model

We consider the classical chiral XY model with six-fold spin anisotropy, D , in the presence of an external magnetic field h . The Hamiltonian of the system is

$$\mathcal{H} = \sum_i \left\{ -\cos(\theta_{i-1} - \theta_i + \pi\Delta/3) + h[1 - \cos(\theta_i)] + D[1 - \cos(6\theta_i)]/36 \right\} \quad (7.1)$$

where θ_i is the angle between the i^{th} spin and the magnetic field orientation. The Hamiltonian (7.1) is a generalization of the six-state chiral XY model introduced by Yokoi *et al.* [108] in connection with ferro-electric chiral smectic liquid crystals [109, 110] and materials like $Cr_{1/3}NbS_2$ [111] which exhibit antisymmetric exchange interactions.

We shall concentrate on the behaviour of the model near the limit $D = \infty$, where n_i , defined as $3\theta_i/\pi$, can take only the integer values $\{0,1,\dots,5\}$. Although we restrict ourselves to one dimension the results apply equally to models with ferromagnetically coupled layers and an uniaxial modulation driven by the interactions (7.1) perpendicular to the layers.

The ground-state configurations of the Hamiltonian (7.1) satisfy

$$\frac{\partial \mathcal{H}}{\partial \theta_i} = 0 \quad \forall i. \quad (7.2)$$

For a given i , equation (7.2) enables us to express θ_{i+1} as a function of θ_i and θ_{i-1} . This fact, together with the observation that n_i can only take a finite number of values, namely $\{0, 1, \dots, 5\}$, is sufficient to conclude that, for $D = \infty$, there will always exist periodic minimal energy configurations. It will be convenient to label a periodic configuration $\{\dots, \theta_N, \theta_1, \theta_2, \dots, \theta_N, \theta_1, \dots\}$ as $\langle n_1, n_2, \dots, n_N \rangle$.

We can now discuss the phase diagram for $D = \infty$, obtained using the Floria-Griffiths algorithm [71], and presented in Fig. 7.2. We have restricted the labelling of the phases to the first quadrant ($0 \leq \Delta \leq 3; h \geq 0$); the remaining phases can be constructed through appropriate symmetry operations on the n_i sequences. The transition lines between regions A and J and regions J and F are first order. The remaining boundaries are multiphase lines, that is loci where all phases (including non-periodic ones) built from arbitrary combinations of the two neighbouring phases are degenerate [100].

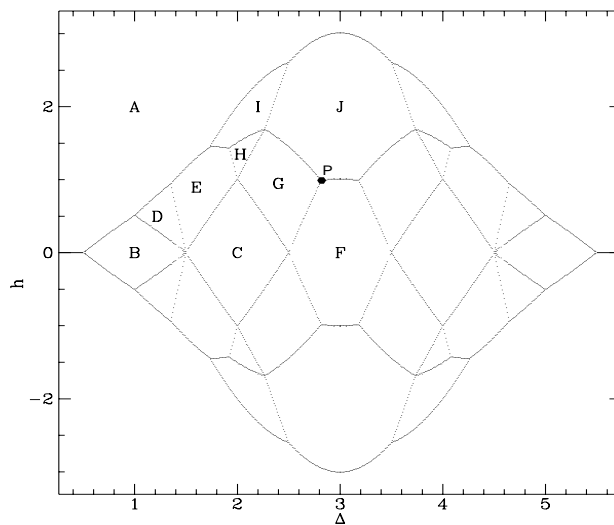


Figure 7.2: Ground state of the Hamiltonian (2.1) for $D = \infty$. A = $\langle 0 \rangle$; B = $\langle 012345 \rangle$; C = $\{ \langle 024 \rangle, \langle 153 \rangle \}$; D = $\langle 01245 \rangle$; E = $\langle 0135 \rangle$; F = $\{ \langle 03 \rangle, \langle 14 \rangle, \langle 25 \rangle \}$; G = $\langle 02514 \rangle$; H = $\{ \langle 025 \rangle, \langle 014 \rangle \}$; I = $\langle 015 \rangle$; J = $\langle 15 \rangle$. The J-A and J-F boundaries (and the symmetric ones under h reversal) are first order.

If the spin anisotropy is reduced from ∞ it seems natural to expect the degeneracy along the multiphase lines to be lifted as the spins soften from the clock positions. Although n_i is no longer constrained to assume integer values, nevertheless, for high values of D , the angles θ_i will be close enough to the clock positions to allow us to continue to use the same labelling scheme introduced before.

We are particularly interested in the possible appearance of Υ -points for finite D . An Υ -point can occur when a first-order transition line separating, say, phases $\langle \alpha \rangle$ and $\langle \beta \rangle$ (that, for simplicity, we now assume to be non-degenerate) approaches a commensurate-incommensurate transition [72,

12, 112]. When this happens, an infinite number of phases spring out from the multicritical point at the end of the first-order line (as represented in Fig. 7.1). The phases appearing are made of sequences of $\langle\alpha\rangle$ and $\langle\beta\rangle$. As $\alpha \neq \beta$ the interfaces separating them, which we shall call $I_{\alpha\beta}$ and $I_{\beta\alpha}$ are also generally distinct. In the example of Fig. 7.1 the general form for a phase in the fan is $\langle\alpha^n I_{\alpha\beta} \beta^m I_{\beta\alpha}\rangle$ (with α^n we denote the repetition of the α sequence n times, i.e. $\langle\alpha^3 I\rangle \equiv \langle\alpha\alpha\alpha I\rangle$), where the integers n, m increase approaching the $\langle\alpha\rangle$ and $\langle\beta\rangle$ boundaries respectively.

The multiphase point \mathbf{P} highlighted in Fig. 7.2 seems to be a good candidate for becoming an Υ -point when D is relaxed from ∞ . In fact, \mathbf{P} lies at the end of a first-order transition line and it seems reasonable to consider the two multiphase lines J-G and G-F as special cases of accumulation lines. Therefore we might expect to observe a structure similar to Fig. 7.1 for small values of $1/D$.

7.3 The interface-interface interaction formalism

When moving from a point inside the Υ structure of Fig. 7.1 towards the α or β phases, one crosses an infinite sequence of phases. Accordingly, the first step in proving the existence of the Υ -point in our model will be to verify that, for small values of $1/D$, each of the J-G and G-F boundaries in Fig. 7.2 splits giving rise to an infinite series of transitions. This can be done using the interface-interface interaction formalism outlined in the previous Chapters.

If we define $\langle\alpha\rangle \equiv J = \langle 51 \rangle$ and $\langle I \rangle \equiv \langle 402 \rangle$ so that $\langle I\alpha \rangle = G = \langle 51402 \rangle$, the degenerate phases on the J_G boundary will have the form [12]

$$\langle\alpha^{n_1} I \alpha^{n_2} I \alpha^{n_3} I \alpha^{n_4} I \dots\rangle. \quad (7.3)$$

It is physically appealing to regard the I block of spins as an interface separating pure α sequences. Following [10] one can conveniently write the energy per spin of phase (7.3) as

$$E = \sum_i \left[e_\alpha^0 n_i l_\alpha + e_I^0 l_I + \sigma + V_\alpha(n_i l_\alpha) + V_{\alpha\alpha}(n_i l_\alpha, n_{i+1} l_\alpha) + \dots \right] / \sum_i (n_i l_\alpha + l_I) \quad (7.4)$$

where l_α (l_I) is the number of spins in phase α (I), e_α^0 (e_I^0) is the energy per spin of $\langle\alpha\rangle$ ($\langle I \rangle$), σ is the creation energy of $\langle I \rangle$, $V_\alpha(x)$ is the interaction energy of two interfaces I separated by a distance x , $V_{\alpha\alpha}(x, y)$ is the interaction energy of three interfaces and so forth. By definition, σ is the energy paid for the creation of an interface, I , in a pure α phase; for this reason σ is often referred to as the “interface tension”.

We start by assuming that the V 's decay sufficiently rapidly with the interface separation to allow us to start our analysis by retaining only V_α . Corrections due to higher-order interactions will be included systematically later on. Although we have introduced the interface-interface interaction approach in connection with the stability of the J – G boundary (that we shall also call $\langle\alpha\rangle$ boundary), the same scheme can be applied to the G-F boundary ($\langle\beta\rangle$ boundary). In the next section we will

consider in turn the stability of both boundaries within the two-interface interaction approximation (the validity of this assumption will be confirmed *a posteriori*).

7.4 The $\langle\alpha\rangle$ boundary

As we explained in the previous section, on the $J - G$ boundary, all phases built with α sequences ($\langle\alpha\rangle = \langle 51 \rangle$) separated by a $|402| \equiv I$ block (i.e. $\langle\alpha^n I \alpha^m \dots\rangle$) are degenerate. Our aim is to study how this degeneracy is lifted when D assumes finite values. When $D = \infty$, all the interface interaction terms are exactly zero. When $1/D$ is small, $V_\alpha(2n)$ dominates the energy contribution from the interface interaction terms. It can be obtained using the reconnection formula [12]

$$V_\alpha(2n) = E_1 + E_2 - E_3 - E_4 \quad (7.5)$$

where E_i is the energy of configuration i as sketched in Fig. 7.3.

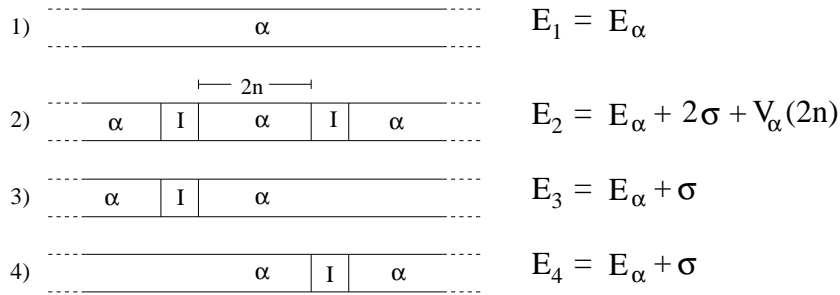


Figure 7.3: Configurations needed to calculate the two-interface interaction.

Equation (7.5) is exact, but is not convenient for our purposes, as we want only the leading term of $V_\alpha(2n)$. In fact, we can exploit the rapid decay of the V_α with n to substitute all infinite segments in Fig. 7.3 with finite (though sufficiently long) ones. Thus equation (7.5) can be approximated by

$$V_\alpha(2n) \approx E_A + E_B - E_C \quad (7.6)$$

where A, B, and C, are the *periodic* configurations sketched in Fig. 7.4. $n_0 + 2n$ and $N - 2n - 2n_I - n_0$ are assumed to be both a large multiple of $2n$ and much greater than n_I .

We label the spins of configurations A, B and C as $\{a_1, a_2, \dots, a_{n_0} \equiv a_0\}$, $\{b_{n_0+1}, \dots, b_N \equiv b_{n_0}\}$ and $\{c_1, c_2, \dots, c_N \equiv c_0\}$, respectively. For D large the spins will deviate from their clock positions $\{a_i^0\}$, $\{b_i^0\}$ and $\{c_i^0\}$ by an angle analytic in D^{-1} [105, 106, 113] and we write

$$a_i = a_i^0 + \tilde{a}_i, \quad b_i = b_i^0 + \tilde{b}_i, \quad c_i = c_i^0 + \tilde{c}_i. \quad (7.7)$$

We can choose to label the spins such that

$$a_i^0 = c_i^0 \quad 1 \leq i \leq n_0, \quad b_i^0 = c_i^0 \quad n_0 + 1 \leq i \leq N. \quad (7.8)$$

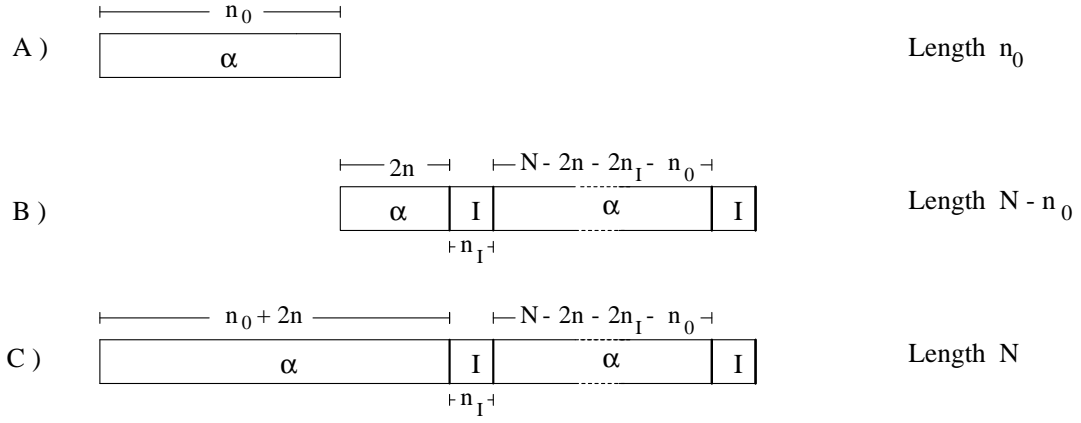


Figure 7.4: Periodic configurations appearing in the approximate reconnection formula (7.6).

In analogy to the inverse anisotropy expansion technique used in Chapter 2, if $1/D$ is sufficiently small we can expand the Hamiltonian (7.1) to second order in the spin deviations $\{\tilde{a}_i\}$, $\{\tilde{b}_i\}$, $\{\tilde{c}_i\}$. Using a superscript tilde to indicate we are using the quadratic expansion for the Hamiltonian, the two-interface interaction can be written

$$\begin{aligned} \tilde{V}_\alpha(2n) = & \tilde{\mathcal{H}}(\tilde{a}_{n_0}, \tilde{a}_1) + \sum_{i=2}^{n_0} \tilde{\mathcal{H}}(\tilde{a}_{i-1}, \tilde{a}_i) + \tilde{\mathcal{H}}(\tilde{b}_N, \tilde{b}_{n_0+1}) + \sum_{i=n_0+2}^N \tilde{\mathcal{H}}(\tilde{b}_{i-1}, \tilde{b}_i) \\ & - \tilde{\mathcal{H}}(\tilde{c}_N, \tilde{c}_1) + \sum_{i=2}^N \tilde{\mathcal{H}}(\tilde{c}_{i-1}, \tilde{c}_i) \end{aligned} \quad (7.9)$$

where

$$\tilde{\mathcal{H}}(\tilde{a}_{i-1}, \tilde{a}_i) = J_{i-1,i}^a \{\tilde{a}_{i-1} - \tilde{a}_i + \Delta_{i-1,i}^a\}^2 + h_i^a (\tilde{a}_i + \epsilon_i^a)^2 + D\tilde{a}_i^2/2 \quad (7.10)$$

with

$$J_{i-1,i}^a = \cos(a_{i-1}^0 - a_i^0 + \pi\Delta/3)/2, \quad (7.11)$$

$$h_i^a = h \cos(a_i^0)/2, \quad (7.12)$$

$$\Delta_{i-1,i}^a = \tan(a_{i-1}^0 - a_i^0 + \pi\Delta/3), \quad (7.13)$$

$$\epsilon_i^a = \tan(a_i^0). \quad (7.14)$$

It follows from (7.8) that

$$\epsilon_i^a = \epsilon_i^b, \quad h_i^a = h_i^b \quad (7.15)$$

for all i and that

$$J_{i-1,i}^a = J_{i-1,i}^c, \quad \Delta_{i-1,i}^a = \Delta_{i-1,i}^c, \quad 2 \leq i \leq n_0 \quad (7.16)$$

$$J_{i-1,i}^b = J_{i-1,i}^c, \quad \Delta_{i-1,i}^b = \Delta_{i-1,i}^c, \quad n_0 + 2 \leq i \leq N. \quad (7.17)$$

For the cases considered here it will be possible to label the phases so that (7.16) is also true for $i = 1$ and (7.17) for $i = n_0 + 1$. Under these circumstances we may drop the a , b and c superscripts

on the quantities defined in (7.11)-(7.14). Using the technique described in Chapter 2 it is then possible to simplify (7.9) using the recursion equations (7.2). After some algebra one obtains

$$\tilde{V}_\alpha(2n) = -J_{0,1} \left\{ (\tilde{a}_{n_0} - \tilde{b}_N)(\tilde{c}_1 - \tilde{c}_{n_0+1}) - (\tilde{a}_1 - \tilde{b}_{n_0+1})(\tilde{c}_N - \tilde{c}_{n_0}) \right\}. \quad (7.18)$$

The angular deviations appearing in (7.18) can be obtained to leading order in $1/D$ by iteratively using the recursion equations (7.2), as shown in Chapter 2 (an example where $\tilde{V}_\alpha(2n)$ is calculated in detail is given in Appendix B.1). The result for general n is

$$\tilde{V}_\alpha(2n) = c_2^n c_4^{n-1} \{s_4 - s_3\}^2 / D^{2n} + \mathcal{O}(1/D^{(2n+1)}) \quad (7.19)$$

where

$$s_i \equiv \sin[\pi(\Delta - i)/3], \quad (7.20)$$

$$c_i \equiv \cos[\pi(\Delta - i)/3]. \quad (7.21)$$

Terms of higher order than quadratic in the Hamiltonian (7.1) will not contribute to the leading term of the interface-interface interaction and hence to leading order $V_\alpha(2n)$ and $\tilde{V}_\alpha(2n)$ will be equal. Therefore we shall not distinguish between them below.

A knowledge of the leading term in the interface-interface interaction, equation (7.19), allows us to take the first step in determining the ground-state configurations. Because we are considering only two-interface interactions the interfaces must be equispaced in the ground state. Inspection of equation (7.19) shows that $V_\alpha(2n)$ is always positive and convex near \mathbf{P} . Therefore we can conclude that, for D large, all transitions $\langle \alpha^n I \rangle \rightarrow \langle \alpha^{n+1} I \rangle$ occur as σ is lowered [10].

The resulting phase diagram is drawn schematically in Fig. 7.5.

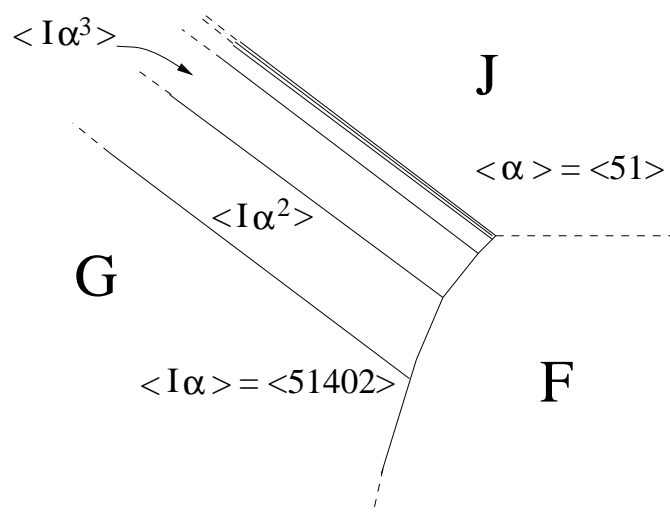


Figure 7.5: Schematic sketch of the splitting of the J-G boundary in the two interface interaction approximation.

To this order of approximation the $\langle\alpha^n I\rangle : \langle\alpha^{n+1} I\rangle$ phase boundaries remain degenerate and higher-order interface interactions can introduce qualitative changes in the phase diagram.

7.5 The $\langle\beta\rangle$ boundary

We now focus our attention on what happens along the G-F boundary (that we will also call $\langle\beta\rangle$ boundary) in the two-interface interaction approximation. In the F region of the phase diagram (Figs. 7.2 and 7.5) three phases coexist when $D = \infty$, namely $\beta_1 = \langle 14\rangle$, $\beta_2 = \langle 25\rangle$ and $\beta_3 = \langle 03\rangle$. However, when D is relaxed, only phases β_1 and β_2 stay degenerate, while phase β_3 has a higher energy.

Consider the boundary between one of the phases $\langle\alpha^n I\rangle$ and region F in Fig. 7.5. Along this boundary, in the absence of interactions between the interfaces $I_1 \equiv (51)^n 4$, $I_2 \equiv 0$ and $I_3 \equiv 2$, all phases

$$\langle(51)^n 4(14)^{m_1} 0(30)^{l_1} 2(52)^{p_1} (51)^n 4(14)^{m_2} 0(30)^{l_2} 2(52)^{p_2} \dots\rangle \quad (7.22)$$

are degenerate.

Now we turn on the two-interface interactions. In this approximation, the possible ground states are periodic and have the form $\langle(51)^n 4(14)^m 0(30)^l 2(52)^p\rangle$, where m , l and p depend on σ . In the following analysis we shall hold n fixed and assume that σ can be varied to trace out the phase sequences. Looking at Fig. 7.5 this corresponds to moving within the $\langle I\alpha^n\rangle$ stripe towards region F.

The energy per spin can be written

$$E = \left\{ (1+2n)E_{I_1} + E_{\beta_1} 2m + E_{I_2} + E_{\beta_2} 2p + E_{I_3} + E_{\beta_3} 2l + \sigma + V_{\beta_1}(2m) + V_{\beta_3}(2l) + V_{\beta_2}(2p) \right\} / L \quad (7.23)$$

where $L = (2m + 2p + 2l + 3 + 2n)$ and σ includes the interface tension of the three interfaces I_1 , I_2 and I_3 .

Simple calculations show that

$$E_{\beta_1} = E_{\beta_2}, \quad E_{\beta_3} = E_{\beta_2} + 3h^2/(8D) + \mathcal{O}(1/D^2). \quad (7.24)$$

Using the analytical techniques summarised in the previous section one can find, to leading order, the two-wall interactions between interfaces bounding phases $\langle\beta_1\rangle$, $\langle\beta_2\rangle$, and $\langle\beta_3\rangle$,

$$\begin{aligned} V_{\beta_1}(2m) = V_{\beta_2}(2p) &= D^{-(2m+2)} \{s_2 - s_3\}^2 c_3^{2m+1}, \\ V_{\beta_3}(2l) &= DV_{\beta_1}(2l)/c_3. \end{aligned} \quad (7.25)$$

We now want to find the values \bar{m} , \bar{p} and \bar{l} which minimise (7.23) for a given n and σ . By symmetry arguments one has $\bar{m} = \bar{p}$. It follows from (7.24) that \bar{l} must be bounded from above.

Indeed an explicit calculation of the energy $\mathcal{O}(1/D)$ shows immediately that $\bar{l} = 0$ or 1 and that the sequence of phases as σ is lowered is, $[\bar{n}, 0, 0, 0] \rightarrow [\bar{n}, 0, 1, 0] \rightarrow \text{F}$, where we used the notation $[n, m, l, p]$ to denote phase $\langle (51)^n 4(14)^m 0(30)^l 2(52)^p \rangle$.

The boundary between $[\bar{n}, 0, 0, 0]$ and $[\bar{n}, 0, 1, 0]$ is non-degenerate and therefore cannot be split by terms of higher order in D^{-1} . The boundary between $[\bar{n}, 0, 1, 0]$ and F remains degenerate to all phases of the form $[\bar{n}, m, 1, m]$. The effect of higher order terms can be deduced by noting that $V_{\beta_1}(2m)$ and $V_{\beta_2}(2p)$ are positive and convex. This implies that all the transitions $[\bar{n}, m, 1, m] \rightarrow [\bar{n}, m+1, 1, m+1]$ are stable [10]. Fig. 7.6 summarises the results of the two-interface interaction analysis.

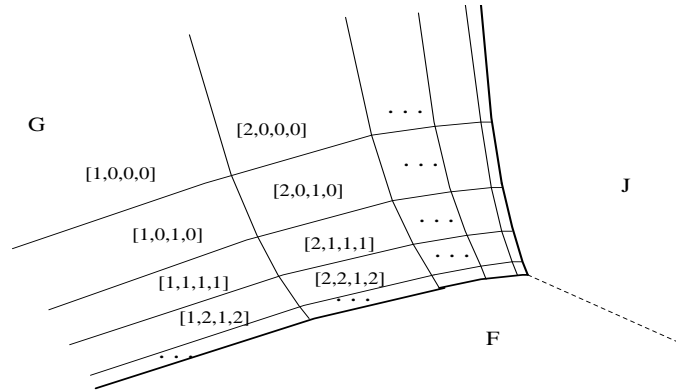


Figure 7.6: Schematic phase diagram near the Y-point in the two-interface interaction approximation. The notation $[n, m, l, p]$ is used to indicate the phase $\langle (51)^n 4(14)^m 0(30)^l 2(52)^p \rangle$. The bold solid lines are accumulation lines. The dashed line is a first order boundary.

7.6 Hyperfine structure

We now restrict our analysis to the richest region of the phase diagram, i.e. where $l = 1$. We already know that, in the two-interface approximation, the possible ground states can be written in the form $\langle \alpha^n I_1 \beta_1^m I_2 \beta_2^m I_3 \rangle \equiv [n, m, m]$, where $I_1 \equiv 4$, $I_2 \equiv 030$, and $I_3 \equiv 2$. Bassler, Sasaki and Griffiths [12] have shown that, for exponentially decaying interface interactions, such as is the case here, the general form of the interaction energy of an arbitrary number of interfaces can be constructed as

$$V_{\alpha\beta_1\beta_2\dots\beta_2}(2n, 2m, 2p, 2q, \dots, 2s) = V_{\alpha}(2n)t_{\alpha\beta_1}V_{\beta_1}(2m)t_{\beta_1\beta_2}V_{\beta_2}(2p)t_{\beta_2\alpha}V_{\alpha}(2q)\dots t_{\beta_1\beta_2}V_{\beta_2}(2s) \quad (7.26)$$

where the V 's are defined in (7.19) and (7.25) and, to leading order, we find

$$\begin{aligned} t_{\beta_1\beta_2} &= D^{-3}\{s_2 - s_3\}^{-2}c_2^2c_3^2, \\ t_{\alpha\beta_1} &= D\{(s_3 - s_2)(s_4 - s_3)\}^{-1}, \\ t_{\beta_2\alpha} &= t_{\alpha\beta_1}. \end{aligned} \quad (7.27)$$

The formulæ (7.27) follow from calculations similar to that described in Appendix B.1. For example taking the phases $A = [n, m, m]$, $B = [n, m + 1, m + 1]$, and $C = [n, m, m, n, m + 1, m + 1]$ the right-hand side of equation (7.18) is equal in leading order to $V_{\beta_1}(2m)t_{\beta_1\beta_2}V_{\beta_2}(2m + 2)$. The quantity $t_{\beta_1\beta_2}$ can then immediately be extracted by using the expression (7.25) for V_{β_1} and V_{β_2} .

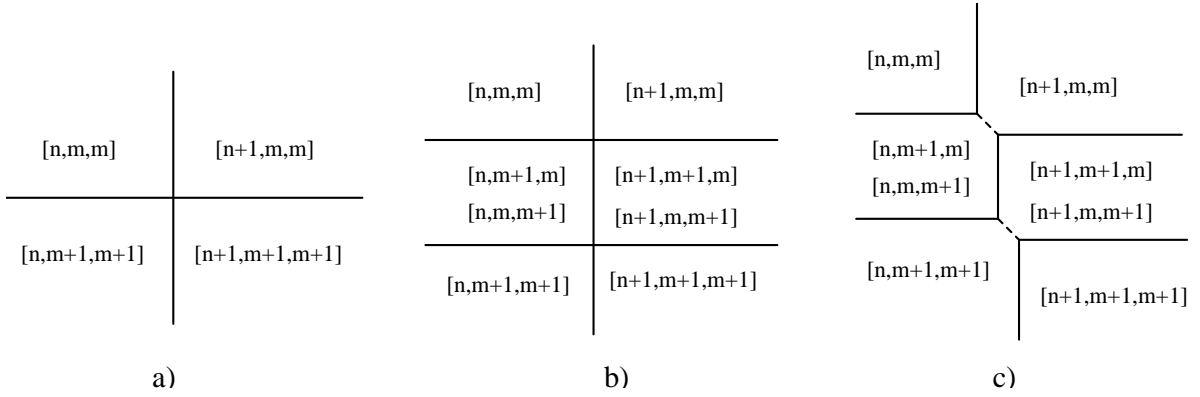


Figure 7.7: Detail of the phase diagram in (a) the two-interface approximation; (b) the three-interface approximation; (c) the four-interface approximation. First order lines are dashed.

With the aid of (7.26) it is possible to examine the effects of three-interface interactions on the superdegenerate boundaries in Fig. 7.6. Consider the general case represented in Fig. 7.7a. All four boundaries are multiphase lines where any sequence of the two neighbouring phases are degenerate within the two-interface interaction approximation. For the $[n, m, m] : [n + 1, m, m]$ and $[n, m + 1, m + 1] : [n + 1, m + 1, m + 1]$ boundaries this exhausts the possibilities and the three-interface interactions are not of sufficiently long range to split the degeneracy. For the $[n, m, m] : [n, m + 1, m + 1]$ ($[n + 1, m, m] : [n + 1, m + 1, m + 1]$) boundary, however, the phases $[n, m + 1, m]$ and $[n, m, m + 1]$ ($[n + 1, m + 1, m]$ and $[n + 1, m, m + 1]$) are also degenerate and there is the possibility that these may be stabilised with respect to $[n, m, m]$ and $[n, m + 1, m + 1]$ ($[n + 1, m, m]$ and $[n + 1, m + 1, m + 1]$) by the three-interface interaction.

To check this we need the energy differences [10, 12]

$$\begin{aligned}
 2E_{[n, m+1, m]} - E_{[n, m, m]} - E_{[n, m+1, m+1]} &= 2E_{[n, m, m+1]} - E_{[n, m, m]} - E_{[n, m+1, m+1]} \\
 &\sim V_{\beta_1\beta_2}(m, m + 1) + V_{\beta_1\beta_2}(m + 1, m) - V_{\beta_1\beta_2}(m + 1, m + 1) - V_{\beta_1\beta_2}(m, m)
 \end{aligned}
 \tag{7.28}$$

which are dominated by $V_{\beta_1\beta_2}(m, m)$ and which are therefore negative. Similarly the $[n + 1, m, m] : [n + 1, m + 1, m + 1]$ boundary is unstable with respect to the formation of $\{[n + 1, m + 1, m], [n + 1, m, m + 1]\}$. The resulting modification to the phase diagram is sketched in Fig. 7.7b.

The V_4 terms do not cause further splitting of the multidegenerate lines of Fig. 7.7b but they qualitatively change the phase diagram near the two points where four lines meet. In the proximity of the upper one the structure of the phase diagram is determined by the signs of the energy differences

[12]

$$\begin{aligned}
\Delta V_1 &= V_{\alpha\beta_1\beta_2}(n, m, m) + V_{\alpha\beta_1\beta_2}(n+1, m+1, m) \\
&\quad - V_{\alpha\beta_1\beta_2}(n+1, m, m) - V_{\alpha\beta_1\beta_2}(n, m+1, m) \\
\Delta V_2 &= V_{\beta_1\beta_2\alpha}(m, m, n) + V_{\beta_1\beta_2\alpha}(m+1, m, n+1) \\
&\quad - V_{\beta_1\beta_2\alpha}(m+1, m, n) - V_{\beta_1\beta_2\alpha}(m, m, n+1)
\end{aligned}
\tag{7.29}$$

With the aid of the factorization formulæ (7.26) it is possible to check that the two energy differences (7.29) are positive. This means that phases $[n+1, m, m]$ and $\{[n, m, m+1], [n, m+1, m]\}$ are separated by a short first-order line; similarly one can show that $\{[n+1, m, m+1], [n+1, m+1, m]\}$ and $[n, m+1, m+1]$ also coexist at a first-order transition. In this approximation the structure of Fig. 7.7b must be modified as in Fig. 7.7c.

The factorization formulæ (7.26) allow us to go further and study the effect on the phase diagram of interface–interface interactions of all orders. Bassler, Sasaki and Griffiths [12] showed that the form of the phase diagram depends upon the sign of the two-interface interactions (7.19) and (7.25) and the t 's, equation (7.27). Here these are all positive corresponding to a case where the superdegenerate boundaries at the end of the first-order lines in Fig. 7.7c split under the effect of higher-order interface–interface interactions, giving rise to a structure analogous to that in Fig. 7.6 (but where the phases have longer periodicity). Furthermore one can carry the analysis further by studying again the splitting near the points where four lines meet and so on, finding a structure similar to the one in Fig. 6(c). The analysis can then be repeated *ad infinitum*, showing that the Υ -point has, indeed, a self-similar, fractal structure.

Fig. 7.8 summarises the results of a numerical simulation of our model. We have discretized the $[0, 2\pi]$ domain for the angles θ_i in 1200 parts and then used the Floria-Griffiths [71] algorithm to find the exact ground state of the discretized model. Some of the short first order transition lines, as in Fig. 7.7c, are visible.

7.7 Conclusions

We have considered a model of XY spins with 6-fold anisotropy and chiral spin interactions. Using an expansion in $1/D$, the inverse spin anisotropy, we have given analytic evidence for the existence of an Υ -point (an accumulation point for two interpenetrating sequences of first-order transitions) in the model.

The phase diagram near the Υ -point has been constructed inductively by calculating the interface–interface interactions to leading order in $1/D$. Following arguments due to Bassler, Sasaki and Griffiths [12] we have argued that the Υ -point has a self-similar, fractal structure.

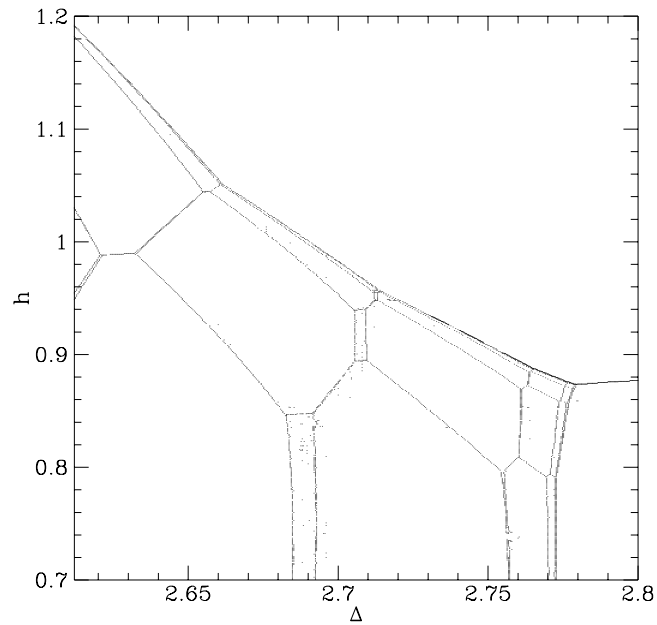


Figure 7.8: Phase diagram obtained through numerical simulation. The $[0, 2\pi]$ interval for the angles has been discretized in 1200 parts. The ground states for each h and Δ was found using the Floria-Griffiths algorithm.

Although the results presented here are rigorous within the leading order analysis of the interface-interface interactions, we cannot rule out the possibility that the neglected higher-order contributions could affect the phase diagram by truncating the sequence of phases springing out from the multiphase lines.

Appendix A

A.1 Stability of the $\langle 2 \rangle - \langle 3 \rangle$ boundary

The leading-order analysis of section 5.6 showed that, in the two-wall interaction approximation, a sequence of phases,

$$\langle 2 \rangle, \langle 3 \rangle, \langle 4 \rangle, \dots, \langle n \rangle, \dots \quad (\text{A.1})$$

appears in the phase diagram of the quantum ANNNI model. The question is whether three- or higher-order interactions can introduce longer-period mixed ground-states between two neighbouring phases of the sequence (A.1).

As discussed in section 5.7, to ascertain whether the $\langle n \rangle | \langle n+1 \rangle$ boundary is stable it is necessary to determine the sign of the structure coefficient

$$F(n, n+1) \equiv V_3(n, n) - 2V_3(n, n+1) + V_3(n+1, n+1). \quad (\text{A.2})$$

In general, the leading order term of $F(n, n+1)$, which is $\mathcal{O}(1/\tilde{D}^{4n-1})$, can be calculated through a second-order expansion of the energy denominators of the V_3 's (see section 5.7). However, for $n = 1$ the term $\mathcal{O}(1/\tilde{D}^3)$ is accidentally zero and terms $\mathcal{O}(1/\tilde{D}^4)$ must be retained. This leads to a lengthy calculation. We now calculate $F(2, 3)$ explicitly, considering each order of perturbation theory in turn.

Second-order perturbation theory

Contributions arise from diagrams spanning a wall which are created and then immediately destroyed (as in the example of Fig. 5.8). The contribution to $V_3(2, 2)$ comes from both first and second neighbour excitations. That to $V_3(2, 3)$ is just from second neighbours because the energy denominator of the first neighbour excitation does not depend on both σ and η . For the same reason there is no contribution at all to $V_3(3, 3)$.

Using a subscript 2 to indicate that we are considering only the terms arising from second order perturbation theory one obtains $\mathcal{O}(1/\tilde{D}^4)$

$$V_2(2, 2) = \frac{8J_2^2}{(4\tilde{D})^3 S} [-J_1^2 + 2J_2(J_1 - J_2)] + \frac{48J_2^3}{(4\tilde{D})^4 S} [-J_1 J_2 + 2J_2^2], \quad (\text{A.3})$$

$$V_2(2, 3) = -\frac{8J_2^4}{(4\tilde{D})^3 S} + \frac{48J_2^4(J_2 + J_1)}{(4\tilde{D})^4 S}, \quad (\text{A.4})$$

$$V_2(3, 3) = 0. \quad (\text{A.5})$$

Third-order perturbation theory

Contributions to $V_3(2, 2)$ in third order perturbation theory arise from diagrams like that shown in Fig. A.1.

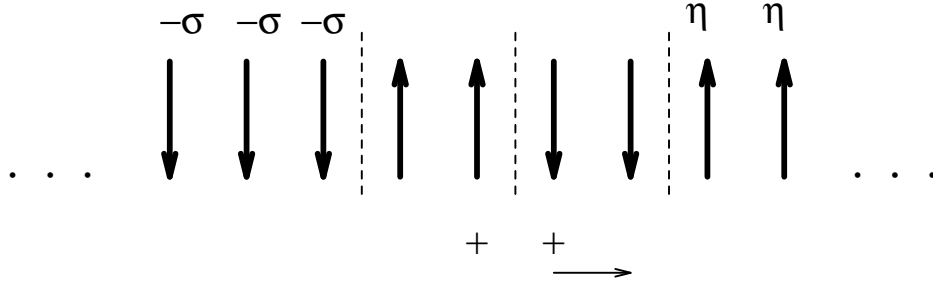


Figure A.1: Example of a term contributing to $V_3(2, 2)$ in third order perturbation theory.

Recalling that the spins on either side of the wall can hop, and that the initial excitation can be between second neighbours, with a subsequent hop to first neighbours gives

$$V_3(2, 2) = \frac{48J_1^2 J_2^2 (2J_2 - J_1)}{(4\tilde{D})^4 S}. \quad (\text{A.6})$$

Similar diagrams contribute to $V_3(2, 3)$. The hop must lie within the domain of 3 spins

$$V_3(2, 3) = \frac{24J_1^2 J_2^3}{(4\tilde{D})^4 S}. \quad (\text{A.7})$$

There is no contribution $V_3(3, 3)$.

Fourth-order perturbation theory

We first consider processes which are proportional to $V_{\parallel}^2 V_{\parallel}^2$. As we discussed in the text, to lowest order in J_2/D we do not need to consider processes which hop beyond the wall. However, since the calculation of $F(2, 3)$ requires a calculation of $V_3(2, 2)$ and $V_3(2, 3)$ including the first higher-order corrections, we need to keep such processes.

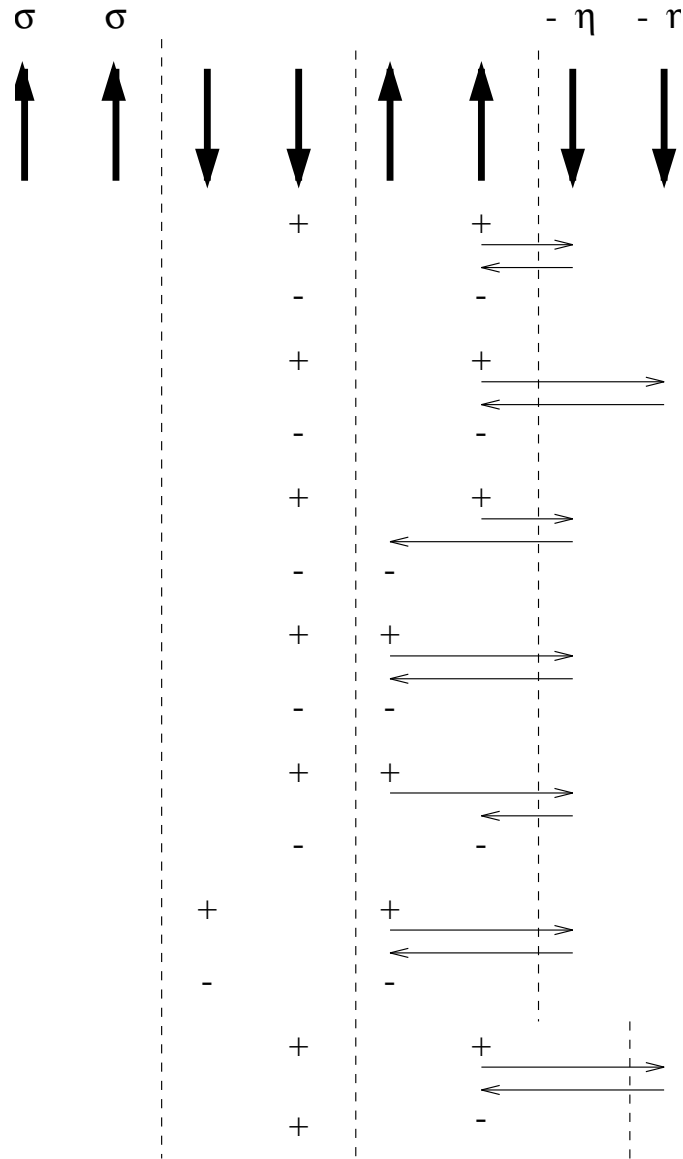


Figure A.2: Processes which can not occur when the wall is as shown and which therefore carry a factor $\delta_{\eta,-1}$ (when the wall is absent $\eta = -1$ and these processes are allowed). The first six diagrams contribute to $V_3(2, 2)$ and the last one to $V_3(2, 3)$. In the last diagram the right-hand block contains three down spins.

We now evaluate contributions from such processes, which we show in Fig. A.2. First of all, since these processes only exist in the *absence* of the right-hand wall, they all carry a factor $\delta_{\eta,-1}$. Secondly their overall sign is negative for even-order (fourth-order) perturbation theory. Also, the contributions to $V_3(2, 2)$ carries a factor of 2 to account for the mirror image diagrams.

Thus from the first diagram of Fig. A.2, we get $E_k(\sigma, \eta)$ of equation (5.16) as

$$E_3(\sigma, \eta) = -2\delta_{\eta, -1} J_1^2 J_2^2 (\mathcal{E}_1 \mathcal{E}_2 \mathcal{E}_3)^{-1}, \quad (\text{A.8})$$

where \mathcal{E}_i is an energy denominator. We have that $\mathcal{E}_i \sim 4\tilde{D} + O(J)$. In particular, we need to include the dependence of \mathcal{E}_i on σ , which we deduce from Fig. 5.10.

For the present purposes it suffices to set $\mathcal{E}_i = 4\tilde{D}$ and $d\mathcal{E}_i/d\sigma = J_2$ for all diagrams of Fig. A.2, except the last one, for which $d\mathcal{E}_i/d\sigma = (J_2 - J_1)$. Thus for the first diagram of Fig. A.2 we have

$$\sum_{\sigma\eta} \sigma\eta E_3(\sigma, \eta) = -12J_1^2 J_2^2 (4\tilde{D})^{-4} (d\mathcal{E}/d\sigma). \quad (\text{A.9})$$

Indicating with $\delta V_4(2, 2)$ and $\delta V_4(2, 3)$ the total contribution to $V_4(2, 2)$ and $V_4(2, 3)$ from the diagrams of Fig. A.2 one has

$$\delta V_4(2, 2) = -(J_2^3/\tilde{D}^4) (48J_1^2 + 24J_2^2 - 12J_1J_2), \quad (\text{A.10})$$

$$\delta V_4(2, 3) = -(6J_2^5/\tilde{D}^4). \quad (\text{A.11})$$

However, one also needs to consider terms proportional to $V_{\mathbb{W}}^4$ where two pairs of excitations are created and destroyed which do indeed turn out to be important. Consider first a set of four spins n_i at sites i and the following processes

- (i) n_1, n_2 excited, n_1, n_2 destroyed, n_3, n_4 excited, n_3, n_4 destroyed
- (ii) n_1, n_2 excited, n_3, n_4 excited, n_3, n_4 destroyed, n_1, n_2 destroyed
- (iii) n_1, n_2 excited, n_3, n_4 excited, n_1, n_2 destroyed, n_3, n_4 destroyed
- (iv) n_3, n_4 excited, n_3, n_4 destroyed, n_1, n_2 excited, n_1, n_2 destroyed
- (v) n_3, n_4 excited, n_1, n_2 excited, n_1, n_2 destroyed, n_3, n_4 destroyed
- (vi) n_3, n_4 excited, n_1, n_2 excited, n_3, n_4 destroyed, n_1, n_2 destroyed

We will be interested in the cases shown in Fig. A.3 where n_1 and n_2 must be first or second neighbours straddling one wall and similarly for n_3 and n_4 with respect to the other wall. Except for the possibility that $n_2 = n_3$, all the n 's are distinct. Because we are working to linear order in $1/S$ (that is ignoring terms higher than quadratic in the boson Hamiltonian) the energy denominator depends on position on the lattice but not on the position of the other excitations. Hence the energy denominators are simply the sum of the energies of the excited spins relative to the ground state energy. We denote them by $E_{ijk\dots}$ when spins $i, j, k \dots$ are excited. Noting that the matrix elements, say M , are common to all processes (i)–(vi) we are now in a position to write down the contribution from these diagrams to fourth order in perturbation theory

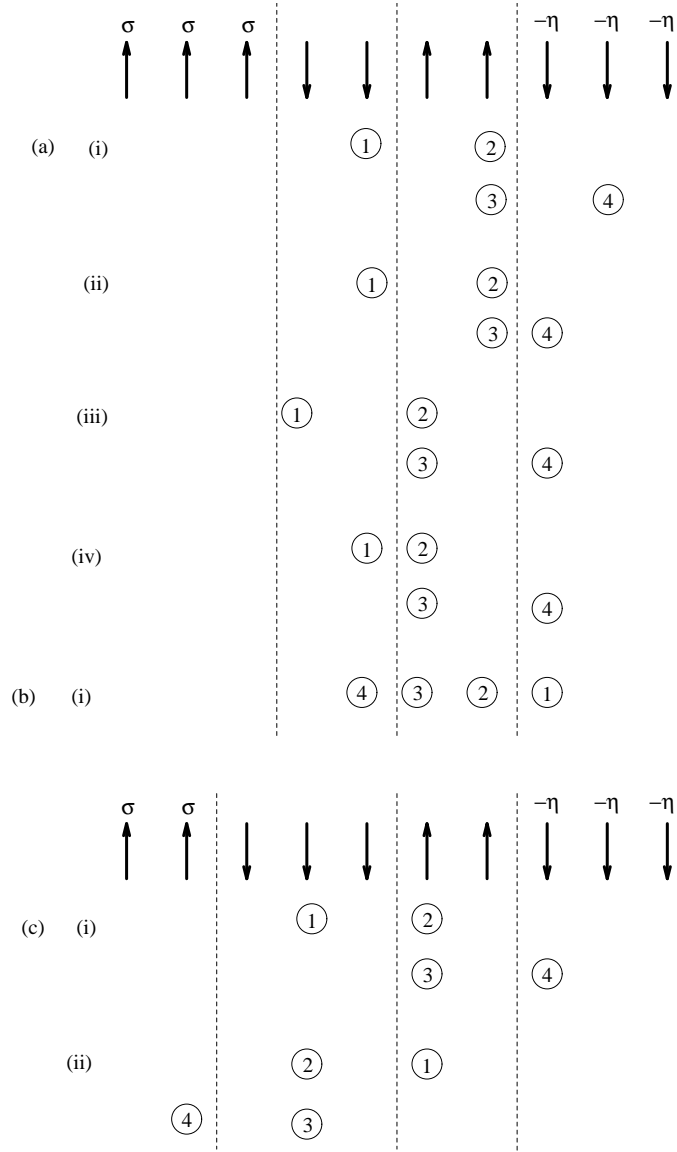


Figure A.3: Terms which contribute to (a) $V_4^{(1)}(2,2)$, (b) $V_4^{(2)}(2,2)$, (c) $V_4^{(3)}(2,2)$. The figures indicate which spins are excited. The way in which all possible orderings of the excitations are accounted for is described in the text (see equations (A8) and (A9) for diagrams (a) and (c) and equation (A10) for diagram (b)). In cases (a) and (b) the diagrams which are mirror images in the center wall must also be accounted for by including a factor of 2.

$$V_4 = \frac{M}{S} \left(\frac{1}{E_{12}^2 E_{34}} + \frac{1}{E_{12} E_{34}^2} - \frac{\xi}{E_{12} E_{1234} E_{12}} - \frac{2\xi}{E_{12} E_{1234} E_{34}} - \frac{\xi}{E_{34} E_{1234} E_{34}} \right) \quad (\text{A.12})$$

where $\xi = 2$ if two excitations are present at the same site (Bose statistics) and $\xi = 1$ for all spins distinct.

Using $E_{1234} = E_{12} + E_{34}$

$$V_4 = \frac{M}{S} (1 - \xi) \frac{E_{12} + E_{34}}{E_{12}^2 E_{34}^2}. \quad (\text{A.13})$$

Putting $\xi = 1$ it is immediately apparent that there is no contribution from diagrams for which all n_i are different. There are however terms $\mathcal{O}(1/\tilde{D}^4)$ when $\xi = 2$. Diagrams of this type which contribute to $V_3(2, 2)$ are shown in Fig. A.3a. Only terms with $\eta = 1$ give a contribution different from E_0 . Therefore when the sum over σ is taken the term proportional to σ is the lowest order which survives. Including a factor 2 for diagrams symmetric with respect to reflection in the center wall of Fig. A.3a one obtains

$$V_4^{(a)}(2, 2) = \frac{12}{(4\tilde{D})^4 S} \left(2J_2^5 - J_1 J_2^4 + 2J_1^2 J_2^3 \right), \quad (\text{A.14})$$

where the superscript indicates a contribution of type a in Fig. A.3.

Similarly the contributions of this type to $V_3(2, 3)$ is shown in Fig. A.3c. They give

$$V_4^{(c)}(2, 3) = \frac{12J_2^5}{(4\tilde{D})^4 S}. \quad (\text{A.15})$$

There is one further contribution to $V_4(2, 2)$. Consider the following order of excitation of four spins

- (i) n_1, n_2 excited, n_3, n_4 excited, n_2, n_4 destroyed, n_1, n_3 destroyed
- (ii) n_1, n_2 excited, n_3, n_4 excited, n_1, n_3 destroyed, n_2, n_4 destroyed
- (iii) n_3, n_4 excited, n_1, n_2 excited, n_1, n_3 destroyed, n_2, n_4 destroyed
- (iv) n_3, n_4 excited, n_1, n_2 excited, n_2, n_4 destroyed, n_1, n_3 destroyed

The pairs (n_1, n_2) , (n_3, n_4) , (n_1, n_3) , (n_2, n_4) , must all be first or second neighbours spanning a wall. This means that the only contribution of this type is to $V_4(2, 2)$ and is shown in Fig. A.3b. Proceeding as before the sum of all orderings gives

$$V_4^{(b)} = -\frac{2M}{S} \frac{E_{1234}}{E_{13} E_{24} E_{12} E_{34}} \quad (\text{A.16})$$

where we have included a factor 2 for the reverse order of the perturbations. Evaluating this for the relevant diagram

$$V_4^{(b)}(2, 2) = \frac{24J_1^2 J_2^3}{(4\tilde{D})^4 S} \quad (\text{A.17})$$

where a factor 2 for the mirror image process has been included.

Finally obtaining $V_3(2, 2)$ from equations (A.10), (A.3), (A.6), (A.14), and (A.17) and $V_3(2, 3)$ from equations (A.11), (A.4), (A.7), and (A.15) we are in a position to calculate the sum of the contributions to $F(2, 3)$ from all the diagrams of Fig. A.3. We obtain

$$\delta F(2, 3) = -\frac{492J_2^5}{(4\tilde{D})^4S} \quad (\text{A.18})$$

where we have used $J_2 = J_1/2 + \mathcal{O}(1/\tilde{D}S)$. Combining this with Eqns. (A.10) and (A.11) we get

$$F(2, 3) = -\frac{392J_2^5}{(4\tilde{D})^4S} . \quad (\text{A.19})$$

This is negative showing that the $\langle 2 \rangle : \langle 3 \rangle$ phase boundary is indeed stable.

i	...	-3	-2	-1	0	1	2	3	4	...					
		*							*						
$3a_i^0/\pi$...	5	1	5	1	5	:	1	5	1	5	1	5	1	...
$3b_{n_0+i}^0/\pi$...	0	2	5	1	5	:	1	5	1	4	0	2	5	...
			*								*				

(B.6)

The *'s mark where a_i^0 first differs from $b_{i+n_0}^0$ when moving away from the dotted interface in either direction.

It follows immediately from (B.4) that

$$(\tilde{a}_3 - \tilde{b}_{n_0+3}) = \frac{1}{D} \left\{ \sin\left[\frac{\pi}{3}\Delta - 3\right] - \sin\left[\frac{\pi}{3}\Delta - 4\right] \right\} \quad (\text{B.7})$$

Two further iterations of (B.5) give

$$\begin{aligned} (\tilde{a}_1 - \tilde{b}_{n_0+1}) &= \frac{1}{D^2} \cos\left[\frac{\pi}{3}\Delta + a_1^0 - a_2^0\right] \cos\left[\frac{\pi}{3}\Delta + a_2^0 - a_3^0\right] (\tilde{a}_3 - \tilde{b}_{n_0+3}) \\ &= \frac{1}{D^3} \cos\left[\frac{\pi}{3}(\Delta - 4)\right] \cos\left[\frac{\pi}{3}(\Delta - 2)\right] \left\{ \sin\left[\frac{\pi}{3}\Delta - 3\right] - \sin\left[\frac{\pi}{3}\Delta - 4\right] \right\}. \end{aligned} \quad (\text{B.8})$$

$(\tilde{a}_{n_0} - \tilde{b}_N)$ may be calculated in an analogous way

$$(\tilde{a}_{n_0} - \tilde{b}_N) = -(\tilde{a}_1 - \tilde{b}_{n_0+1}). \quad (\text{B.9})$$

Similarly

$$(\tilde{c}_1 - \tilde{c}_{n_0+1}) = (\tilde{c}_N - \tilde{c}_{n_0}) = (\tilde{a}_1 - \tilde{b}_{n_0+1}). \quad (\text{B.10})$$

Using $J_{0,1} = \cos[\frac{\pi}{3}(\Delta - 2)]/2$, from the definition (7.11) and substituting (B.8)–(B.10) into (7.18) gives

$$\tilde{V}_\alpha(6) = -\frac{1}{D^6} \left\{ \sin\left[\frac{\pi}{3}\Delta - 4\right] - \sin\left[\frac{\pi}{3}\Delta - 3\right] \right\}^2 \cos\left[\frac{\pi}{3}(\Delta - 4)\right]^2 \cos\left[\frac{\pi}{3}(\Delta - 2)\right]^3. \quad (\text{B.11})$$

It is important to point out that the labelling used in equation (B.1) is not unique. Any labelling which satisfies (7.16) for $1 \leq i \leq n_0$ and (7.17) for $1 \leq n_0 + 1 \leq N$ will give the correct results for $\tilde{V}_\alpha(6)$. However in general $(\tilde{a}_1 - \tilde{a}_{n_0+1})$ etc. will contain lower powers of $1/D$ which cancel when the difference in (7.18) is taken. The choice given above, which maximises the distance of the position (*) where a_i^0 first differs from $b_{n_0+1}^0$ avoids such cancellation and leads to the easiest calculation.

It is important to mention that because the interface-interface interactions decay very rapidly (exponentially) with increasing interface–interface distance the values of $n_0 + 2n$ and $N - 2n - 2n_I - n_0$ need not in fact be much larger than $2n$ and n_I . That sufficiently large values have been chosen can be checked *a posteriori* by verifying that increasing the values of n_0 and N does not change the result (B.11).

Finally we give an explicit expression for the interface energy σ defined in (7.4). A leading order calculation gives

$$\sigma = c_2 + c_4 - 2c_3 + \frac{1}{D} \{s_2^2 - 2s_3^2 - 2s_2s_4 + 4s_3s_4 - s_4^2 + h\sqrt{3}(s_2 - 2s_3 + s_4)\} + \mathcal{O}(D^{-2}) \quad (\text{B.12})$$

where

$$s_i \equiv \sin[\pi(\Delta - i)/3], \quad (\text{B.13})$$

$$c_i \equiv \cos[\pi(\Delta - i)/3]. \quad (\text{B.14})$$

Bibliography

- [1] J. Rossat-Mignod, P. Burlet, J. Villain, H. Bartholin, T.-S. Wang, D. Florence, and O. Vogt. *Phys. Rev. B*, **16**, 440, (1977).
- [2] J. Rossat-Mignod, P. Burlet, H. Bartholin, O. Vogt, and R. Langier. *J. Phys. C*, **13**, 6381, (1980).
- [3] R. J. Elliott. *Phys. Rev. B*, **124**, 346, (1961).
- [4] J. Villain in **Structures et Instabilités**. C. Godréche, editor, page 1. Editions de physique, Les Ulis, France, (1986).
- [5] A. M. Szpilka. *Domain wall interactions and spatially modulated phases*. Ph. D. thesis, Cornell University, (1985).
- [6] M. E. Fisher and W. Selke. *Phys. Rev. Lett.*, **44**, 1502, (1980).
- [7] P. Bak and J. von Boehm. *Phys. Rev. B*, **21**, 5297, (1980).
- [8] W. Selke and P. M. Duxbury. *Z. Phys. B*, **57**, 49, (1984).
- [9] J. Villain and M. B. Gordon. *J. Phys. C*, **13**, 3117, (1980).
- [10] M.E. Fisher and A.M. Szpilka. *Phys Rev. B*, **36**, 644, (1987).
- [11] M. Barma and V. Subrahmanyam. *Phase Transitions*, **16/17**, 303, (1989).
- [12] K. E. Bassler, K. Sasaki, and R. B. Griffiths. *J. Stat. Phys.*, **62**, 45, (1991).
- [13] J. W. Cahn. *J. Chem. Phys.*, **66**, 3667, (1977).
- [14] D. B. Abraham. *Phys. Rev. Lett.*, **44**, 1165, (1980).
- [15] P.M. Duxbury and J.M. Yeomans. *J. Phys. A*, **18**, L983, (1985).
- [16] M.J. De Oliveira and R.B. Griffiths. *Surf. Sci*, **71**, 687, (1978).
- [17] S. Dietrich in **Phase Transitions and Critical Phenomena**. C. Domb and J. L. Lebowitz, editors, volume 12, page 1. Academic, New York, (1988).

- [18] M. Schick R. Pandit and M. Wortis. *Phys. Rev. B*, **26**, 5112, (1982).
- [19] C. Micheletti and J. M. Yeomans. *Europhys. Lett.*, **28**, 4659, (1994).
- [20] A.B. Harris, C. Micheletti, and J.M. Yeomans. *Phys. Rev. B* *52*, **52**, 6684, (1995).
- [21] J. Jensen and A.R. Mackintosh. **Rare Earth Magnetism**. Oxford University Press, Oxford, (1991).
- [22] J. Jensen and A.R. Mackintosh. *Phys. Rev. Lett.*, **64**, 2699, (1990).
- [23] F. Seno, J. M. Yeomans, R. Harbord, and D. Y. K. Ko. *Phys. Rev. B*, **49**, 6412, (1994).
- [24] F. Seno, J. M. Yeomans, R. Harbord, and D. Y. K. Ko. *Tur. J. Phys.*, **18**, 361, (1994).
- [25] K. Sasaki. *J. Stat. Phys.*, **68**, 1013, (1992).
- [26] F.J. Dyson. *Phys. Rev.*, **102**, 1217, 1230, (1956).
- [27] S. V. Maleev. *Sov. Phys. – JETP*, **6**, 776, (1958).
- [28] T. Holstein and H. Primakov. *Phys. Rev.*, **58**, 1098, (1940).
- [29] C. Kittel. **Quantum Theory of solids**. J. Wiley & Sons, New York, (1963).
- [30] I. Afflek in **Fields, strings and critical phenomena**. E. Brézin and J. Zinn-Justin, editors, page 565. North Holland, (1990).
- [31] A. Messiah. *Quantum Mechanics*. North-Holland, Amsterdam, (1966).
- [32] R.B. Stinchcombe. *J. Phys. C*, **6**, 2459, (1973).
- [33] P.G. de Gennes. *Solid St. Commun.*, **1**, 132, (1963).
- [34] T. Kanata, K. Yoshikawa, and N. Okada. *Phys. Rev. B*, **37**, 5852, (1987).
- [35] W. L. Zhong, B. Jiang, P. L. Zhang, J. M. Ma, H. M. Chang, H. Z. Yang, and L. X. Li. *J. Phys. Cond. Mat.*, **5**, 2619, (1993).
- [36] C. L. Wang, S. R. P. Smith, and D. R. Tilley. *J. Phys. Cond. Mat.*, **6**, 9633, (1994).
- [37] W. P. Wolf. *J. Phys. (Paris)*, **32**, 26, (1971).
- [38] A. H. Cooke, D. T. Edmonds, C. B. P. Finn, and W. P. Wolf. *J. Phys. Soc. Japan*, **17**, 481, (1962).
- [39] Y.-L. and B. R. Cooper. *Phys. Rev.*, **172**, 539, (1968).
- [40] B. R. Cooper and O. Vogt. *J. Phys. (Paris)*, **32**, 958, (1971).

- [41] M. Henkel, A.B. Harris, and M. Cieplak. *Phys. Rev. B*, **52**, 4371, (1995).
- [42] J. D. Weeks. *Phys. Rev. Lett.*, **31**, 549, (1973).
- [43] C. Micheletti A. B. Harris and J. M. Yeomans. Complete wetting in the three-dimensionalising model. *J. Stat. Phys.* (in press), (1996).
- [44] C.L. Henley. *Phys. Rev. Lett.*, **62**, 2056, (1989).
- [45] E.F. Shender. *Sov. Phys. JETP*, **56**, 178, (1982).
- [46] A.B. Harris. private communication.
- [47] J.W. Negele and H. Orland. **Quantum Many-Particle Systems**. Addison-Wesley, (1988).
- [48] J.B. Kogut. *Rev. Mod. Phys.*, **51**, 669, (1979).
- [49] P. Pfeuty. *Ann. Phys.*, **57**, 79, (1970).
- [50] E. Fradkin and L. Susskind. *Phys. Rev. D*, **17**, 2637, (1978).
- [51] M. Susuki. *Prog. Theor. Phys.*, **56**, 1454, (1976).
- [52] R. W. Wang, D. L. Mills, E. E. Fullerton, J. E. Mattson, and S. D. Bader. *Phys. Rev. Lett.*, **72**, 920, (1994).
- [53] R. W. Wang, D. L. Mills, E. E. Fullerton, J. E. Mattson, and S. D. Bader. *Phys. Rev. B*, **50**, 3931, (1994).
- [54] B. L. Johnson and R. E. Camley. *Phys. Rev. B*, **44**, 9997, (1991).
- [55] B. L. Johnson and R. E. Camley. *J. Phys. Cond. Mat.*, **5**, 3727, (1993).
- [56] L. Trallori, P. Politi, A. Rettori, M. G. Pini, and J. Villain. *J. Phys. C*, **7**, L451, (1995).
- [57] P. Grunberg, R. Schreiber, Y. Pang, M. B. Brodsky, and H. Sowers. *Phys. Rev. Lett.*, **57**, 2422, (1986).
- [58] L. Néel. *Ann. Phys. (Paris)*, **5**, 232, (1936).
- [59] D.L. Mills. *Phys. Rev. Lett.*, **68**, 18, (1973).
- [60] F. Keffer and H. Chow. *Phys. Rev. Lett.*, **31**, 1061, (1973).
- [61] L. Trallori, P. Politi, A. Rettori, M. G. Pini, and J. Villain. *Phys. Rev. Lett.*, **72**, 1925, (1994).
- [62] L. Trallori, M. G. Pini, A. Rettori, M. Macciò, and P. Politi. *Mean-field study of surface and interface properties in terms of nonlinear maps*, **Preprint**, (1996).

- [63] W. Chou and R. B. Griffiths. *Phys. Rev B*, **34**, 6219, (1986).
- [64] R. B. Griffiths C. Micheletti and J. M. Yeomans. Surface spin-flop phases and bulk discommensurations in antiferromagnets. Oxford University preprint OUTP 96/23/S, (1996).
- [65] A.B. Harris, C. Micheletti, and J.M. Yeomans. *Phys. Rev. Lett.*, **74**, 3045, (1995).
- [66] A. D. Johnson, C. Norris, J. W. M. Frenken, H. S. Derbyshire, and J. E. Mac Donald. *Phys. Rev. B*, **44**, 1134, (1991).
- [67] V. Heine and L. D. Marks. *Surf. Sci.*, **165**, 65, (1986).
- [68] F. Ercolessi, E. Tosatti, and M. Parrinello. *Phys. Rev. Lett.*, **57**, 719, (1986).
- [69] J. Villain. in *Transizioni di Fase di Superficie*. Lectures given at the “Scuola Nazionale di Struttura della Materia”, Torino, (1995).
- [70] L. Pietronero. in *Enciclopedia Italiana di fisica*, volume 2. (1993).
- [71] L. M. Floria and R. B. Griffiths. *Numer. Math.*, **55**, 565, (1989).
- [72] R. B. Griffiths in **Fundamental problems in statistical mechanics**. van Beijeren, editor, volume 7, page 69. Elsevier Science, (1990).
- [73] D. Pandey and P. Krishna. *J. Cryst. Growth Charact.*, **7**, 213, (1984).
- [74] D. de Fontaine and J. Kulik. *Acta Metall.*, **33**, 1137, (1987).
- [75] J. Kulik and D. de Fontaine. *Mater. Res. Soc. Symp. Proc.*, **21**, 255, (1984).
- [76] A. Loiseau, G. Van Tendeloo, R. Portier, and F. Ducastelle. *J. Phys. (Paris)*, **46**, 595, (1985).
- [77] M.E. Fisher and A.M. Szpilka. *Phys Rev. B*, **36**, 5343, (1987).
- [78] M.E. Fisher and A.M. Szpilka. *Phys. Rev. Lett.* , **57**, 1044, (1986).
- [79] J. M. Yeomans. **Solid State Physics**, volume 21. Academic Press, Orlando, (1988).
- [80] W. Selke. *Phys. Report*, **170**, 213, (1988).
- [81] W. Selke. **Phase transitions and Critical Phenomena**, volume 15. Academic Press, New York, (1992).
- [82] G. V. Uimin. *J. Phys. Lett.*, **43**, L665, (1982).
- [83] V. L. Pokrovsky and G. Uimin. *J. Phys. C*, **15**, L353, (1982).
- [84] V. L. Pokrovsky and G. Uimin. *JETP*, **82**, 1640, (1982).

- [85] B. Lebech, K. Clausen, and O. Vogt. *J. Phys. C*, **13**, 1725, (1980).
- [86] J. Rossat-Mignod, P. Burlet, L.P. Regnault, and C. Vettier. *J. Magn. Magn. Mat.*, **90**, 5, (1990).
- [87] H. Horiuchi, K. Horioka, and N. Morimoto. *J. Mineral Soc. Jpn*, **2**, 253, (1990).
- [88] G. D. Price and J. M. Yeomans. *Acta Crystallogr. B*, **40**, 448, (1984).
- [89] M. Akaogi, S. Akimoto, K. Horioka, K. Takahashi, and H. Horiuchi. *J. Solid State Chem.*, **44**, 257, (1982).
- [90] G. D. Price, S. C. Parker, and J. M. Yeomans. *Acta Crystallogr. B*, **B41**, 231, (1985).
- [91] M. E. Fisher and W. Selke. *Philos. Trans. R. Soc. (London)*, **A302**, 1, (1981).
- [92] F. Hadrović. in *One-dimensional modulated magnetic structures*. Summer-project report (Oxford University), (1995).
- [93] R. J. Elliott, J. A. Krumhansl, and P. L. Leath. *Rev. Mod. Phys.*, **46**, 465, (1974).
- [94] L. M. Falicov and J. C. Kimball. *Phys. Rev. Lett.*, **22**, 997, (1969).
- [95] J. K. Freericks and L. M. Falicov. *Phys. Rev. B*, **41**, 2163, (1990).
- [96] R. Ramirez and L. M. Falicov. *Phys. Rev. B*, **3**, 2455, (1971).
- [97] Ch. Gruber, J. L. Lebowitz, and N. Macris. *Phys. Rev B*, **48**, 4312, (1993).
- [98] Ch. Gruber, D. Udelschi, and J. Jędrzejewski. *J. Stat. Phys*, **76**, 125, (1994).
- [99] P. Lemberger. *J. Phys. A*, **25**, 715, (1992).
- [100] M. E. Fisher and W. Selke. *Phys. Rev. Lett.*, **44**, 1502, (1980).
- [101] A. B. Harris C. Micheletti and J. M. Yeomans. A devil's staircase in the falicov-kimball model. Oxford University preprint OUTF 96/22/S, (1996).
- [102] P. Bak. *Rep. Prog. Phys.*, **45**, 587, (1982).
- [103] K. Sasaki. *Physica A*, **171**, 80, (1991).
- [104] J. Jensen. Theory of commensurable magnetic structures in holmium. *preprint*, (1996).
- [105] F. Seno and J. M. Yeomans. *Phys. Rev. B*, **50**, 10385, (1994).
- [106] F. Seno and J. M. Yeomans. *Phys. Rev. B*, **52**, 9550, (1995).
- [107] C. Micheletti, F. Seno, and J. M. Yeomans. *Phys. Rev. B*, **52**, 4353, (1995).

- [108] C. S. O. Yokoi, L.H. Tang, and W. R. Chou. *Phys. Rev. B*, **37**, 2173, (1988).
- [109] P. G. de Gennes. **The Physics of Liquid Crystals**. Oxford University Press, Oxford.
- [110] L. Strzelecki R. B. Meyer, L. Liebert and P. Keller. *J. Phys. Lett. (Paris)*, **171**, L69, (1975).
- [111] T. Moriya and T. Miyadai. *Solid State Comm.*, **42**, 209, (1982).
- [112] J. P. M. Chaiken and T. C. Lubensky. **Principles of condensed matter physics**. Cambridge University Press, Cambridge, (1995).
- [113] C. Baesens. in Topics in Mathematical Physics (lecture notes). Warwick University, (1993).